FREQUENCY-DEPENDENT ELECTRIC POWER LINE MODELING FOR STEADY STATE HARMONIC ANALYSIS

by

Bikash Poudel

A dissertation submitted to the faculty of
The University of North Carolina at Charlotte
in partial fulfillment of the requirements
for the degree of Doctor of Philosophy in
Electrical Engineering

Charlotte

2016

Approved by:

Dr. Valentina Cecchi

Dr. Sukumar Kamalasadan

Dr. Zia Salami

Dr. Brett Q. Tempest

ABSTRACT

BIKASH POUDEL. Frequency-dependent electric power line modeling for steady state harmonic analysis. (Under the direction of DR. VALENTINA CECCHI)

The modern electric power system is experiencing an increased level of harmonic frequency components because of the growing use of power electronic devices, such as converters, and nonlinear loads, such as rectifier-end loads. Electric power line models commonly used in system level studies have been historically developed with the assumption that only the fundamental frequency-component (50 or 60 Hz) propagates in the system. These conventional line models, such as the PI and the exact PI models, are therefore sufficiently accurate to represent the line behavior at the fundamental frequency; they are not however as accurate when the propagation of harmonic frequencies is of interest. Frequency-dependent characteristics of electric power lines and subsequent development of frequency-dependent line models have been historically focused on capturing transient behavior, such as resulting from switching and element energizing events, in which the harmonic content is high. Transient analysis is not sufficient to study the harmonic components since the present grid has significant level of steady state harmonic components. Moreover, the models developed for transient analysis are not applicable in frequency domain simulation environments. Although time domain analysis can be performed to study the steady state voltages and currents in large systems, it is unnecessary and computationally burdensome.

This research work focuses on the investigation and derivation of a frequency-dependent electric power line model for steady state harmonic studies characterized by a single generic model which can be used for both overhead and underground electric power lines of any length. In order to achieve this goal, first an analytical benchmark model is derived using the analytical equations of the distributed line model expressed in hyperbolic functions and incorporating frequency dependent ef-

fects such as the effect of ground return and the skin effect. Two frequency-dependent line modeling approaches are first studied: the multi-segment line model structure and an approximation based line modeling approach. This investigation led to the development of the proposed frequency-dependent electric power line model, which is characterized by a PI structure and represented by a passive circuit realization. The developed frequency-dependent line modeling approaches are evaluated in terms of their effectiveness in system level studies such as harmonic power flow algorithms. Test cases are developed to run harmonic power flow using the different line models. The proposed models are compared with the currently-used models, i.e. the PI and the exact PI models, as well as with the benchmark analytical model. Metrics for comparison are series impedance, shunt admittance and line terminal behavior (harmonic voltage magnitudes and phases). It is observed that the proposed model is easily integrated in the system level analysis tools, such as harmonic power flow, and results in a significantly improved accuracy over the currently-used simple PI or exact PI models.

ACKNOWLEDGEMENTS

First and foremost, I would like to thank my advisor, Dr. Valentina Cecchi, for all her support, encouragement, guidance and patience in this research work. Her valuable advices, suggestions and feedbacks have enabled and motivated me throughout the course of developing this thesis. It has been an honor and privilege to work with her.

I would also like to express my gratitude to Dr. Sukumar Kamalasadan, Dr. Zia Salami and Dr. Brett Q. Tempest for agreeing to be in my thesis committee and offering me their time and meaningful suggestions. I highly appreciate the Graduate Student Support Plan (GASP) award and teaching assistantship, research assistantship and travel grants I received from UNC Charlotte and Dr. Cecchi.

I am thankful to the entire faculty, staffs, fellow students and everyone who helped me directly or indirectly and made my stay at UNC Charlotte enjoyable and fruitful.

I would like to express my heartfelt indebtedness to my parents, siblings and in-laws for their enduring love and support. Finally, my very special admiration to my wife, Neelima, for her patience, understanding, moral support, love and care throughout my doctoral program at UNC Charlotte.

DEDICATION

Gnyani Devi in Nepali language means goddess of wisdom.

To my mother, *Gnyani Devi*.

ज्ञानी देवी

TABLE OF CONTENTS

LIST OF FIGURES

LIST OF TABLES

LIST OF SYMBOLS AND ABBREVIATIONS

δ	Skin depth
δ_i^B	i^{th} harmonic frequency voltage angle at bus B
ϵ	Electrical permitivity
γ	Propagation constant
λ	Average mean error in percentage
μ	Electrical permeability
ω	Electrical frequency in radians
ρ	Electrical resistivity
A	Cross section area
a_n	n^{th} pole in pole residue function
C	Capacitance
c_n	c^{th} residue in pole residue function
D	Distance between any two conductors
d	Constant in pole residue function
f	Electrical frequency in Hz
G	Conductance
H	Magnetic field
h	Linear multiplier in pole residue function
H_{ij}	Distance between conductor i and image j

I	Current
i	Current density
I_r	Line receiving-end current
I_s	Line sending-end current
I_{ed}	Eddy current
L	Inductance
l	Line length
L_{int}	Inductane due to internal flux linkage
R	Resistance
R_{ac}	ac resistance
R_{dc}	dc resistance
S_{ij}	Distance between conductor i and image j
V_r	Line receiving-end voltage
V_s	Line sending-end voltage
Y	Line shunt admittance
y	Per unit length line series admittance
Y_c	Characteristic admittance
Z	Line series impedance
z	Per unit length line series impedance
Z'_a	Line series impedance from analytical model

Z_c	Characteristic impedance
ACSR	Aluminum Conductor Steel Reinforced
AWG	American Wire Gauge
EMT	Electro-magnetic Transient
FDLM	Frequency-Dependent Line Model
GMD	Geometric mean distance
GMR	Geometric mean radius
HPF	Harmonic Power Flow
IEEE	Institute of Electrical and Electronics Engineers
LED	Light Emitting Diode
PCC	Point of Common Coupling
THD	Total harmonic distortion

CHAPTER 1: INTRODUCTION

1.1 Overview

The work presented in this thesis focuses on the development and derivation of frequency-dependent power line models for steady state analysis. Historically, steady state models for electric power lines have been developed assuming that only the fundamental frequency component propagates in the grid; hence power line model parameters are calculated and calibrated at fundamental frequency only. In this work, the line models incorporating the propagation of non-fundamental frequencies are developed to address the frequency-dependent nature of transmission line electrical parameters. Multiple frequency-dependent line modeling approaches are first investigated. Finally, a general steady state frequency-dependent line model is derived and integrated within system level analysis tools such as Harmonic Power Flow (HPF). The proposed model always has a PI structure and yields better harmonic voltages and currents calculations as compared to the commonly used simple PI or the exact PI models.

This chapter presents the following topics:

- Background and motivation for this work;
- Research objectives;
- List of main contributions;
- Organization of the thesis.

1.2 Background and Motivation

Electric power lines are a major integral component of the electric power systems. The North American electric power system is often considered one of the largest and complex man-made structure and engineering system. Power lines deliver bulk

electric power to individual houses to business, services and industries and power delivery is crucial in almost every aspect of the modern society. Historically, the power system loads were considered linear, and it was assumed that only the fundamental sinusoidal power signal is propagating in the grid. Power lines were modeled by lumped parameter configuration or a uniformly distributed configuration considering the assumption of only the fundamental frequency component of either 50 Hz or 60 Hz propagating in the grid. However, such modeling is not sufficient in accurate study of the steady-state harmonics propagating in the modern grid.

1.2.1 Addressing the Harmonic Frequencies

The assumption of linear power system is no longer valid. The use of nonlinear elements are growing in the modern power grid and also the renewable energy sources such as wind and solar power penetration is increasing. Power electronic devices such as converters and controllers are in use to make the grid smarter, safer and more efficient. On the consumer side, the nonlinear loads like fluorescent bulbs, LED lights, and loads with rectifier ends have been increasing. These power electronic devices and nonlinear loads are contributing to the injection of a higher level of harmonics in the grid. The harmonic currents injected into the grid affect the power quality; the distortion levels of voltage and currents are measured as a metric of power quality. The amount of current distortion caused by different types of loads are shown in Table 1.1. (Adapted from [1]). An example of a typical compact LED lamp current waveform [2] is shown in Figure 1.1. The corresponding harmonic spectrum is shown in Figure 1.2.

Table 1.1: Current distortions for different types of loads generating harmonics.

Type of Load	Current Distortion
Fluorescent Lighting	20%
Single Phase Power Supply	80%
6 Pulse Converter, capacitive smoothing, no series inductance	80%
6 Pulse Converter, capacitive smoothing with series inductance>30%	40%
6 Pulse Converter, capacitive smoothing with large inductor	28%
12 Pulse Converter	15%
ac Voltage Regulator	varies with firing angle

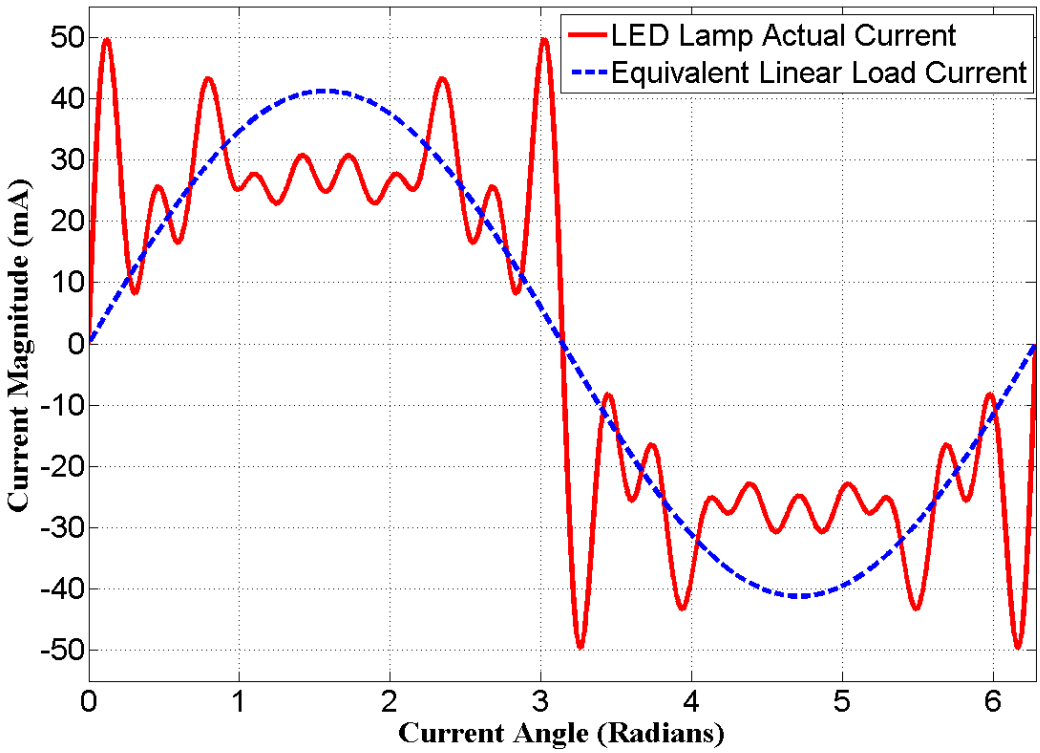

Figure 1.1: Philips 7 watts LED lamp current waveform.

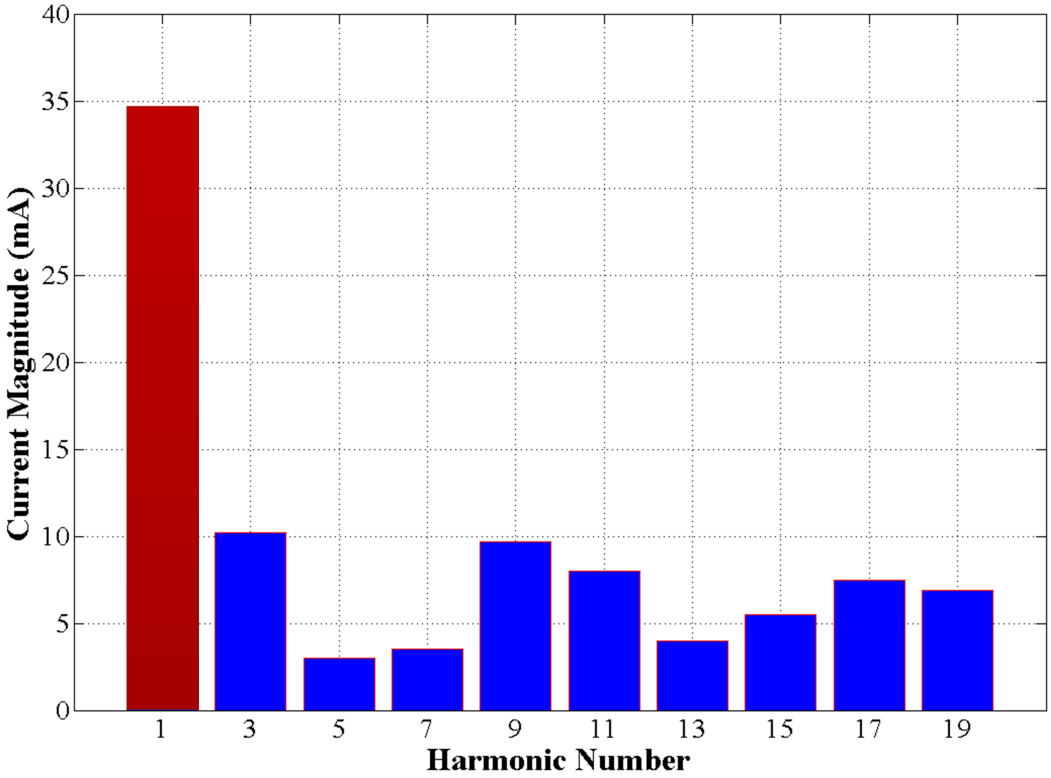

Figure 1.2: Philips 7 watts LED lamp harmonic current spectrum.

The increased level of harmonics causes waveform distortion and is a major power quality concern for the electric power industry [3, 4]. The IEEE recommended limits of distortion levels [4] have been adopted by utilities and power quality requirements have been set accordingly. The recommended voltage distortion limits and the current distortion limits are show in Table 1.2 and 1.3. Filtering out the unnecessary harmonics is an option; however, trying to filter out all possible harmonics is costly [5]. For this reason, some level of harmonics is always present in the grid and the harmonic components are propagating in the power lines. An example of harmonics injected at a point of common coupling (PCC) by a steel mill power served by Southeastern Electric Power Company [6] is shown in Figure 1.3. In light of propagation of the multiple frequencies in the power grid, the conventional power line models derived for studies at only the fundamental frequency are no longer accurate. Thus, re-evaluation of power line models to address the nonlinearity and propagation of harmonics in the system is deemed necessary.

Table 1.2: Voltage distortion limits.

Bus Voltage at PCC	Individual Harmonic (%)	Total Harmonic Distortion (%)
V$\leq$ 1.0 kV	5.0	8.0
1.0 kV $<$ V $\leq$ 69 kV	3.0	5.0
69 kV $<$ V $\leq$ 161 kV	1.5	2.5
V$>$161 kV	1.0	1.5[a]

[a]THD can be up to 2% if the cause is HVDC terminal.

Table 1.3: Current distortion limits (120 V to 69 kV rated).

Maximum Harmonic Current Distortion in Percent of I_L						
Individual Harmonic Order (Odd Harmonics)						
I_{sc}/I_L	$h<11$	$11\leq h<17$	$17\leq h<23$	$23\leq h<35$	$h\geq 35$	TDD
<20	4.0	2.0	1.5	0.6	0.3	5.0
$20<50$	7.0	3.5	2.5	1.0	0.5	8.0
$50<100$	10	4.5	4.0	1.5	0.7	12.0
$100<1000$	12.0	5.5	5.0	2.0	1.0	15.0
>1000	15.0	7.0	6.0	2.5	1.4	20.0

I_{sc} is maximum short-circuit current at PCC and I_L is the fundamental component maximum demand load current at PCC. Even harmonics are limited to 25% of the odd harmonics above.

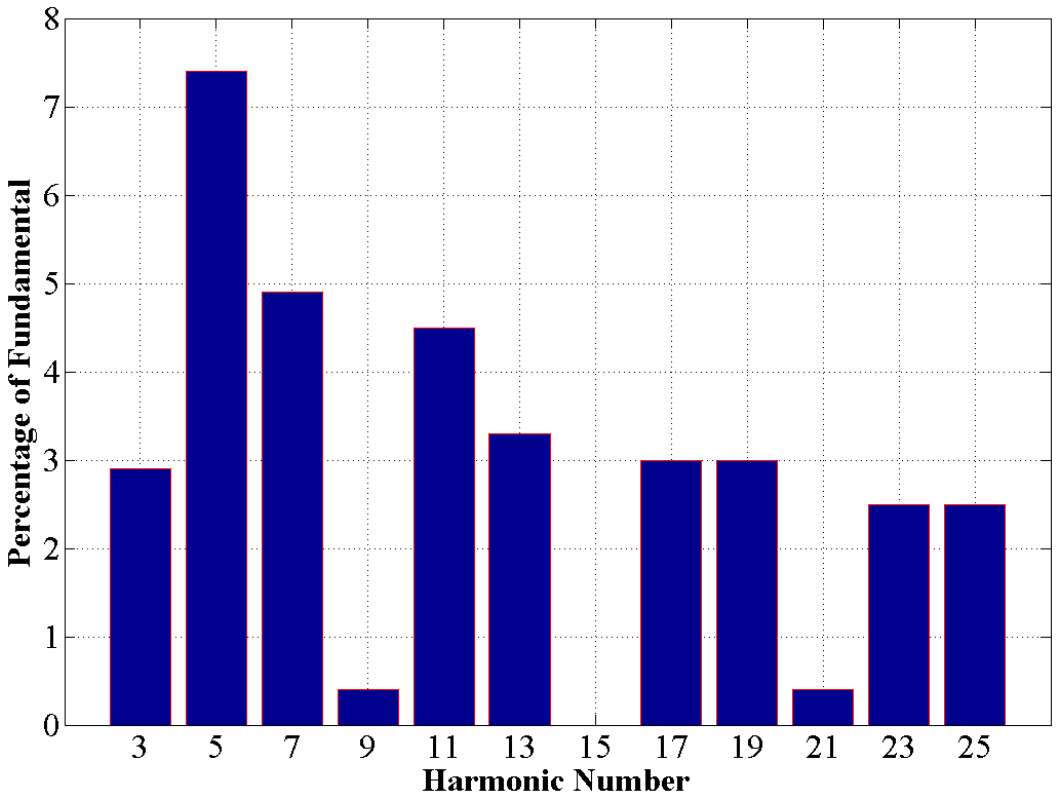

Figure 1.3: Harmonic currents injected at PCC (A site measurement of steel mill power served by Southeastern Electric Power Company).

1.2.2 Steady State Application

Most of the literature on frequency-dependent line models are focused on Electro-Magnetic Transient (EMT) simulations [7] and are used in commercial softwares like PSCAD [8] for precise time domain simulations. The time domain models account for harmonics propagation, however they are focused on transient studies. Hence, the simulations are in time domain and these models cannot be used for steady state analysis in the frequency domain. The focus of this work is to develop frequency-dependent power line models for steady state harmonic analysis. The literature review of frequency-dependent line models for EMT analysis [9–17] and steady state applications [18–24] are presented in Chapter 3.

The modeling approaches proposed in this thesis have the traditional PI structure. This allows the proposed models to be easily integrated in the conventional steady state analytical tools like power flow. The proposed model, along with other commonly used steady state models have been used in HPF to test and compare the effectiveness of the proposed models in study of the propagation of steady state harmonic frequencies. Among multiple HPF tools, the semi-iterative HPF has been used to calculate steady state voltages and currents at different buses or nodes of the test cases.

1.3 Research objectives

In this work, different approaches for frequency-dependent line modeling for steady state analysis are investigated. In summary, the main objectives of the work are,

- Derivation of a frequency-dependent electric power line model for steady state harmonic studies characterized by a single generic model which can be used for all types of electric power lines. For this task, the objectives can be further detailed as,
  - Defining and deriving an analytical benchmark model to evaluate the proposed and other line models.

  - Investigation of different frequency-dependent line modeling approaches such as multi-segment frequency-dependent line modeling.
  - Development of a highly accurate frequency-dependent line model characterized by a PI structure.
  - Presenting a circuit representation of the proposed model using only passive circuit elements.
- Evaluation and testing of the proposed model. For this task, the objectives can be further detailed as,
  - Development of semi-iterative Harmonic Power Flow algorithm to evaluate the effectiveness of the proposed models.
  - Development of test cases to run Harmonic Power Flow.

1.4 Main Contributions of the Thesis

The summary of the contributions are summarized as follows.

- A single generic vector fitting-based frequency dependent line model to be used in frequency domain analysis is proposed. The proposed model results in much higher accuracy than the simple PI, the cascaded PI or the constant exact PI models.
- The proposed frequency-dependent line modeling approach removes the necessity to run time domain simulations while still retaining very accurate frequency-dependent characteristics. This makes the model computationally efficient, and the simulation execution time faster.
- The PI structure of this proposed model allows for simple implementation in existing system-level analysis algorithms such as harmonic power flow.
- The proposed model can be synthesized in an R-L-C network and is therefore implementable in conventional simulation software. The use of passive elements also aids in maintaining model stability.
- The effect of using multi-segment frequency-dependent line models to study

the propagation of the harmonics in the grid in frequency domain is studied. In general, the HPF results obtained using the multi-segment frequency-dependent line models are closer to the results obtained using the frequency-dependent line models in PSCAD than the ones obtained using a single-segment line model.

- An approach for analyzing frequency-dependent impedance of a transmission line by deriving an analytical expression for the real part of this impedance, defined as apparent resistance, as a function of frequency and line length was presented. Results have shown that during the run of the digital simulation, the approximated equation is executed 250 times faster than the analytical equation. This approach can be used to derive expression for imaginary part of the impedance as well as admittances of the lines.
- Simplified polynomial expressions of first and second order are derived for frequency-dependent parameters of the line i.e. series impedance and shunt admittance. These simplified expressions replace the analytical expressions for series impedance and shunt admittance which uses hyperbolic, Bessel and Kelvin functions. Results have shown that during the run of the digital simulation, the approximated equation is executed 250 times faster than the analytical equation.
- An analytical distributed model including the frequency-dependent effects such as the skin effect and the effect of ground return is derived. This model is derived to use as a benchmark model for comparison.
- The derived analytical model can be used for higher accuracy. However, for each frequency of interest, a separate analytical model has to be used. The proposed model avoids this problem by providing a single generic model for all harmonic frequencies of interest without much affecting the accuracy of analytical model.
- A semi-iterative HPF algorithm is derived which is used as a test tool to evaluate the proposed line models.

1.5 Thesis Organization

This thesis is organized as follows:

- Chapter 2: In this chapter, frequency-dependent characteristics of transmission line parameters such as the skin effect and the effect of ground return are discussed. Frequency-dependent line modeling for steady state analysis are reviewed. A brief review of time domain transmission line models is also presented to create a background in order to highlight the differences between the proposed steady state models and the time domain models in chapter 5.
- Chapter 3: In this chapter, the benchmark model is derived. The limitations of the currently used lumped parameter models as well as distributed line model are presented. Literature review of the frequency dependent line modeling techniques on both time and frequency domain are presented. Approaches for frequency-dependent line modeling techniques used in this work are discussed. The line model evaluation tools and softwares are also presented.
- Chapter 4: In this chapter, the initial investigation of the different approaches for frequency-dependent line modeling techniques are presented. Specifically, multi-segment frequency-dependent transmission line models, an approach for modeling frequency-dependent apparent resistance of transmission line and simplified polynomial approximated model for frequency dependent distribution line are presented.
- Chapter 5: In this chapter, the proposed novel frequency-dependent electric power line model for steady state harmonic analysis is presented. The passive circuit realization of the model is also derived.
- Chapter 6: In this chapter, the simulation results on multiple test cases are presented. The proposed line model is compared with other commonly used line models in terms of calculated line impedances, bus voltages, harmonic distortions at different buses and harmonic losses. An example of the passive network

is also obtained.

- Chapter 7: In this chapter, the list of contributions are mentioned. Then the differences between the proposed model and the EMT model are highlighted. Finally, the possible areas and considerations for future works are presented.

CHAPTER 2: REVIEW OF ELECTRIC POWER LINE MODELING

2.1 Overview

Electric power transmission lines are an important component in the bulk transfer of electrical energy. Transmission lines interconnect the generators with the substations. Distribution lines then enable the transmission of electricity to the consumers. This chapter presents a review of electric power line modeling. Specifically, the following topics are discussed:

- Transmission line electrical parameters;
- Frequency dependence of line parameters, with special attention to the effect of ground return and the skin effect; and
- Line models for steady state analysis.

2.2 Transmission Line Electrical Parameters

All electric power lines exhibit the four electrical properties i.e. resistance, inductance, capacitance and the conductance. From a circuit point of view, the resistance and inductance constitute the series impedance; capacitance and conductance constitute the shunt admittance. The series impedance and shunt admittance are the major elements in consideration for transmission line modeling. The line series impedance and shunt admittances are given by,

$$Z = (R + j\omega L)\,\Omega \text{ and,} \tag{2.1}$$

$$Y = (G + j\omega C)\ \text{S}, \tag{2.2}$$

where R and L are series resistance and inductance of the line and G and C are the shunt conductance and capacitance of the line and ω is the frequency of the voltage or current signal propagating in the line. Most often, these parameters are expressed

in terms of per unit length of the line, and are the result of the conductor properties and the electromagnetic fields associated with it. The electrical parameters are now briefly reviewed in the following subsections.

2.2.1 Series Resistance

The series resistance of the conductor is an important electrical property, affecting the majority of the real power losses in the power system. The dc resistance of a solid round conductor at temperature T Kelvin is given by,

$$R_{dc} = \frac{\rho l}{A}\,\Omega, \tag{2.3}$$

where, ρ is the resistivity of the conductor in Ωm at temperature T Kelvin, l is its length in meter and A is its cross sectional area in square meters. Most of the power line transmission carry alternating current, and causes the ac resistance to be higher than the dc resistance. This is due to the skin effect, which is described later in sub-section 2.3.1. The effective ac resistance of a conductor can be expressed is in terms of power loss and the current flowing through the conductor as follows,

$$R_{ac} = \frac{power\ loss\ in\ conductor}{|I|^2}\,\Omega, \tag{2.4}$$

where I is the rms current in the conductor in amperes. Copper and aluminium are the most commonly used metals in power conductors because of their high conductivity and availability among metals [25].

2.2.2 Series Inductance

The inductance is calculated as the flux linkage per ampere flowing in the conductor. It therefore represents the voltage induced by the flux linkage. The inductance depends on line geometry, i.e. cable size and spacing between the cables in a multi-conductor case. For a single conductor, the inductance due to internal flux linkage is given as [26],

$$L_{int} = \frac{\mu}{8\pi}\,\mathrm{H/m}, \tag{2.5}$$

where μ is the permeability of the conductor in Hm^{-1}.

For a two conductor case, the flux emanating from one conductor links with the other and affects the inductance of the conductor. If two conductors with radius r_1 and r_2 are separated by a distance D, as shown in Figure 2.1, the inductance due to external flux linkage is added to the internal inductance.

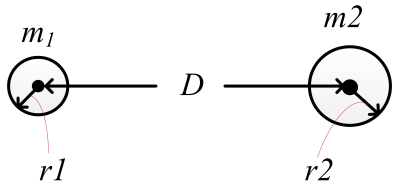

Figure 2.1: Conductors of different radii separated by distance D.

The resulting inductance for conductor 1 is then given as,

$$L_1 = \left(\frac{1}{2} + 2\ln\frac{D}{r_1}\right) \times \frac{\mu}{4\pi}\,\mathrm{H/m}. \tag{2.6}$$

Stranded conductors come under the general classification of composite conductors, which means conductors composed of two or more elements of strands electrically in parallel. Lets consider the composite conductors, with all elements identical and carrying equal currents, as shown in Figure 2.2.

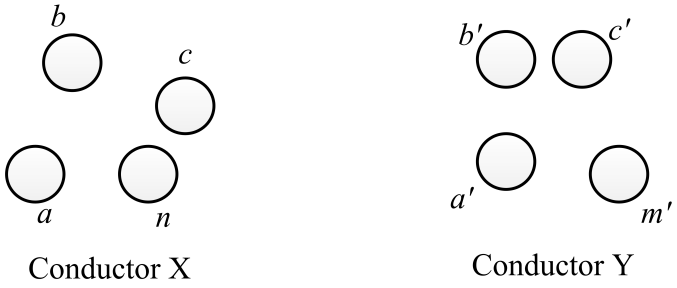

Figure 2.2: Single phase line with two composite conductors.

The resulting inductance for conductor bundle X is given as,

$$L_X = 2 \times 10^{-7}\left(\ln\frac{GMD}{GMR}\right)\,\mathrm{H/m}, \tag{2.7}$$

where GMD is geometric mean distance between the two composite conductors and

GMR is the geometric mean radius of the conductor bundle X. Using these concepts, inductance for various conductors with various geometry can be calculated [26].

2.2.3 Shunt Admittance

Shunt admittance has two components, i.e. shunt conductance and shunt capacitance. The shunt admittance exists between the conductor or between conductor and the ground. The conductance, accounts for the leakage current at the insulators of overhead lines and through the insulation of the cables. The shunt conductance is usually very low and its contribution to shunt admittance is negligible. Hence, for general purpose, the capacitance is considered. Due to the potential difference between the conductors, the power line exhibit capacitive property. If two conductors with radius r_1 and r_2 are separated by a distance D, as shown in Figure 2.1, the capacitance between the conductors is given as [27],

$$C_{12} = \frac{2\pi\varepsilon}{\ln(D^2/r_1 r_2)}\ \mathrm{F/m}, \tag{2.8}$$

where ε is the permitivity of the surrounding material around the conductor. The capacitance to ground is half the capacitance between the conductors. The representation is show in Figure 2.3.

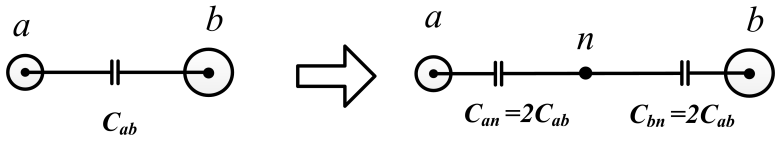

Figure 2.3: Representation of line to line and line to neutral capacitance.

For a bundled conductors as shown in Figure 2.2, the capacitance can be expressed as,

$$C = \frac{2\pi\varepsilon}{\ln(D_{eq}/d)}\ \mathrm{F/m}, \tag{2.9}$$

where D_{eq} is the geometric mean distance between the conductors, and d is geometric mean radius of the conductor.

The capacitance of a transmission line is affected by earth, as its presence alters the electric field of the line [27]. If the earth is assumed to be a perfect conductor as an infinite horizontal plane, the electric field of charged conductors above earth is not the same as it would be if the equipotential surface of the earth were not present. Lets consider a three phase line with return path through the earth. Potential difference exists between the conductors and the earth. The earth has a charge equal in magnitude to that of conductor but opposite in charge. The electric flux from the charges on the conductor to the charges on the earth is perpendicular to the earth's equipotential surface. Lets imagine a fictitious conductor of the same size and shape as the overhead conductor lying directly below the original conductor above the plane of the ground. The fictitious conductor is below the surface of the earth by a distance equal to the distance of the overhead conductor above the earth as shown in Figure 2.4. If the earth is removed and charge equal and opposite to that on the overhead conductor is assumed on the fictitious conductor, the plane midway between the original conductor and the fictitious conductor is an equipotential surface and occupies the same position as the equipotential surface of the earth. The electric flux between the overhead conductor and this equipotential surface is the same as that which existed between the conductor and the earth. Thus, for purpose of calculation of capacitance, the earth may be replaced by a fictitious charged conductor below the surface of the earth by a distance equal to that of the overhead conductor above the earth. Such a conductor has a charge equal in magnitude and opposite in sign to that of the original conductor and is called method of image conductor. Including the earth effect, using the method of image conductor, the capacitance is given as,

$$C_n = \frac{2\pi\varepsilon}{\ln\left(\frac{D_{eq}}{d}\right) - \ln\left(\frac{\sqrt[3]{H_{12}H_{23}H_{31}}}{\sqrt[3]{H_1H_2H_3}}\right)} \text{ F/m to neutral,} \tag{2.10}$$

where H_i is the distance between the conductor i and its image, H_{ij} is the distance

between the conductor i and image j. Using these concepts, the capacitance for various conductors with various geometry can be calculated [27].

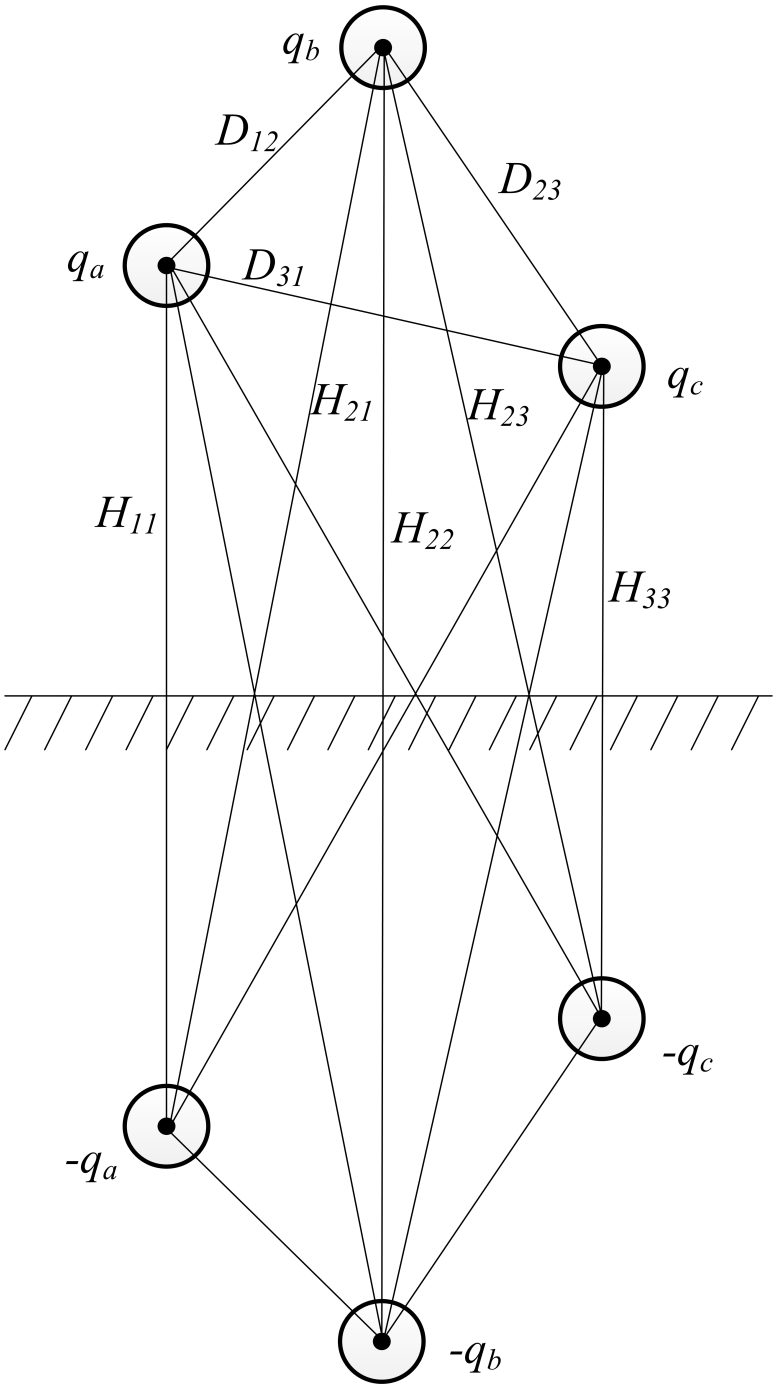

Figure 2.4: Three phase line and its image.

2.3 Frequency Dependence of Line Parameters

The line parameters are dependent on multiple factors like line length, conductor geometry, temperature, frequency etc. Since this work is devoted to the study of frequency-dependence of line models, the frequency-dependence of the line parameters are discussed. The line series impedance and the shunt admittances change with the change in frequency. Equation (2.1) and (2.2) can be rewritten as,

$$Z = (R_{ac} + j\omega L)\,\Omega \text{ and,} \tag{2.11}$$

$$Y = (G + j\omega C)\text{ S.} \tag{2.12}$$

The series reactance, $j\omega L$, as seen from the Equation (2.11), is directly proportional to the frequency ω. Similarly, the shunt capacitance is also directly proportional to the frequency as seen from Equation (2.12). Apart from this, the series resistance and series reactance are dependent on other frequency-dependent factors such as the skin effect and the effect of ground return. The shunt admittance, is however not affected by the skin effect. The inclusion of frequency-dependent factors in calculating shunt and series parameters are discussed later in detail in Chapter 3. Factors contributing to the frequency-dependence of the line parameters are discussed in following sections.

2.3.1 Skin Effect

The phenomenon by which alternating current tends to flow on the outer edge of the conductor is called skin effect. Skin effect causes the current density to be largest at the outer surface, or skin, of the conductor, and the current density decreases with greater depths in the conductor. Figure 2.5 shows a cross section of a conductor carrying an ac current. In the Figure, the darker the shade, the higher the current density. It is found that due to skin effect, resistance increases with increase in frequency [28]. The skin effect is caused by the opposing eddy currents induced by the changing magnetic field created by ac current, and it can be explained with the help of Figure 2.6.

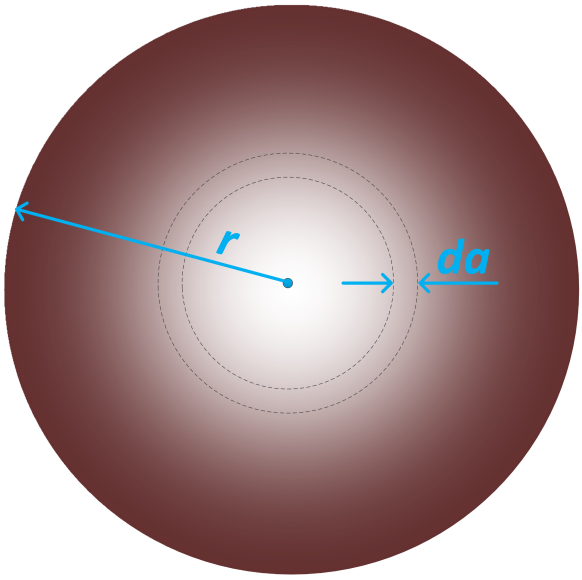

Figure 2.5: Cross section of a wire-skin effect graphical representation.

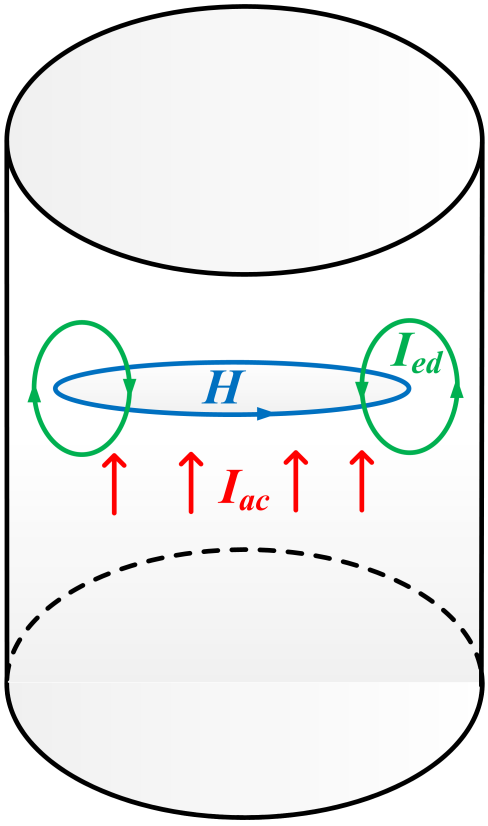

Figure 2.6: Rotating eddy currents causing skin effect.

If we assume that the ac current I_{ac} is flowing from top to bottom of a cylindrical conductor as shown in Figure 2.6, then the changing electric field of ac current will create a changing magnetic field H. The magnetic field H then create the eddy currents I_{ed}. The circulating eddy currents oppose the main ac current flowing in the conductor around the core, but has same direction on the outer edge. For this reason, the electrons in the core are pushed towards the edge. At large enough frequencies, there is almost no current flowing from the center and most current is flowing at outer surface and within certain depth from the surface. The current density decreases from exponentially from the surface to the core and is given by,

$$i = i_s e^{-\frac{d}{\delta}} \tag{2.13}$$

where i is the current density at distance d from the surface, i_s is the current density at the surface and δ is the skin depth. Skin depth can be defined as the depth below the surface of the conductor where the current density has fallen to 37% of the current density at the surface. It can be calculated as [29],

$$\delta = \sqrt{\frac{\rho}{\pi f \mu}}. \tag{2.14}$$

The differential equation for alternating current as a function of distributed current density in a round wire can be expressed by,

$$I = \int_{a=0}^{r} i(2\pi a)\, da\,, \tag{2.15}$$

where I is the current in amperes, i is the current density in amperes per square cm, a is the distance from the center of the wire and r is the radius of the wire in cm. The current density can be solved and expressed in terms of Bessel functions [30, 31] of zeroth order. The Bessel function in turn can be expressed in terms of kelvin functions. The current density can then be expressed as,

$$i = i_\circ\{\mathrm{ber}(ma) + \mathrm{bei}(ma)\}, \tag{2.16}$$

where $i_\circ$ is the current density at the center,

m is the property of the material given in c.g.s units by,

$$m = \sqrt{\frac{4\pi\omega}{10^9\rho}} \tag{2.17}$$

the ber and bei are kelvin functions of zeroth order given by the series sum,

$$\mathrm{ber}(x) = 1 + \sum_{k=1}^{N} \frac{(-1)^k}{[(2k)!]^2} \left(\frac{x}{2}\right)^{4k} \tag{2.18}$$

$$\mathrm{bei}(x) = \sum_{k=1}^{N} \frac{(-1)^k}{[(2k+1)!]^2} \left(\frac{x}{2}\right)^{4k+2} \tag{2.19}$$

The current density can then be expressed in terms of current as,

$$i = \frac{Im}{2\pi r} \left(\frac{\mathrm{ber}(ma) + j\mathrm{bei}(ma)}{\mathrm{bei}'(mr) - j\mathrm{ber}'(mr)} \right). \tag{2.20}$$

Since there is no drop due to internal flux at the surface where $a = r$, the impedance of the wire due to resistance and internal flux is,

$$Z_{eff} = \frac{\rho m}{2\pi r} \left(\frac{\mathrm{ber}(mr) + j\mathrm{bei}(mr)}{\mathrm{bei}'(mr) - j\mathrm{ber}'(mr)} \right). \tag{2.21}$$

The real part of the Z_{eff} is the resistance. As dc resistance is,

$$R_{dc} = \frac{\rho}{\pi r^2}, \tag{2.22}$$

the skin effect ratio is given by,

$$\frac{R_{ac}}{R_{dc}} = \mathrm{Re}\left[\frac{mr}{2} \left(\frac{\mathrm{ber}(mr) + j\mathrm{bei}(mr)}{\mathrm{bei}'(mr) - j\mathrm{ber}'(mr)} \right) \right]. \tag{2.23}$$

An example of the No. 30 AWG copper wire skin effect ratios for different frequencies [28] are shown in Table 2.1. The data are experimentally measured values for different settings. Setting A is 48 parallel strands of No. 30 copper, setting B is 48 spiralled strands for No. 30 copper and setting C is solid round copper equivalent conductor. The temperature was maintained between 21° to 23° Celsius. For

overhead ACSR cables mostly used for power transmission, the skin effect ratio for fundamental frequency of 60 Hz of some select cables [32] are shown in Table 2.2. The skin effect ratio is calculated for 20° Celsius.

Table 2.1: Skin effect ratio for 3 different settings of No. 30 AWG copper wire.

frequency	$\boldsymbol{R_{ac}/R_{dc}}$ for 3 Cable Settings		
kHz	Setting A	Setting B	Setting C
5	1.004	1.006	1.008
10	1.028	1.040	1.062
20	1.10	1.14	1.21
30	1.21	1.29	1.41
40	1.31	1.43	1.59
50	1.41	1.56	1.76
60	1.50	1.68	1.91
70	1.60	1.79	2.05
80	1.69	1.91	2.07
90	1.77	2.01	2.28
100	1.86	2.11	2.38

Table 2.2: Skin effect ratio for some select cables at 60 Hz.

Code word	Aluminum area, cmil	Stranding Al/St	diameter inch	R_{ac}/R_{dc}
Waxwing	266,800	18/1	0.609	1.0226
Ostrich	300,000	26/7	0.642	1.0219
Merlin	336,400	18/1	0.684	1.0235
Chickadee	397,500	18/1	0.743	1.0244
Pelican	477,000	18/1	0.814	1.0267
Dove	556,500	26/7	0.927	1.0259
Rook	636,000	24/7	0.977	1.0286
Drake	795,000	26/7	1.108	1.0324
Rail	954,000	45/7	1.165	1.0432
Ortolan	1,033,500	45/7	1.213	1.0479
Finch	1,113,000	54/19	1.293	1.0459
Lapwing	1,590,000	45/7	1.502	1.0824
Falcon	1,590,000	54/19	1.545	1.0732
Bluebird	2,156,000	84/19	1.762	1.1269

2.3.2 Effect of Ground Return

To study the frequency dependence of transmission line parameters, Carson's equations [33] are widely used. Carson's equations take into account the effect of ground return by utilizing the method of image conductors as discussed in previous subsection. Figure 2.7 shows two conductors and their images.

Referring to Figure 2.7, the self impedance in ohms per mile of the line is given as,

$$Z_{ii} = r_i + 4\omega P_{ii} G + j(X_i + 2\omega G \cdot \ln \frac{S_{ii}}{RD_i} + 4\omega Q_{ii} G). \tag{2.24}$$

The mutual impedance in ohms per mile of the line is given as,

$$Z_{ij} = 4\omega P_{ii} G + j(2\omega G \cdot \ln \frac{S_{ii}}{D_{ij}} + 4\omega Q_{ii} G), \tag{2.25}$$

where he variables X_i, P_{ij} and Q_{ij} are given as,

$$X_i = 2\omega G \cdot \ln \frac{RD_i}{GMR_i} \quad \Omega/\text{mile} \tag{2.26}$$

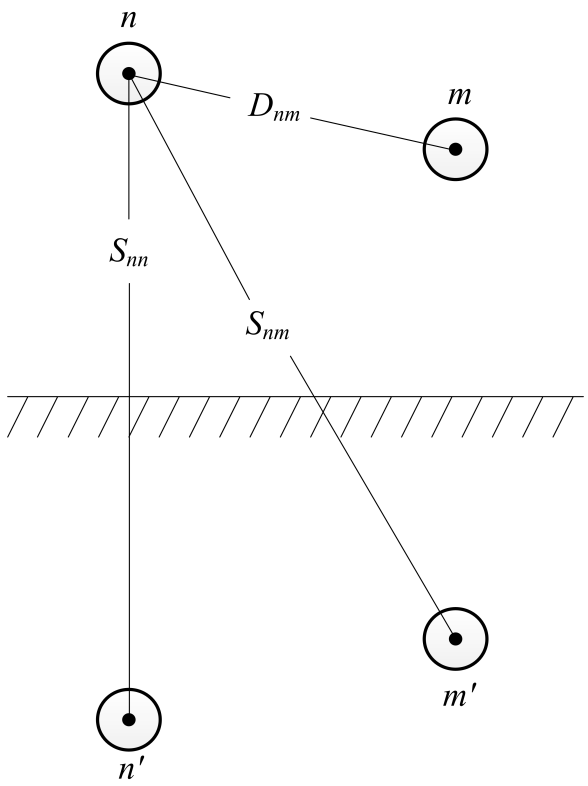

Figure 2.7: Conductors and their images.

$$P_{ij} = \frac{\pi}{8} - \frac{1}{3\sqrt{2}} k_{ij} \cos(\theta_{ij}) + \frac{k_{ij}^2}{16} \cos(2\theta_{ij}) \cdot \left(0.6728 + \ln\frac{2}{k_{ij}}\right) \tag{2.27}$$

$$Q_{ij} = -0.0386 + \frac{1}{2} \cdot \ln\frac{2}{k_{ij}} + \frac{1}{3\sqrt{2}} k_{ij} \cos(\theta_{ij}) \tag{2.28}$$

and the variable k_{ij} is given by,

$$k_{ij} = 8.565 \times 10^{-4} \cdot S_{ij} \cdot \sqrt{\frac{f}{\rho}} \tag{2.29}$$

The variables mentioned in these equations are;

r_i=resistance of conductor i in Ω/mile

$\omega = 2\pi f$ = system angular frequency in raidans per second

$G = 0.1609347 \times 10^{-3}$ Ω/mile

RD_i = radius of conductor i in feet

GMR_i = Geometric mean radius of conductor i in feet

f = system frequency in Hertz

ρ = resistivity of earth in Ω-meters

D_{ij} = distance between conductors i and j in feet

S_{ij} = distance between conductors i and image j in feet

θ_{ij} = angle between a pair of lines drawn from conductor i to its own image and to the image of conductor j

2.3.3 Other Frequency-Dependent Effects

Similar to the skin effect, in case of multiple conductors in parallel, the magnetic field of one conductor will affect the current density distribution in adjacent conductor. This effect is known as proximity effect [34]. This changes the effective resistance of the conductor. The proximity effect is pronounced if the ratio of distance between the cables to the diameter of the cable is small [35]. In case of power lines, the ratio is very high and this effect is negligible [35–38]. Sometimes, the communication cables may run along with power lines and cause electromagnetic interferences for higher frequencies. This effect is also negligible for steady state harmonics in power systems [35]. The conductor strands bundled together will have appreciable proximity effect, however when bundled together in circular fashion like bundled ACSR cables, the proximity effect is negligible [39]. Old conductors have rough surface and corona discharge can occur for higher frequencies, and increases the effective resistance of the cable and create more leakage [40]. For this research, the cable surface is assumed to be smooth and corona discharge from uneven surface is ignored.

2.4 Electric Power Line Models for Steady State Analysis

Modeling the electric power lines is one of the earlier and critical step in the analysis of power system. Electric power lines can be represented in multiple ways, and the most common ones are explained briefly in following sections.

Transmission lines are usually represented by lumped parameter models or the distributed parameter model. The transmission lines are commonly classified in terms

of length, and for short and medium length lines, the lumped parameter model offer a good accuracy. The lumped parameters of resistance, inductance, conductance and capacitance are idealized elements connected with perfectly conducting wires. The long lines, however, are represented more accurately by distributed parameter model. The short, medium and long lines are explained briefly in following subsections.

2.4.1 Short Line Model

A line with length of less than 50 miles (80 km) is considered short line. Shunt admittance is so small that it can be ignored for short line and only the series impedance can represent the line [41]. The line series impedance is simply the per unit impedance multiplied by the length of the line.

$$Z = (r + j\omega L)l = R + jX, \tag{2.30}$$

where, r and L are the per unit length resistance and inductance of the line, R and X are the total resistance and reactance of the line. The line model is shown in Figure 2.8.

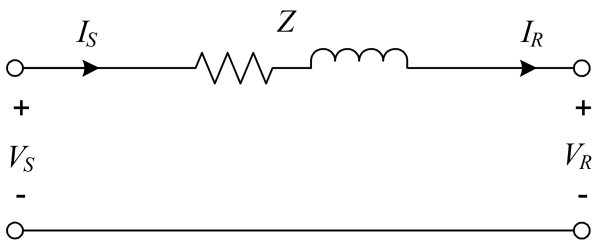

Figure 2.8: Short line model.

The relationship between sending end voltage and current are related as follows,

$$V_S = V_R + ZI_R, \tag{2.31}$$

$$I_S = I_R, \tag{2.32}$$

where V_S and I_S are the sending-end voltage and current and V_R and I_R are receiving-end voltage and current.

2.4.2 Medium Line Model

A line with length above 50 miles (80 km) and below 150 miles (250 km) is considered a medium length line. For medium length lines, the shunt capacitance is appreciable and is considered by placing a lumped capacitance at each end of the line. This model is known as the PI model. The PI model type is shown in Figure 2.9 and is one of the more commonly used lumped parameter models for steady state analysis.

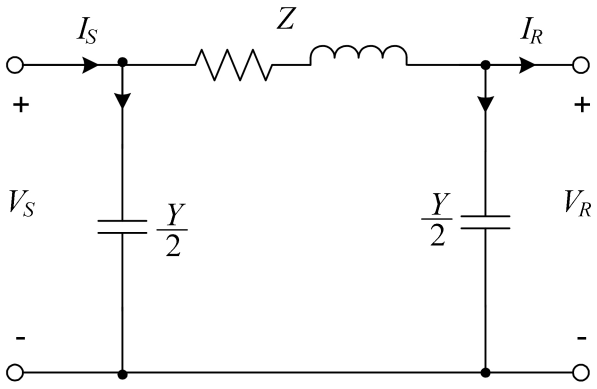

Figure 2.9: PI model.

For a PI model, the sending-end and receiving-end voltages and currents are related as follows:

$$V_S = AV_R + BI_R, \tag{2.33}$$

$$I_S = CV_R + DI_R, \tag{2.34}$$

where V_S and I_S are the sending-end voltage and current and V_R and I_R are receiving-end voltage and current. The A, B, C and D are given by,

$$A = 1 + \frac{ZY}{2}, \tag{2.35}$$

$$B = Z, \tag{2.36}$$

$$C = Y\left(1 + \frac{ZY}{4}\right), \tag{2.37}$$

$$D = 1 + \frac{ZY}{2}, \tag{2.38}$$

where Y is the shunt admittance and Z is the series impedance of the line as expressed in (2.12) and (2.11). The accuracy with which the lumped parameter represents the distributed parameter model decreases with increasing frequency [42].

2.4.3 Distributed Parameter Models

As discussed previously, unlike in the lumped parameter model, in reality, these shunt and series parameters are distributed in nature as shown in Figure 2.10. Differential equations are used to derive the line model and distributed line model is the best representation of the line.

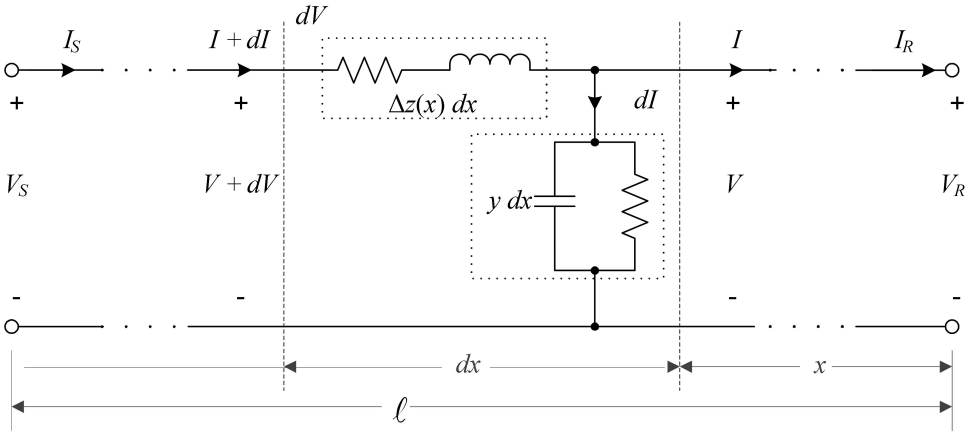

Figure 2.10: Distributed line model-a differential section of length dx.

The relationship between sending-end voltage and current to receiving-end voltage and current is given by [27, 43] as,

$$V_S = \cosh(\gamma l) V_R + Z_c \sinh(\gamma l) I_R. \tag{2.39}$$

$$I_S = \frac{1}{Z_c} \sinh(\gamma l) V_R + \cosh(\gamma l) I_R. \tag{2.40}$$

The parameter γ is known as propagation constant and Z_c is known as characteristic

impedance. These parameters are given by,

$$\gamma = \sqrt{yz} = \sqrt{(r + j\omega L)(g + j\omega C)}, \tag{2.41}$$

$$Z_c = \sqrt{\frac{z}{y}} = \sqrt{\frac{(r + j\omega L)}{(g + j\omega C)}}, \tag{2.42}$$

where, y is the per unit length shunt admittance, z is the per unit series impedance, r is the per unit series resistance, L is the per unit series inductance, g is the per unit shunt conductance, and C is the per unit shunt capacitance.

2.4.4 Exact PI Model

An exact PI model is the PI-equivalent of the distributed line model. The PI-equivalent is derived because the PI structure can be readily and easily used in some of the steady state analysis algorithms like power flow tools. Comparing (2.33) and (2.34) with (2.39) and (2.40), the new A', B', C' and D' parameters are obtained as,

$$A' = \cosh(\gamma l). \tag{2.43}$$

$$B' = Z_c \sinh(\gamma l). \tag{2.44}$$

$$C' = \frac{1}{Z_c} \sinh(\gamma l). \tag{2.45}$$

$$D' = \cosh(\gamma l). \tag{2.46}$$

Comparing (2.35)-(2.38) with (2.43)-(2.46), the new series impedance and shunt admittance are obtained as,

$$Z' = Z_c \sinh(\gamma l). \tag{2.47}$$

$$Y' = \frac{2}{Z_c} \tanh(\frac{\gamma l}{2}). \tag{2.48}$$

These new Z' and Y' are series and shunt parameters of the exact PI model.

2.5 Time Domain Line Models

The main objective of this work includes the development of accurate frequency-dependent electrical power line models for steady state harmonic analysis. Accurate frequency-dependent power line models are already available, however they are in time domain. Hence, the proposed phasor domain frequency-dependent line model and the currently available time domain frequency-dependent line models have noticeable differences. To clarify the differences between the proposed phasor domain frequency-dependent line model and the currently available time domain frequency-dependent line models, a brief discussion of the time domain line models is presented.

2.5.1 Bergeron Line Model

When voltage and current signals travel along the line, the voltage and current can be expressed as a one-dimensional wave equation [44]. The solution [45] of this wave equation is commonly termed as traveling wave model [7]. To study the minute details of the transmission line models behavior in time domain environment, a discrete-time representation of the traveling wave model was proposed by Bergeron [46]. This model is effective to use in time domain computer simulations incorporating the frequency-dependence of the line parameters. Based on this model, at a distance x from the sending end of the line, the voltage and current expressions in a lossless line are given by,

$$I(x,t) = i^{+}(x - vt) + i^{-}(x + vt) \tag{2.49}$$

$$V(x,t) = Z_c[i^{+}(x - vt) + i^{-}(x + vt)] \tag{2.50}$$

where + and − represent the forward and backward travelling waves. If it takes time τ for a wave to travel from node k to node m, the Bergeron line model can be represented as shown in Figure 2.11.

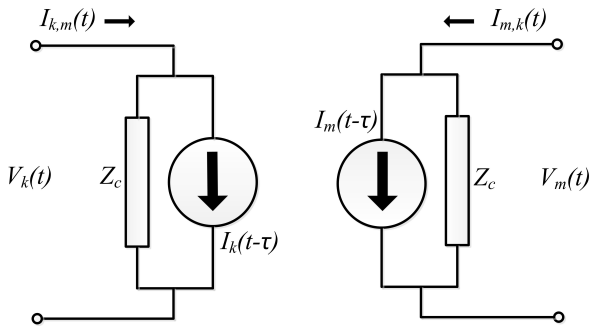

Figure 2.11: Bergeron line mode connecting node k and m.

In this model, the two node voltages are expressed in terms of node currents. The voltage wave at node k takes time τ to reach node m. The line is assumed to be lossless in this calculations. After the computation of voltages and currents is done in lossless line, the losses are adjusted later [46].

2.5.2 Lossy Time Domain Line Model

The solution of the Bergeron line model first considers the line to be lossless and losses are accounted later. A lot of work has been done to include the lossy nature of the line and many transmission line models have been proposed utilizing the concept of modal transformation to decouple the phases. One of the most robust and widely used model was proposed by J. Marti [11]. The weighing function A is defined, which along with the characteristic impedance Z_c are approximated using rational approximations and realized in circuit by using Foster Realizations [47, 48]. This approximation has the same structure as shown in Figure 2.11.

The rational approximation technique of a complex number is accurate in cases where the magnitude is changing and the phase has minimal change. Improving on the approximation, Gustavsen proposed a Vector Fitting technique [49]. Using this Vector Fitting technique, a frequency-dependent transmission line model was proposed [15]. The propagation H and characteristic admittance Y_c are approximated using Vector Fitting technique. These models are currently being used by time domain simulation softwares [8, 50].

In the next chapter, motivation for the development of phasor domain frequency-dependent line model is presented. Research objectives, goals and methods of frequency-dependent line modeling approaches are also discussed briefly.

CHAPTER 3: PROBLEM STATEMENT AND PROPOSED APPROACHES

3.1 Overview

The work presented in this thesis focuses on the development of frequency-dependent electric power line models for steady state harmonic analysis. Most of the literature on frequency-dependent line models are focused on Electro-Magnetic Transient (EMT) simulations [7] and are used in commercial softwares like PSCAD [8] for precise time domain simulations. The time domain models account for harmonics propagation, however they are focused on transient studies. Hence, the simulations are in time domain and these models cannot be used efficiently for steady state analysis in the frequency domain. The focus of this work is to develop frequency-dependent power line models for steady state harmonic analysis. In this work, multiple steady state modeling approaches have been investigated. One of the objective of this work is also to present the proposed model in PI structure to make it readily implementable in the steady state analysis algorithms such as HPF. Speed and accuracy of the proposed model are also investigated to gauge its effectiveness in system level studies.

In this chapter, first the research goals and assumptions are presented. Then a synthesized review of the literature on frequency-dependent line models is presented. Then the analytical benchmark model is presented, which is derived using the analytical equations of distributed line models expressed in hyperbolic functions and also incorporating all frequency dependent effects such as the effect of ground return and the skin effect. Then the errors and limitations of the currently used frequency-dependent steady state models are highlighted. An overview of the proposed approaches to model frequency-dependent power lines are presented. The software tools used in this research are mentioned. Finally, HPF algorithms, which are used to test and evaluate

the proposed line models are discussed.

3.2 Research Goals

In this work, different approaches for frequency-dependent line modeling for steady state analysis are investigated. In summary, the main research goals of this work are,

- Derivation of a frequency-dependent electric power line model for steady state harmonic studies characterized by a single generic model which can be used for all types of electric power lines. For this task, the objectives can be further detailed as,
  - Defining and deriving an analytical benchmark model to evaluate the proposed and other line models. The analytical benchmark model is explained in detail in following subsection of this chapter.
  - Investigation of different approaches of frequency-dependent line modeling approaches such as multi-segment frequency-dependent line modeling. These multiple approaches of frequency-dependent line modeling approaches are briefly stated in following subsections of this chapter, and then discussed in detail in chapter 4.
  - Development of a highly accurate frequency-dependent line model characterized by a PI structure. The details of this line modeling approach is presented in chapter 5.
  - Presenting a circuit representation of the proposed model using only passive circuit elements. The details of this circuit representation technique is discussed in chapter 5.
- Evaluation and testing of the proposed model. For this task, the objectives can be further detailed as,
  - Development of semi-iterative HPF algorithm to evaluate the effectiveness of the proposed models. A brief discussion of iterative as well as semi-iterative HPF algorithm is presented in following subsections of this

chapter.

- Development of test cases to run HPF. The IEEE 13 node test feeder topology is considered, and this test case is developed to in such a way that HPF using different line models can be executed. The test case and the simulation results are presented in chapter 6.

3.3 Assumptions and Considerations

Few assumptions and considerations are made in this research work to meet the expected goals and objectives. Some of the major assumptions are listed below. Other contextual assumptions are mentioned in the text whenever relevant and necessary.

- To compare the simulation results obtained using the proposed model and claim the accuracy obtained, an analytical model is derived and considered the benchmark model. The real time field data is not practically feasible as multiple arbitrary current injections of various magnitudes have been injected to see how system behaves under different conditions.
- Frequency-dependent effects such as the effect of ground return and the skin effect are considered into account. Proximity effect, effect of rough conductor surface and any other electromagnetic interferences are ignored.
- Semi-iterative HPF is used an analysis tool. Fundamental component load flow is iterative and the harmonic load flow is non-iterative.
- Three different types of conductors are considered i.e. overhead ACSR, underground concentric neutral and underground tape shielded conductors.
- For the vector fitted modeling approach, only up to the 25^{th} harmonics is considered.
- For HPF, the linear loads are considered to be static impedance loads and it is assuemd that the current characteristics of the nonlinear load are already known.

3.4 Literature Review: Frequency-Dependent Line Models

After the development of commercial digital simulators in 1950s and 1960s [51], various accurate simulation models of transmission lines were proposed [52]. Significant efforts have been invested in developing frequency-dependent transmission line models for electromagnetic transient (EMT) studies [9–17]. EMT simulation software like EMTP-ATP [7] and PSCAD [8] use these models for precise time domain simulations. These models account for harmonics propagation, however they are focused on transient studies. Hence, the simulations are in the time domain and the models cannot be used efficiently for studies in the frequency domain. Doing time domain harmonic power flow simulations for large systems is computationally burdensome, slower in time and in many cases unnecessary for steady state analysis. The frequency-dependent line model proposed in this thesis yields higher accuracy than commonly used models, resulting in comparable accuracy to EMT models without the need to run expensive time-domain simulations.

A frequency-domain line modeling approach was proposed in [18] and embedded in a harmonic power flow algorithm in [19]. The approach creates a fixed multi-segment lumped parameter model structure for each frequency of interest; however, it does not provide a generic model to be used for all harmonics of interest. In [20], a method to derive a closed form expression for frequency-dependent parameters was presented; the method looks into individual parameter's frequency-dependency, yet again does not provide a generic model structure that could be used in steady state harmonic analysis. Details of this model are presented in the next chapter. A concept of representing three phase line by cascaded PI was presented in [21]; the circuit representation is in modal domain, unlike the proposed model which is in frequency domain. The work in [22] presents frequency domain models for harmonic calculations, where sequence impedances are considered instead of phase impedances. The work in [23] presents an approach to model three-phase frequency-dependent lines with entirely

passive elements using the Padé approximation [53]. These models do not always have a PI structure. During the investigation of frequency-dependent line modeling approaches as a part of this thesis, a generic frequency-dependent transmission line model [24] based on the Vector Fitting approximation method [49] is proposed, a single balanced overhead transposed transmission line is considered as the test case. After this preliminary investigation, a comprehensive frequency-dependent electric power line modeling approach is proposed, which can model single- and multi-phase, balanced and unbalanced, electric power lines and presents a passive circuit realization for the proposed model. The proposed model is always characterized by a single generic PI structure, thereby making it easily implementable in steady state analysis tools such as power flow algorithms.

3.5 Frequency-Dependent Benchmark Model

When the proposed model is implemented in steady state tools such as power flow algorithms, the results thus obtained has to be compared with real field observations or some benchmark models. The real time field data is not practically feasible as multiple arbitrary current injections of various magnitudes have been injected to see how system behaves under different conditions. Hence, an analytical model is derived and considered the benchmark model. In order to incorporate frequency-dependent characteristics, such as effect of ground return and skin effect, first, an updated distributed line model is derived. The per unit length series impedance and shunt admittance are given by,

$$z = (r + j\omega L)\,\Omega \text{ and,} \tag{3.1}$$

$$y = (g + j\omega C)\ \text{S}, \tag{3.2}$$

The benchmark model is derived using the following step by step procedure:

1. In order to account for the effect of ground return, the per unit length series impedance (3.1) is calculated using Carson's equations [33]. The per unit length impedance is of the complex form,

$$z_g = (p + jq)\,\Omega. \tag{3.3}$$

2. The real part of the newly updated series impedance p in Equation 3.3, i.e. the resistive component obtained using Carson's equations, is adjusted to account for the skin effect [54]. This results in updated frequency-dependent per unit length series impedance as,

$$z_a(f) = (r_a + j\omega L_a)\,\Omega\,, \tag{3.4}$$

where the subscript a indicates analytical model.

3. The per unit length shunt admittance (3.2) is calculated using the method of images [27]. This results in updated frequency-dependent per unit length shunt admittance as,

$$y_a(f) = (g_a + j\omega C_a)\ \mathrm{S}. \tag{3.5}$$

4. $z_a(f)$ and $y_a(f)$ are then substituted into Equations (2.41) and (2.42) to obtain the analytical model γ_a and $Z_{c,a}$;

$$\gamma_a = \sqrt{y_a z_a} = \sqrt{(r_a + j\omega L_a)(g_a + j\omega C_a)}, \tag{3.6}$$

$$Z_{c,a} = \sqrt{\frac{z_a}{y_a}} = \sqrt{\frac{(r_a + j\omega L_a)}{(g_a + j\omega C_a)}}. \tag{3.7}$$

5. The frequency-dependent analytical model γ_a and $Z_{c,a}$ are then used to find the exact PI equivalent series impedance $Z'_a(f)$ and shunt admittance $Y'_a(f)$ of a given line length, l using,

$$Z'_a(f) = Z_{c,a} \sinh(\gamma_a l), \tag{3.8}$$

$$Y'_a(f) = \frac{2}{Z_{c,a}} \tanh(\frac{\gamma_a l}{2}). \tag{3.9}$$

6. Steps 1 to 5 are repeated for each frequency of interest. Thus, calculated $Z'_a(f)$ and $Y'_a(f)$ are used as series and shunt elements in the traditional PI model structure as shown in Figure 3.1.

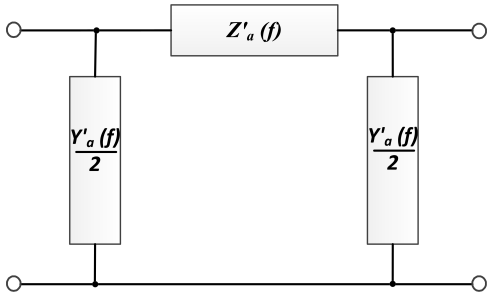

Figure 3.1: Analytical model in traditional PI structure.

7. For each frequency, different values of $Z'_a(f)$ and $Y'_a(f)$ are obtained. Hence, for N number of frequencies of interest, there are N PI-structure models:

$$Z'_a(f) = \{Z'_a(f_1), Z'_a(f_2), ..., Z'_a(f_N)\}, \tag{3.10}$$

$$Y'_a(f) = \{Y'_a(f_1), Y'_a(f_2), ..., Y'_a(f_N)\}. \tag{3.11}$$

where $f_1, f_2, ..., f_N$ are the frequencies of interest. Hence each element of the $Z'_a(f)$ and $Y'_a(f)$ incorporate all frequency-dependent characteristics. A compact form of each element of $Z'_a(f)$ and $Y'_a(f)$ can be expressed as,

$$Z'_a(f_i) = \sqrt{\frac{(r_{dc}s(f_i) + j\omega L_a)}{(g_a + j\omega C_a)}} \times \sinh\left(l\sqrt{(r_{dc}s(f_i) + j\omega L_a)(g_a + j\omega C_a)}\right), \tag{3.12}$$

$$Y'_a(f_i) = 2\sqrt{\frac{(g_a + j\omega C_a)}{(r_{dc}s(f_i) + j\omega L_a)}} \times \tanh\left(\frac{l\sqrt{(r_{dc}s(f_i) + j\omega L_a)(g_a + j\omega C_a)}}{2}\right). \tag{3.13}$$

where, f_i is the i^{th} frequency of interest, r_{dc} is the dc value of the resistance of the line, $s(f_i)$ is the skin effect ratio of the line at the frequency f_i.

It is also noted that for multi-phase lines, each series impedance and shunt admittance would be a matrix of size $(phase \times phase)$. This set of N PI-structures as shown in Figure 3.2 is referred to as the analytical model and taken as benchmark for model comparison.

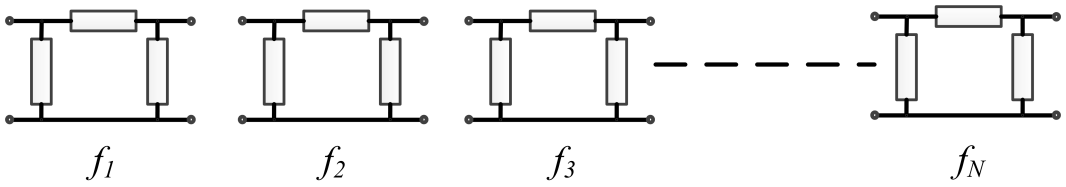

Figure 3.2: Analytical model: set of N PI-structures.

3.6 Frequency Dependent Steady State Models: Errors and Limitations

The accuracy with which the lumped parameter model represents the distributed parameters of electric power lines decreases with increasing frequency [42]. Hence, to study the propagation of harmonics in the system, the use of lumped parameter line models does not yield accurate harmonic calculations. Distributed parameter model can be used for best representation of the transmission line. However, for N number of harmonic frequencies of interest, N number of distributed line models are needed as described in previous section and shown in Figure 3.2. In this thesis, a single frequency-dependent line model is proposed, which retains almost the same accuracy as offered by N set of exact PI models, which is the analytical model. Frequency-dependent characteristics of single distributed exact PI model are described in the following sub-sections. The errors arising from this single distributed parameter models are presented and these are highly minimized in the proposed model.

3.6.1 Limitations of Lumped Parameter Model

For steady state analysis, a line frequency-dependent series and shunt parameters are calculated at 50 or 60 Hz only i.e. step 1 to 5 of sub-section 3.5 is executed for only one frequency. The values computed for z and y are put in the form given by,

$$z_{ep}(f) = (p + jq)\,\Omega. \tag{3.14}$$

where the subscript ep indicates exact PI model. Then the real part p represents the resistance and the imaginary part q the inductive reactance, and the circuit representation is done accordingly with a resistor and an inductor. The resistance is kept constant for all frequencies and the inductive reactance is changed linearly with

frequency. This model is referred to in this paper as the *constant exact PI model*. Hence, the *constant exact PI model* is actually an exact PI model where the frequency dependency of the line parameters are calibrated at 60 Hz. This model results in exact values for 60 Hz and generates error for other frequencies. For 60 Hz, steps 1 to 5 of section 3.5 are executed in case of both constant exact PI model and analytical model. Hence, at 60 Hz,

$$z_{ep}(60) = z_a(60). \tag{3.15}$$

Lets say, the series impedance is to be calculated at n^{th} harmonic frequency i.e. at $(60 \times n)$ Hz. For constant exact PI model, it is simply,

$$z_{ep}(60n) = p + n(jq)\,\Omega. \tag{3.16}$$

But, to calculate the series impedance at n^{th} harmonic frequency for the analytical model, steps 1 to 5 of section 3.5 are executed again. Hence, at n^{th} harmonic frequency,

$$z_{ep}(60n) \neq z_a(60). \tag{3.17}$$

For a unit length line of falcon cable type, this error is evident in Figure 3.3 where series resistance and inductive reactance are plotted for up to the 25^{th} harmonic frequency. The difference between the analytical model and the constant exact PI model in both resistance and reactance keeps increasing as frequency increases. The proposed frequency-dependent line model highly minimizes this error.

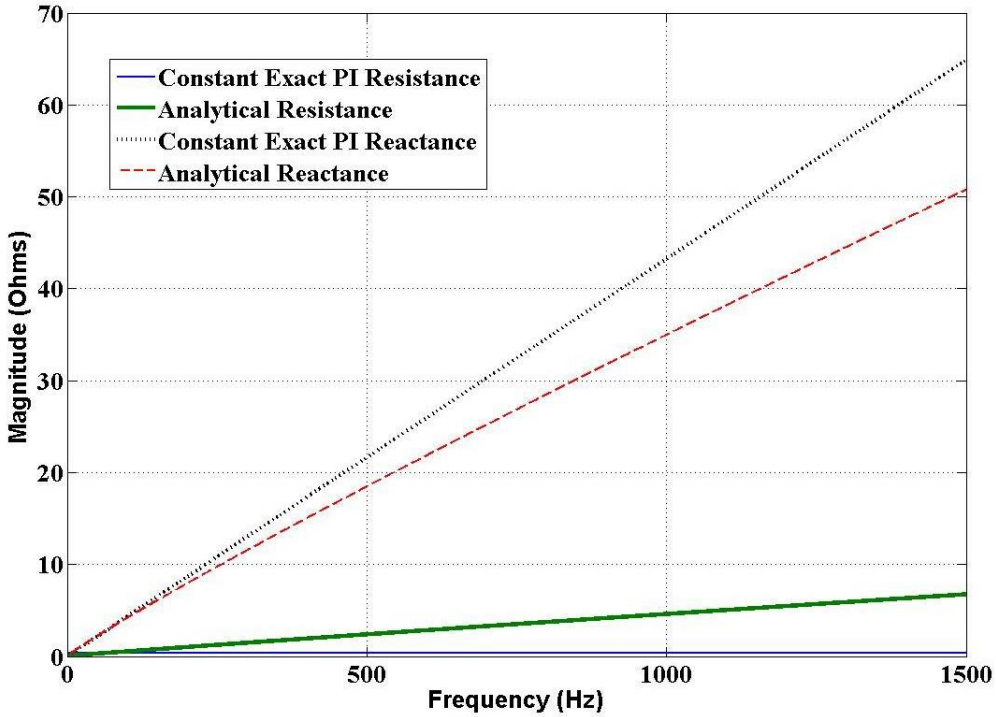

Figure 3.3: Resistance and reactance of a unit-length line of falcon cable type for the *constant exact PI* model and the *analytical model*.

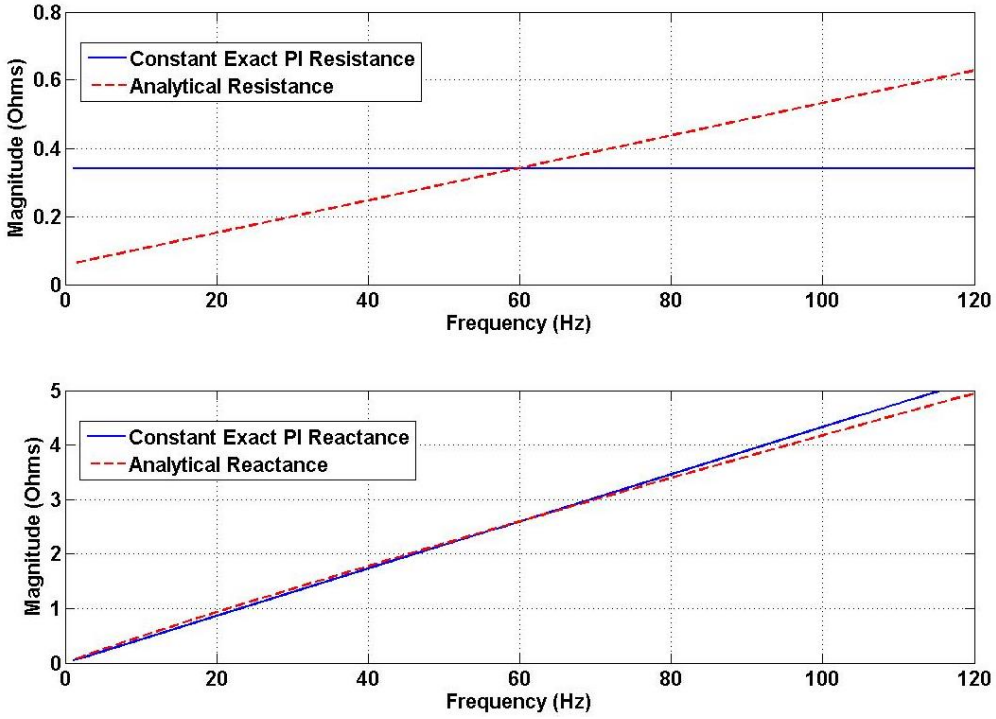

Figure 3.4: Figure 3.3 zoomed in around 60 Hz.

3.6.2 Usage of Distributed Line Model

Distributed parameter model can be used for best representation of the electric power lines. However, for N number of harmonic frequencies of interest, N number of distributed line models are needed. Because of this, a single circuit representation of the distributed line model cannot be achieved. Also, the time required to calculate the A, B, C, D parameters of distributed models is quite significant. For each frequency of interest, Carson's equation, Kelvin functions in loop, hyperbolic functions and a number of simple algebraic expressions of complex numbers have to be calculated.

On the other hand, lets rewrite Equations (3.12) and (3.13), which calculates the series impedance and shunt admittance of the line at i^{th} frequency of interest:

$$Z'_a(f_i) = \sqrt{\frac{(r_{dc}s(f_i) + j\omega L_a)}{(g_a + j\omega C_a)}} \times \sinh\left(l\sqrt{(r_{dc}s(f_i) + j\omega L_a)(g_a + j\omega C_a)}\right), \tag{3.18}$$

$$Y'_a(f_i) = 2\sqrt{\frac{(g_a + j\omega C_a)}{(r_{dc}s(f_i) + j\omega L_a)}} \times \tanh\left(\frac{l\sqrt{(r_{dc}s(f_i) + j\omega L_a)(g_a + j\omega C_a)}}{2}\right). \tag{3.19}$$

Observing the Equations (3.18) and (3.19), it is evident that the series impedance $Z'_a(f_i)$ and shunt admittance $Y'_a(f_i)$ are dependent on frequency. However, the information on how much the frequency is affecting the value of the series impedance or shunt admittance is not clear. During the investigation of multiple approaches for frequency-dependent line modeling, an approach to simplify the expression for the series impedance $Z'_a(f_i)$ and shunt admittance $Y'_a(f_i)$ is presented, which provides a comprehensive understanding of how the frequency is affecting these parameters with the advantage of higher speed of execution. This approach along with other approaches are described briefly in following sections, and details of the modeling approaches are presented in chapter 4 and 5.

3.7 Proposed Approaches for Frequency-Dependent Line Modeling

Multiple methods of frequency-dependent electric power line modeling have been investigated for this research work. All the methods are intended to study the propa-

gation of steady state harmonics. A brief overview of the investigated approaches are given here. Details of these developed methodologies are then discussed in the next chapter.

Multi-Segment Model: The multi-segment frequency-dependent transmission line modeling approach to capture the frequency-dependent terminal behavior of the transmission lines is investigated. The multi-segment line modeling approach from [18] is considered. The proposed method determines the appropriate segmentation of lumped parameter models for non-fundamental frequencies of interest. In this approach, the line model structure is also dependent on the harmonic frequency level. The model segmentation is in fact defined for a specific line (line length, conductor type and geometry) and for each harmonic frequency. The line model structure used is characterized by multiple uniform lumped parameter segments. The information about the segmented structure is calculated and stored off-line. Individual harmonics are treated one at a time utilizing different line model structures for different frequencies, or alternatively, individual harmonics can be treated one at a time utilizing the line model structure developed for the highest frequency of interest. The final HPF results are obtained by superimposing all the harmonic components. A description of this methodology is presented in chapter 4.

Simplified Polynomial Approximation Model: An analytical expression capturing the frequency-dependent characteristics of real part of the line series impedance (apparent resistance) is derived; the imaginary part can then be treated in a similar manner. The apparent resistance is expressed in terms of frequency and line length, assuming all other influencing variables to be constant. Various numerical approximation techniques, which implement least square methods are applied to obtain a final approximated expression for this apparent resistance. Computational time and error between the analytical equation and the simplified approximated equation are compared. Specifically for distribution lines, the expressions for all four line parameters

are simplified to a simple first and second order polynomial functions. Results have shown that during the run of the digital simulation, the proposed equations are executed much faster than the analytical equations. A description of this methodology is presented in chapter 4.

Vector Fitted Approximation Model: In this approach, the vector fitting technique, used in frequency-dependent transmission line modeling for electromagnetic transient (EMT) analysis, is used to approximate the analytical model and derive a frequency-dependent frequency domain model. A generic frequency-dependent line model with a single structure is derived. A passive circuit realization of the proposed model in a PI structure is presented and can be directly implemented in steady-state analysis tools such as harmonic power flow solvers. Multiple test cases are simulated. Results show that the proposed model yields more accurate harmonic voltages and currents as compared to the commonly-used models such as the simple PI model. It is also shown that steady state results obtained using the proposed model are very close to the ones obtained using the EMT model, achieving comparable accuracy without having to run time domain simulations.

3.8 Line Model Evaluation Tools

The proposed line models have to be evaluated and compared against the benchmark analytical model and other commonly used models. Harmonic power flow is one of the best algorithm to evaluate line models to study the propagation of steady state harmonics. HPF is performed in various test cases using multiple software tools for line models evaluation, testing and verification.

3.8.1 Software Tools

For this research, most of the calculations and computations are done in Matlab [50]. Matlab based add ons like Matpower [55] has also been used to run power flows. To compare the multi-segmented frequency-dependent line model with EMT models, PSCAD [8] has been used. For IEEE 13 node distribution test case, CYMDIST [56]

has been used to run power flow. Mathematica [57] has been used to compute symbolic calculations during the investigation of these various approaches for frequency-dependent line modeling. Example screen shot of PSCAD schematics of three bus system built to run harmonic load flow is shown in Figure 3.5 and screen shot of CYMEDIST schematics of IEEE 13 node test feeder built for load flow is shown in Figure 3.6.

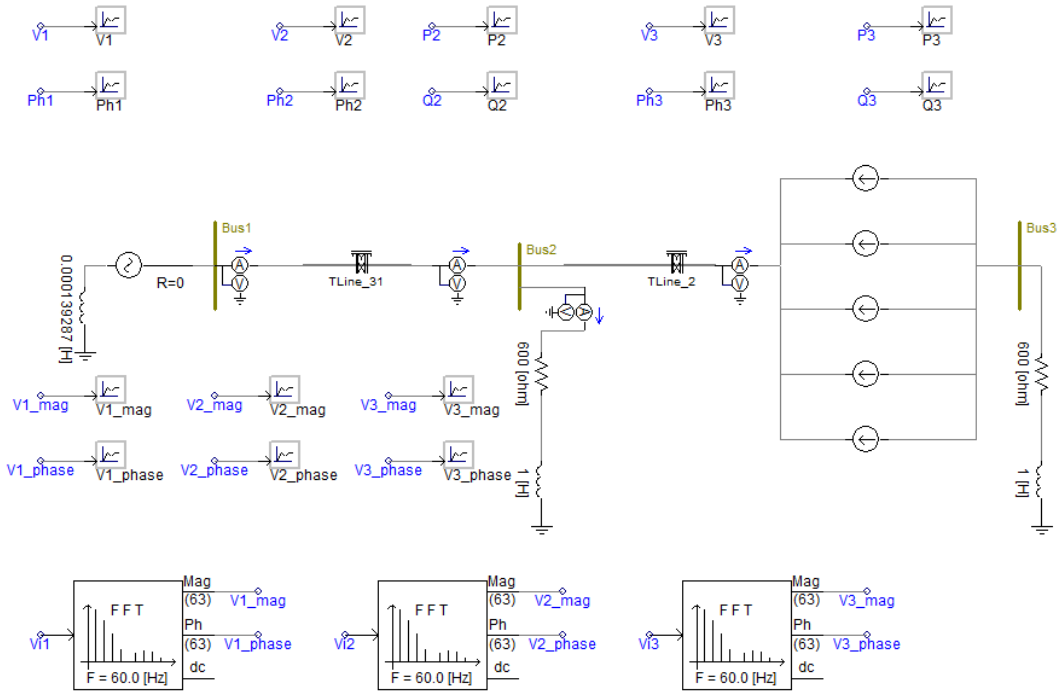

Figure 3.5: PSCAD schematics of three bus system.

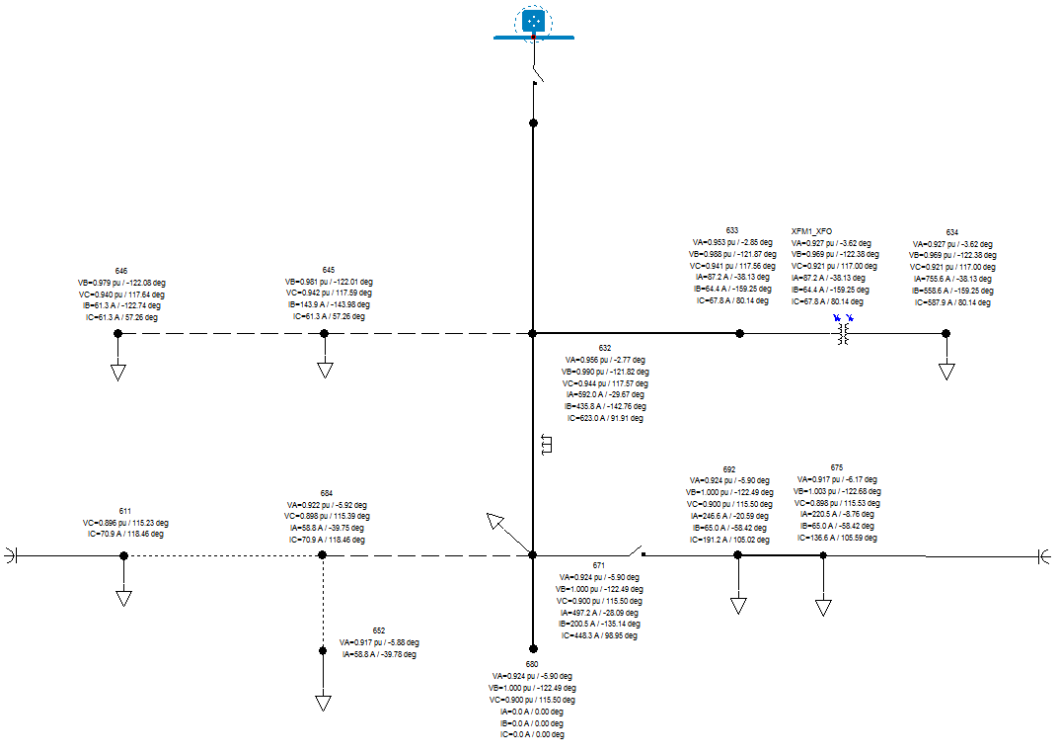

Figure 3.6: CYMEDIST schematics of IEEE 13 node test feeder.

3.8.2 Harmonic Power Flow

Harmonic power flow is a technique to assess the power flow with a distorted waveform using the spectral components of the waveform called as harmonics [5]. These harmonics are found from Fourier Transform methods. HPF results give information about harmonic voltages at all the buses of the system [58] and the effect of harmonics on each bus can be assessed. Conventional power flow solves for the solution matrix X, which has voltage magnitudes and phases at all the buses,

$$X = [V_1^B, \delta_1^B], \tag{3.20}$$

where V_1^B is the fundamental component voltage magnitude at bus B, δ_1^B is the fundamental compoent voltage angle at bus B and B goes from 1 to N_B, N_B being the total number of buses. For HPF, the solution matrix X contains the fundamental as well as harmonic voltage magnitudes and phases at all the buses,

$$X = [V_1^B, \delta_1^B, V_2^B, \delta_2^B, V_3^B, \delta_3^B, ...V_h^B, \delta_h^B] = [V_i^B, \delta_i^B], \tag{3.21}$$

where V_i^B is the i^{th} harmonic component voltage magnitude at bus B and δ_i^B is the i^{th} harmonic component voltage angle at bus B. B goes from 1 to N_B, N_B being the total number of buses and i goes from 1 to h, h being the total number of harmonics under consideration. There are multiple methods of HPFs [59–62]; based on computation approach, they can be classified into iterative and non-iterative method. The HPF methods could be in frequency domain, in time domain and in hybrid frequency-time domain [5]. Frequency domain HPFs are discussed and used in this work.

3.8.2.1 Iterative Harmonic Power Flow

The iterative HPF was proposed by Xia and Heydt [58]. It considers the interaction between harmonics and the control variables in the harmonic producing loads. Multiple methods of iterative HPFs have been proposed [59–62]. Here, HPF technique of [58] is briefly explained.

In this method, as in case of conventional power flow, we start with the known values and find out the unknown values.

- Line parameters of all the lines
- Total number of buses (N_B) which includes both linear buses (n) and non linear buses (m) and ($N_B = n + m$).
- Total number of harmonics (h) to consider excluding the fundamental.
- Active and reactive powers at all the linear buses.
- Active power, apparent power and expression for load currents at non linear buses.

To apply Newton-Raphson method, the number of unknown variables must be equal to the number of independent equations. For iterative harmonic power flow, the number of unknowns are

- Voltage magnitude and angle for the fundamental frequency at each bus, except the swing bus ($2(n-1)$).
- Harmonic voltage magnitude and phases at all buses ($2nh$).

- Active and reactive power at swing bus for fundamental frequency (2).
- Control parameters describing each non-linear bus ($2m$).

The total number of unknowns is hence $2(n-1)+2nh+2+2m = 2n(1+h)+2m$. Now the total number of independent equations have to be listed out. They are:

- Active and reactive power mismatch for fundamental frequency at each linear buse, except the swing bus ($2(n-m-1)$.
- Voltage magnitude and angle at swing bus for fundamental frequency (2).
- Real and imaginary current balance for fundamental frequency at each non-linear bus ($2m$).
- Real and imaginary current balance for each harmonics excluding the fundamental at all the buses ($2nh$).
- Total active and reactive power mismatch at each non-linear bus ($2m$).

The total number of known independent equations are hence $2(n-m-1)+2+2m+2nh+2m = 2n(1+h)+2m$ which is equal to the total number of unknowns as calculated above.

3.8.2.2 Non-Iterative Harmonic Power Flow

Before iterative HPF was introduced, the non-iterative harmonic network analysis techniques [63, 64] were used. The technique is based on direct linear solution of the harmonic currents and assume no harmonic interactions as,

$$[V_i] = [Y_i]^{-1}[I_i] \quad \text{for } i \neq 1, \tag{3.22}$$

where V_i is the i^{th} harmonic component voltage matrix, Y_i is the i^{th} harmonic component system admittance matrix, I_i is the i^{th} harmonic component current matrix and i goes from 2 to h, h being the total number of harmonics under consideration. Computationally, the non iterative HPF is much faster in comparison to the iterative HPF which has to evaluate a lot of mathematical expressions in a matrix in iterative fashion, and takes a longer time to execute. Although the accuracy of the iterative HPF is better than the non-iterative HPF, because of the simplicity of the

non-iterative method, it is still in use. Sun et al. [65] have shown that with newer converter models, the non-iterative methods have not significant difference in accuracy as compared to iterative methods. For this research work, the non-iterative HPF is used. Initially, the fundamental frequency load flow is performed in conventional way, using Newton Raphson or Gauss Seidel methods. Then the harmonic voltages in the system is calculated by using bus current injections and system impedance matrix. The different harmonic components are superimposed to obtain the final result. Loads are assumed as static impedances and the harmonic interactions between the network and non-linear devices are ignored. The non-iterative HPF flowchart is shown in Figure 3.7. The development of the frequency-dependent power line models and the implementation of HPF is discussed in next chapter.

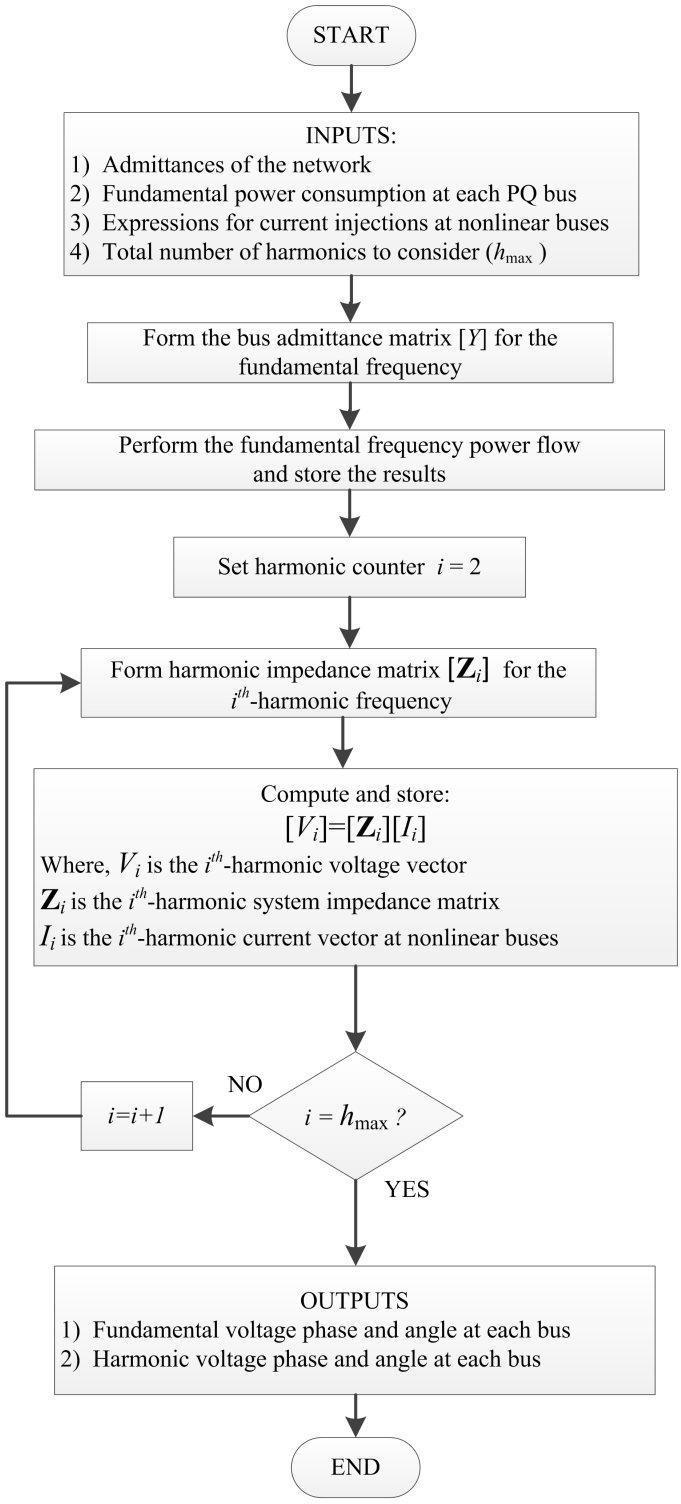

Figure 3.7: Non iterative harmonic power flow flowchart.

CHAPTER 4: INVESTIGATION OF FREQUENCY-DEPENDENT LINE MODELING APPROACHES

4.1 Overview

This chapter discusses the investigation of the frequency-dependent power line modeling approaches. Mainly, two frequency-dependent line modeling approaches have been investigated;

- The multi-segment frequency-dependent transmission line modeling approach to capture the frequency-dependent terminal behavior of the transmission lines, and
- An approach for deriving analytical expression capturing the frequency-dependent characteristics of real part of the line series impedance(apparent resistance).

For all modeling approaches, model derivation is shown and the proposed models are compared with the benchmark model, as well as other commonly used models. First, the multi-segment frequency-dependent transmission line modeling approach to capture the frequency-dependent terminal behavior of the transmission lines is investigated. For this approach, a three bus system test case is considered and harmonic power flow is done. The resulting harmonic voltage magnitudes and angles obtained using different line models are compared with the frequency-dependent multi-segmented line model. Second, an analytical expression capturing the frequency-dependent characteristics of real part of the line series impedance(apparent resistance) is derived and investigated. For this approach, the frequency-dependent apparent resistance obtained from the proposed model are compared with the frequency-dependent apparent resistance obtained from the analytical benchmark model. Simulation results, errors and advantages of the proposed modeling approaches are also discussed.

4.2 Multi-Segment Frequency-Dependent Transmission Line Modeling Approach

The transmission line modeling approach from [18] is implemented to derive the multi-segment frequency-dependent transmission line model. The multi-segment frequency-dependent transmission line modeling approach is focused on capturing the frequency-dependent terminal behavior of the transmission lines. This method uses the frequency scan technique [5] and is based on the comparison of the uniformly distributed transmission line model,which is viewed as the benchmark, with finitely segmented models. The accuracy of the finitely segmented line models with respect to the uniformly distributed line model is defined in terms of metrics of voltage attenuation and phase shift along the line.

4.2.1 Line Model Segmentation

For each harmonic frequency and for every transmission line in the system under study, known receiving-end voltage and current are considered. Then the sending-end voltage obtained using a segmented lumped parameter line model is compared to that obtained using the distributed parameter line model. The number of segments is increased until the desired level of accuracy is reached. The calculation is repeated for all frequencies of interest. A flowchart of the line model segmentation procedure is shown in Figure 4.1. The resulting number of segments for each line model versus the harmonic level is stored in a table. Hence, the final output of this procedure is a table with harmonic frequency and its corresponding number of segments required which falls within the error limit considered in the beginning. An example is shown in Table 4.1. A more detailed description of the modeling methodology can be found in [18].

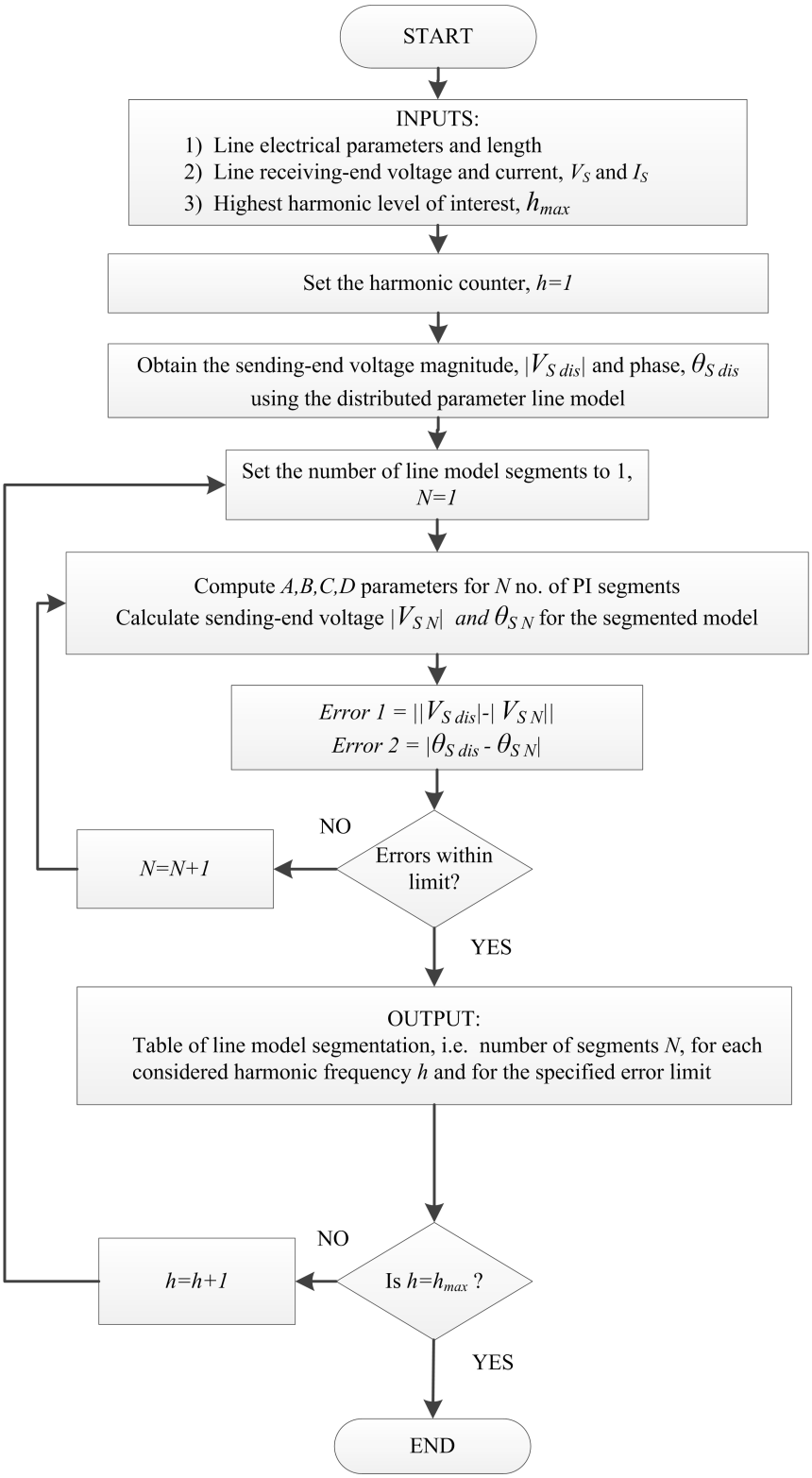

Figure 4.1: Line model segmentation flowchart.

Table 4.1: Line segmentation for 40 miles and 170 miles falcon conductor type.

Falcon conductor 40 miles line		Falcon conductor 170 miles line	
Harmonics	No. of Segments	Harmonics	No. of Segments
1	1	1	1
2	1	2	1
3	1	3	2
4	1	4	2
5	1	5	2
6	1	6	3
7	1	7	3
8	1	8	3
9	1	9	5
10	1	10	6
11	2	11	6
12	2	12	6
13	2	13	6
14	2	14	6
15	2	15	6
16	2	16	9
17	2	17	12
18	2	18	12
19	2	19	13
20	2	20	13
21	2	21	13
22	2	22	13
23	2	23	13
24	2	24	13
25	2	25	18
26	2	26	22
27	2	27	22
28	2	28	23
29	2	29	23
30	2	30	23
31	3	31	23
32	3	32	23
33	4	33	23
34	4	34	29
35	4	35	30
36	4	36	30

4.2.2 Calculation of Equivalent Impedances and Admittances

After the information about line model segmentation is obtained, the system's $\mathbf{Y}$ matrix is required for employing the non-iterative power flow method. Hence, for each line, an equivalent model is developed and corresponding impedances and admittance are obtained. For a single PI-type lumped parameter segment, as shown

in Figure (2.9), relationships between sending-end voltages and currents are expressed as follows:

$$V_s = AV_r + BI_r, \tag{4.1}$$

$$I_s = CV_r + DI_r, \tag{4.2}$$

where V_s and I_s are the sending-end voltage and current and V_r and I_r are receiving-end voltage and current. A, B, C and D are given by (2.35)-(2.38). A multi-segment PI-model structure can be represented as shown in Figure 4.2. If there are N uniform segments, we will have a new series impedance Z_N and a new shunt admittance Y_N for each segment.

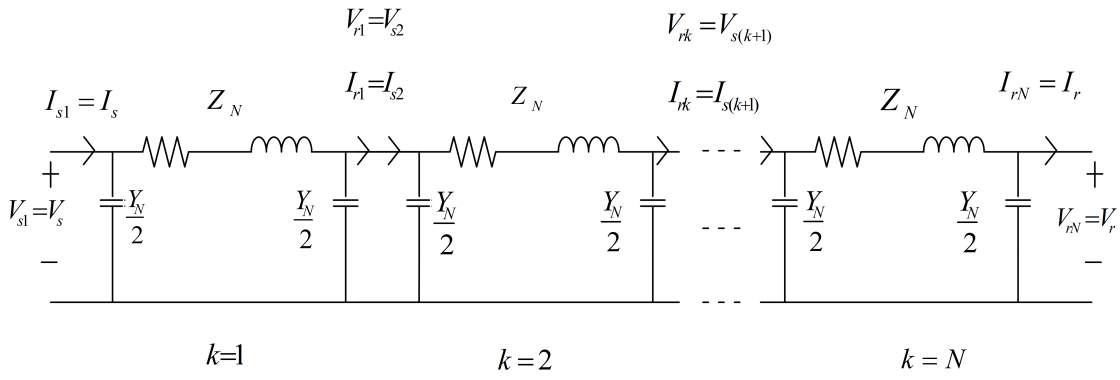

Figure 4.2: Multi segment line model.

The relationship of the impedance Z_l and admittance Y_l of a single-segment PI model with an N-segment PI model impedance Z_N and admittance Y_N of the same line is given by:

$$Z_N = \frac{Z_l}{N}. \tag{4.3}$$

$$Y_N = \frac{Y_l}{N}. \tag{4.4}$$

Let V_{sk} and I_{sk} be the k^{th} segment sending-end voltage and current and V_{rk} and I_{rk} be the k^{th} segment receiving-end voltage and current. Then for the first PI segment, $(k = 1)$,

$$V_{s1} = A_N V_{r1} + B_N I_{r1}, \tag{4.5}$$

$$I_{s1} = C_N V_{r1} + D_N I_{r1}, \tag{4.6}$$

and so on up to N^{th} segment. The general term is:

$$V_{sk} = A_N V_{rk} + B_N I_{rk}, \tag{4.7}$$

$$I_{sk} = C_N V_{rk} + D_N I_{rk}. \tag{4.8}$$

Also, the following expression is true,

$$V_{rk} = V_{s(k+1)}, \tag{4.9}$$

$$I_{rk} = I_{s(k+1)}. \tag{4.10}$$

The intermediate voltage and current expressions could be eliminated and the equations can be expressed in terms of the line sending and receiving end voltage and current V_s and I_s. For example, if there are three segments, then the following expressions are obtained:

$$V_s = (A_3^3 + 2A_3B_3C_3 + B_3C_3D_3)V_r + (A_3^2 + B_3C_3 + A_3D_3 + D_3^2)I_r \tag{4.11}$$

$$I_s = C_3(A_3^2 + B_3C_3 + A_3D_3 + D_3^2)V_r + (A_3 + B_3C_3 + 2B_3C_3D_3 + D_3^3)I_r \tag{4.12}$$

Irrespective of the number of segments, the final expression is of the form,

$$V_s = A'V_r + B'I_r \tag{4.13}$$

$$I_s = C'V_r + D'I_r \tag{4.14}$$

where A', B', C' and D' are the new equivalent parameters and the equations are of the form (4.1) and (4.2). Hence we can express the multi-segment line model into an equivalent PI model. Using (2.35) -(2.38) for the equivalent parameters, a new set of equivalent Z' and Y' are obtained. These new Z' and Y' are then used to develop the system $\mathbf{Y}$ matrix to be used in the non-iterative HPF.

4.2.3 Test Case Study

A test case is set up to validate functionality of the proposed model in the HPF tool and to compare it to the other line models: the single lumped parameter segment model and the frequency-dependent model as described in [15] used in PSCAD. After

the HPF is done, the resulting bus voltages obtained using different line models are compared against each other. The test case is a three-bus system. The generator is connected at Bus 1, a PQ load at Bus 2 and a nonlinear load at Bus 3. The circuit diagram of the test system is shown in Figure 4.3 below.

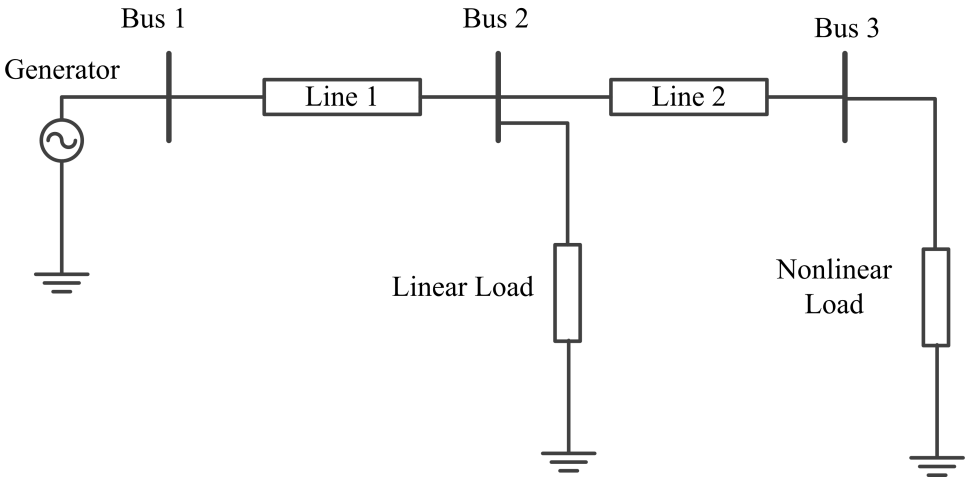

Figure 4.3: 3 bus test case schematics.

A brief description of each component in the test system follows.

- Generator: The Generator is set at 138 kV. Bus 1 is considered the reference bus. The generator is modeled as an ideal voltage source with an inductance behind it to represent the reactance of the generator.
- Transmission Lines: Two transmission lines are present. Line 1 is 42 miles long and line 2 is 170 miles long. Falcon cable [66] is used and the tower height is 30 meters.
- Loads: A linear PQ load is connected at Bus 2. A nonlinear load is connected at Bus 3. The nonlinear load is modeled by current sources. The nature of the nonlinearity is arbitrarily chosen to include four harmonics. Along with the fundamental frequency, the third, twelfth, nineteenth and twenty-fifth harmonics are considered. The amplitude of the 3rd harmonic current is 31.8% of the amplitude of the fundamental current and the amplitude of the 12th, 19th and 25th harmonic currents are all 27.4 % of the amplitude of the fundamental

current, as seen in (4.15). The amplitude of the harmonics are made higher as compared to a real life scenario to more easily visualize the propagation of harmonics in the system. The load characteristics are defined as:

- Load 1 (Bus 2) Constant power load: power consumption $= 23.6 + 10j$ MVar.
- Load 2 (Bus 3) Constant current load: current expression given by:

$$I^3 = 182\sqrt{2}\sin(377t - 0.549) + 58\sqrt{2}\sin(1131t - 1.221) + 50\sqrt{2}\sin(4524t) + 50\sqrt{2}\sin(7163t - 1.047) + 50\sqrt{2}\sin(9425t - 1.134). \quad (4.15)$$

For comparison, HPF is performed using the three line models as described below:

- Line Model 1: This frequency dependent line model (FDLM) is described in [15] and is considered to be the most robust and accurate to date [8]. The FDLM is used by the EMTP software and is formulated in the phase domain. The transmission line is characterized by the frequency dependent propagation function H and characteristic impedance matrix Y_c where H and Y_c are fitted accurately by rational functions. This model is usually utilized for transient analysis. The circuit representation of this model is given in Figure 4.4.
- Line Model 2: This is the proposed frequency dependent transmission line model structure. It is a uniformly-segmented lumped-parameter model where the model structure, i.e. the number of segments, changes according to the harmonic frequency. The circuit representation of this model is given in Figure 4.5.
- Line Model 3: This model is a single lumped parameter model. Its structure remains the same for all the frequencies; however the series impedance and shunt admittance are adjusted based on the frequency. The circuit representation of this model is given in Figure 4.6.

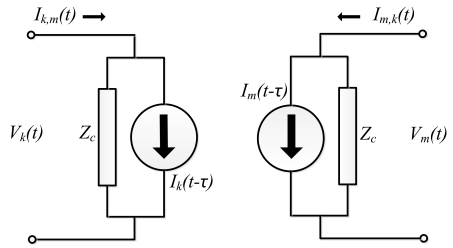

Figure 4.4: Circuit representation of line model 1 connecting node k and m.

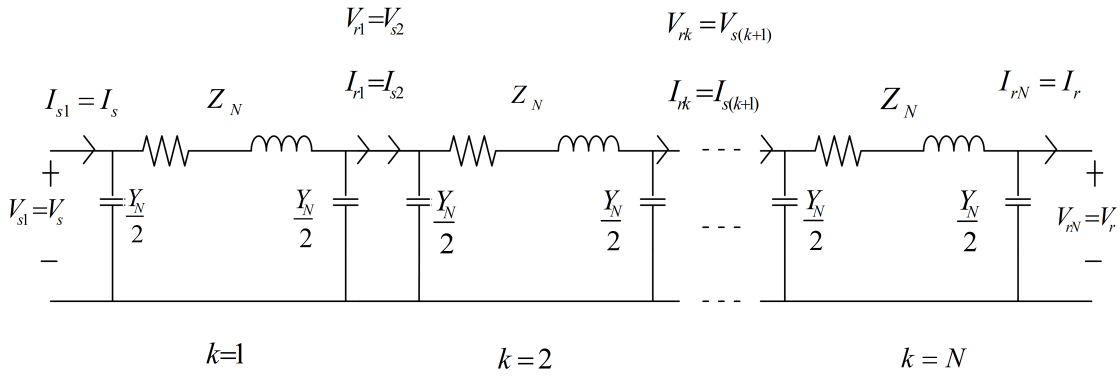

Figure 4.5: Line model 2: multi-segment line model.

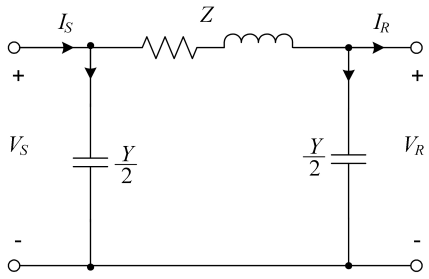

Figure 4.6: Line model 3: PI model.

4.2.4 Simulation Results and Observation

The HPF algorithm as shown in Figure (3.7) is implemented in this test case for the line model 2 and line model 3. HPF for Line Model 1 is performed in the time domain in PSCAD and steady state voltage magnitudes and phase angles are calculated for comparison purposes. The phase angles in three modeling approaches did not show appreciable difference, hence, the resulting harmonic voltage magnitudes for all the buses are summarized in Table 4.2. Also shown in Table 4.2 is the percentage difference between the voltage magnitude obtained using Line Model 1 and the ones

using the other two models. The percentage difference is calculated using,

$$\%\, diff = \left| \frac{|V_{Line\, model\, 3}| - |V_{Line\, model\, 1\, or\, 2}|}{|V_{Line\, model\, 3}|} \right| \times 100\% \tag{4.16}$$

As seen from the table, harmonic voltages obtained at all buses using Line Model 3 have a relatively large percentage difference from the harmonic voltages obtained using FDLM (Line Model 1). Looking at the percentage difference between the voltage magnitudes at all the buses using Line Model 1 and Line Model 2, it is observed that the voltage profile obtained from Line Model 2 is much closer to the voltage profile of Line Model 1.

The difference can also be seen distinctly in the plot of instantaneous voltages at all buses. Figure 4.7, 4.8 and 4.9 show the instantaneous voltages at Buses 1, 2 and 3 respectively. From the voltage plot at Buses 2 and 3, it is seen that Line Model 3 has suppressed the spikes significantly and harmonic voltages are not seen as clearly as with the other two line models. HPF with Line Model 2 has shown that the voltage ripples are represented fairly well as compared to the HPF using the FDLM (Line Model 1). The plot of the voltage at Bus 1 is almost a pure sinusoidal because the harmonics are not propagating from Bus 3 to Bus 1. The harmonic pollution generated at Bus 3 however clearly propagates to Bus 2.

Table 4.2: Harmonic voltage magnitudes using different line models.

	Fundamental Frequency Voltage Magnitude				
	Line Model 1	Line Model 2		Line Model 3	
	$\|V\|$ in kV	$\|V\|$ in kV	% diff	$\|V\|$ in kV	% diff
Bus 1	138.00	138.00	0.00	138.00	0.00
Bus 2	137.90	137.58	0.23	137.58	0.23
Bus 3	137.66	135.93	1.26	135.93	1.26

	Third Harmonic Voltage Magnitude				
	Line Model 1	Line Model 2		Line Model 3	
	$\|V\|$ in kV	$\|V\|$ in kV	% diff	$\|V\|$ in kV	% diff
Bus 1	0.037	0.038	3.48	0.042	12.67
Bus 2	17.32	18.72	8.03	20.38	17.62
Bus 3	65.51	74.28	13.33	92.32	40.84

	Twelfth Harmonic Voltage Magnitude				
	Line Model 1	Line Model 2		Line Model 3	
	$\|V\|$ in kV	$\|V\|$ in kV	% diff	$\|V\|$ in kV	% diff
Bus 1	0.053	0.047	11.33	0.002	95.33
Bus 2	20.22	19.46	3.76	1.19	94.08
Bus 3	21.61	17.37	19.63	7.51	65.22

	Nineteenth Harmonic Voltage Magnitude				
	Line Model 1	Line Model 2		Line Model 3	
	$\|V\|$ in kV	$\|V\|$ in kV	% diff	$\|V\|$ in kV	% diff
Bus 1	0.076	0.068	11.34	0.000	99.50
Bus 2	20.99	21.025	0.13	0.18	99.13
Bus 3	20.08	15.137	24.62	4.35	78.31

	Twenty-fifth Harmonic Voltage Magnitude				
	Line Model 1	Line Model 2		Line Model 3	
	$\|V\|$ in kV	$\|V\|$ in kV	% diff	$\|V\|$ in kV	% diff
Bus 1	0.152	0.159	4.40	0.000	99.90
Bus 2	26.074	28.96	11.08	0.071	99.72
Bus 3	33.582	34.79	3.60	3.245	90.33

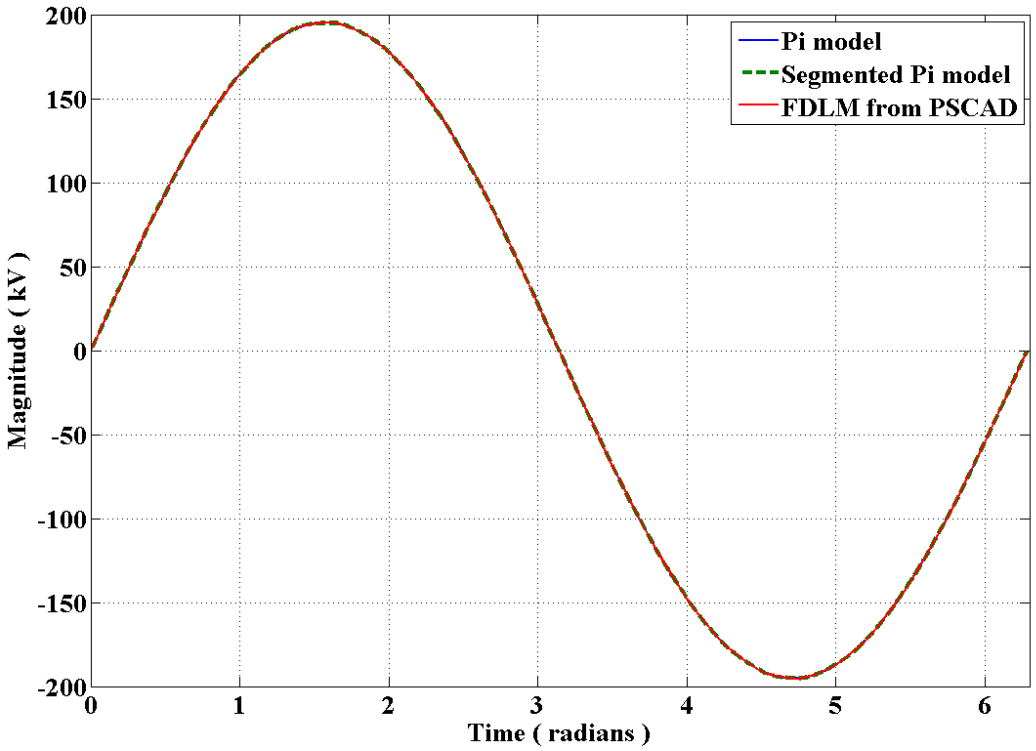

Figure 4.7: Instantaneous voltage at Bus 1.

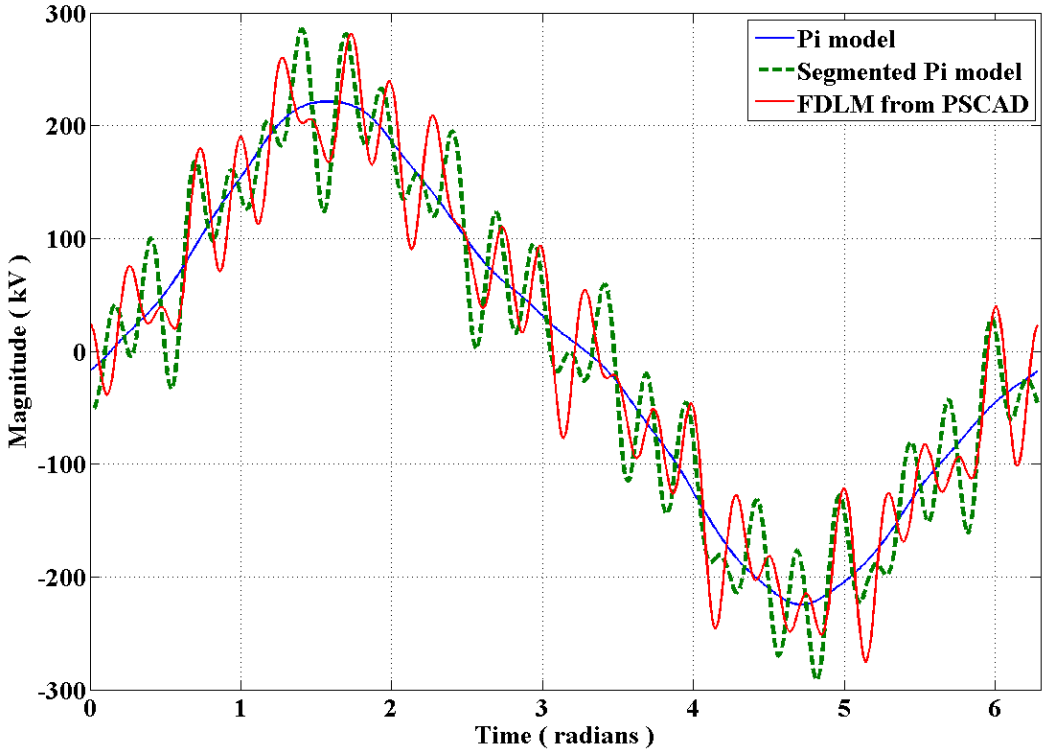

Figure 4.8: Instantaneous voltage at Bus 2.

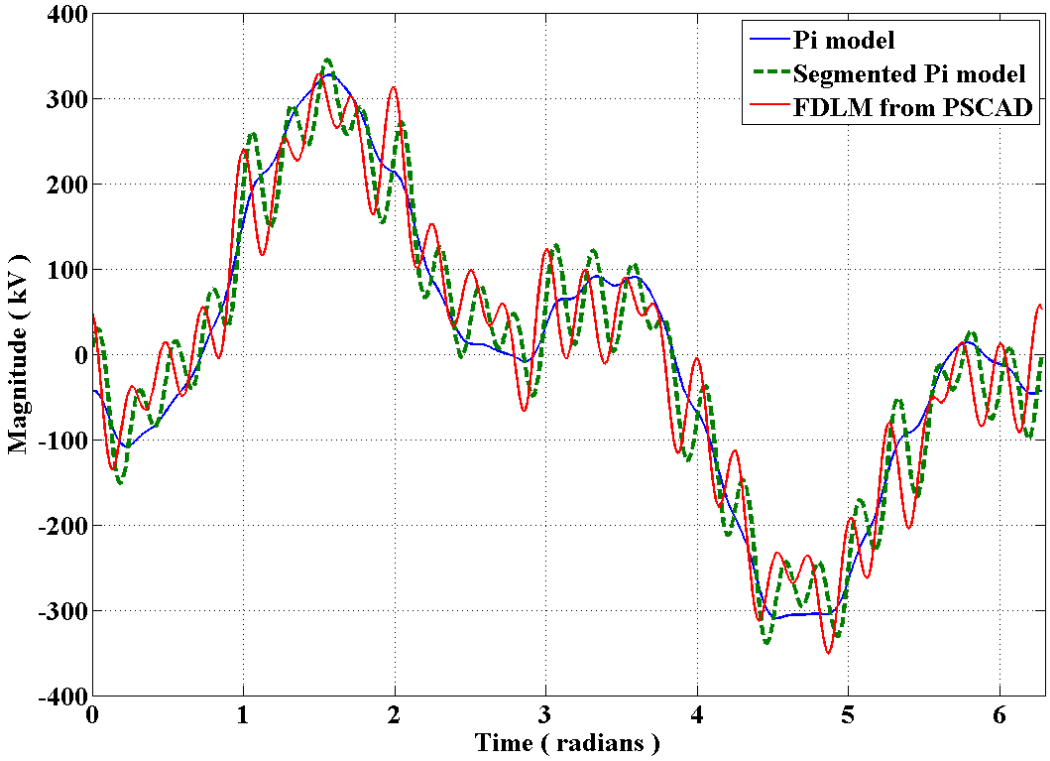

Figure 4.9: Instantaneous voltage at Bus 3.

4.2.5 Discussion

Section 4.2 presented a Harmonic Power Flow tool that uses frequency-dependent line models. The proposed HPF method employs a frequency-dependent line model structure and a non-iterative power flow technique. The tool has been coded in Matlab and a test study was performed for a three-bus power system with a non-linear load injecting harmonic currents. Results of the test studies using the proposed HPF tool are compared to results obtained using a single lumped parameter segment line model (i.e. the traditional PI model) as well as using the frequency-dependent line model used in the PSCAD software. In general, the results obtained using the proposed HPF tool with frequency-dependent line model structures are closer to the results obtained using the frequency-dependent line models in PSCAD than the ones obtained using a single-segment line model. The Other modeling approach to study frequency-dependent characteristics is presented in following section.

4.3 An Approach for Modeling Frequency-Dependent Impedance of Power Lines

The multi-segment frequency-dependent line model has a dynamic structure which changes with the frequency of interest. In order to develop a single generic structure and also to improve on the accuracy of the multi-segment frequency-dependent line model, a novel approach for modeling frequency-dependent impedance of a power transmission line is investigated. An analytical expression capturing the frequency-dependent characteristics of real part of the line series impedance(apparent resistance) is derived. This section focuses on the real part of this frequency-dependent impedance, which is referred to as apparent resistance; the imaginary part can then be treated in a similar manner. The apparent resistance is expressed in terms of frequency and line length, assuming all other influencing variables e.g. temperature, to be constant. Various numerical approximation techniques, which implement least square methods are applied to obtain a final approximated expression for this apparent resistance. Computational time and error between the analytical equation and the simplified approximated equation are compared. Results have shown that during the run of the digital simulation, the proposed equation is executed much faster than the analytical equations.

4.3.1 Apparent Resistance

In chapter 3 section 3.5, benchmark model was discussed. Rewriting the equation (3.12),

$$Z'_a(f_i) = \sqrt{\frac{(r_{dc}s(f_i) + j\omega L_a)}{(g_a + j\omega C_a)}} \times \sinh\left(l\sqrt{(r_{dc}s(f_i) + j\omega L_a)(g_a + j\omega C_a)}\right), \tag{4.17}$$

$Z'_a(f_i)$ being a complex number, Equation (4.17) can be expressed as real and imaginary components,

$$Z'_a(f_i) = \mathrm{Re}[Z'_a(f_i)] + j\,\mathrm{Im}[Z'_a(f_i)]. \tag{4.18}$$

It is clear that $\mathrm{Re}[Z'_a(f_i)]$ is dependent on frequency. Usually the real part of the impedance represents the resistance. In this case, $\mathrm{Re}[Z'_a(f_i)]$ is not the actual resistance of the line, but the overall resistive characteristic offered by the line. This property cannot be analyzed physically but can be analyzed in mathematical terms. This term is called in this work as *apparent resistance*. This phenomenon of frequency-dependency of $\mathrm{Re}[Z'_a(f_i)]$ which comes out from rearrangement of the equation is termed as *apparent effect* in this work. Without replacing the numerical values of the parameters, it is difficult to analyze the apparent resistance. To derive the final expression of the frequency-dependent impedance, as discussed in chapter 3 section 3.5, a lot of steps and equations are to be executed. Hence, such process lacks sufficient information on how the variables constitute the apparent resistance. To avoid going through all those steps and use the equations mentioned there, a simpler expression for apparent resistance is defined. Different numerical approximation techniques are used to find a new closed form equation for the apparent resistance. Figure 4.10 shows the 3 dimensional plot of the apparent resistance against the line length and frequency for falcon conductor type. The conductor parameters are taken from [27].

Figure 4.11 shows the 3 dimensional plot of the resistance including both apparent and skin effects of a the line for falcon cable type. After adding skin effects, it is clear that there is rise in resistance value as frequency increases.

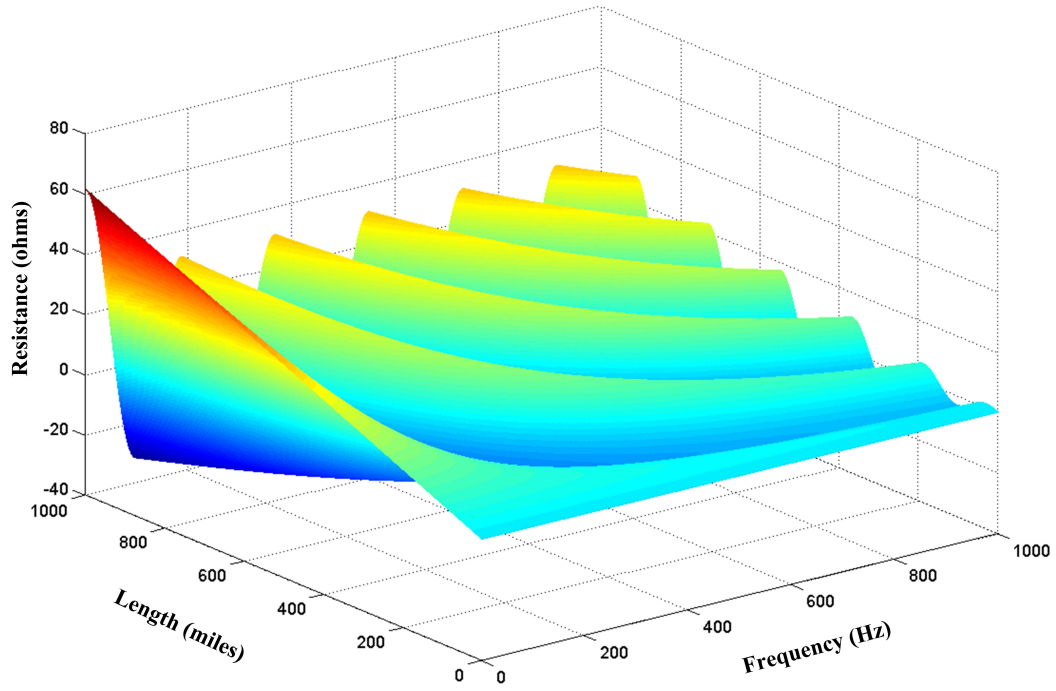

Figure 4.10: Resistance of a transmission line as function of length and frequency for falcon conductor type.

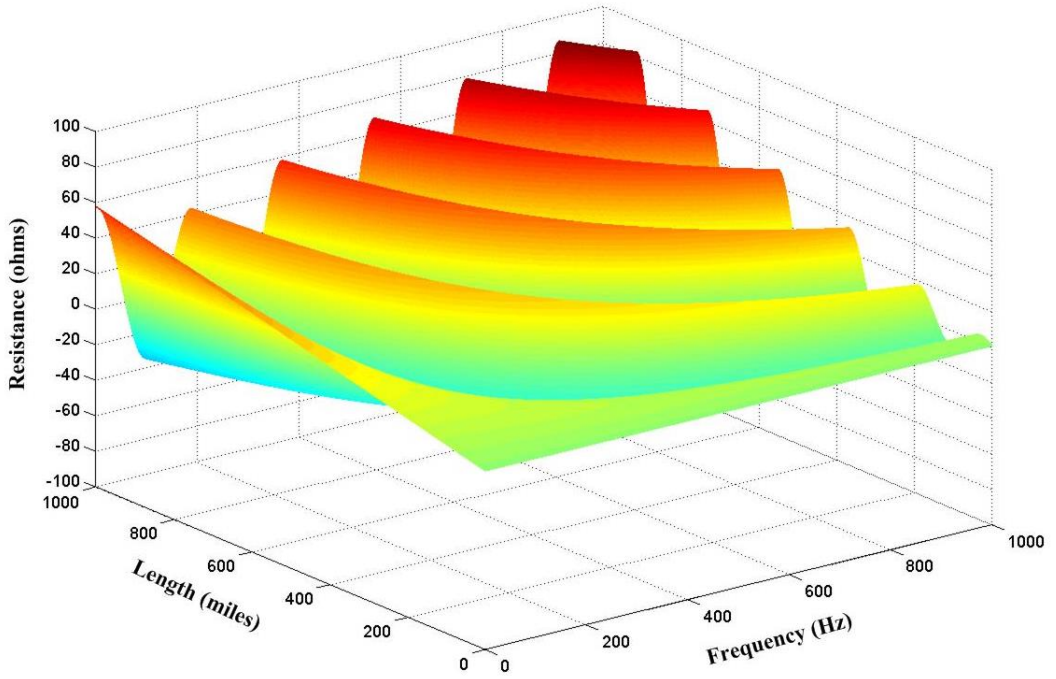

Figure 4.11: Resistance of the line with skin effect as function of length and frequency for falcon conductor type.

4.3.2 Approximation Methods

As discussed in chapter 3 section 3.5, to derive an expression for series impedance, a lot of steps are involved and a number of complex expressions are executed. Symbolic representation of the real part of the impedance i.e. the apparent resistance is mathematically rigorous. Hence, one conductor type is taken as a test case, and numerical substitution is done. Figure 4.10 and 4.11 show how resistance is dependent on both length and frequency. Then the numerical approximation is applied on thus calculated apparent resistance to derive a simpler form expression. Then, instead of going through all the steps mentioned in the derivation fo analytical model, the simpler expression derived can be used. It is expected that the approximated expression will be executed much faster than the analytical ones. The accuracy and complexity may vary depending on the numerical techniques being used. In this work, numerical polynomial and exponential approximations using least square methods [67] are implemented. These approximation techniques were selected for their simplicity. Matlab is used for computations in this work.

4.3.2.1 Polynomial Approximation

For the purpose of clarity, let's consider the quadratic equation of the form,

$$y = a + bx + cx^2, \tag{4.19}$$

to fit the set of n data points $(x_1, y_1), (x_2, y_2), ..., (x_n, y_n)$. If y' is the calculated value, then error for n^{th} data point,

$$e_n = y_n - y'_n. \tag{4.20}$$

Then the sum of the squares of the errors is given as,

$$\begin{aligned} E =& [y_1 - (a + bx_1 + cx_1^2)]^2 + [y_2 - (a + bx_2 + cx_2^2)]^2 + ... \\ &+ [y_n - (a + bx_n + cx_n^2)]^2. \end{aligned} \tag{4.21}$$

For error E to be minimum, the following expressions must be true,

$$\frac{\partial E}{\partial a} = 0,\ \frac{\partial E}{\partial b} = 0,\ \frac{\partial E}{\partial c} = 0. \tag{4.22}$$

Using (4.21) and (4.22),

$$\Sigma y_i = na + b\Sigma x_i + c\Sigma x_i^2. \tag{4.23}$$

$$\Sigma x_i y_i = a\Sigma x_i + b\Sigma x_i^2 + c\Sigma x_i^3. \tag{4.24}$$

$$\Sigma x_i^2 y_i = a\Sigma x_i^2 + b\Sigma x_i^3 + c\Sigma x_i^4. \tag{4.25}$$

Equation (4.23) to (4.25) are in linear form which can be solved simultaneously to find the values of a, b and c.

4.3.2.2 Exponential Approximation

Let's consider the exponential function to approximate as,

$$y = ae^{bx}, \tag{4.26}$$

where a and b are the co-efficients to be determined and x and y are the variables under consideration. Taking logarithms on both sides in (4.26),

$$log_{10}(y) = log_{10}(a) + bx\, log_{10}(e). \tag{4.27}$$

This equation is in the linear form,

$$Y = mX + C, \tag{4.28}$$

where,

$$Y = log_{10}(y), \tag{4.29}$$

$$m = b\ log_{10}(e), \tag{4.30}$$

$$C = log_{10}(a). \tag{4.31}$$

After the conversion of logarithmic function into linear form, the polynomial approximation method as described in previous subsection is used to determine the co-efficients a and b.

4.3.3 Approximation Procedure

Real part of (4.17) is approximated using standard mathematical functions. The steps given below are followed to determine the final expression for the apparent resistance.

Step 1. Detection of Oscillation: The apparent resistance has an oscillatory behavior which resembles the cosine function. Denoting this oscillation frequency as f_{rs}, the amplitude of the resistance is represented by

$$A = \cos(f_{rs}), \tag{4.32}$$

where f_{rs} is a function of two dependent variables, i.e. length of the line and frequency of the signal, which has to be calculated. The resistance of a 1000 mile long line and a 300 mile long line of falcon conductor type, plotted against frequency of the signal are shown in Figures 4.12 and 4.13, respectively.

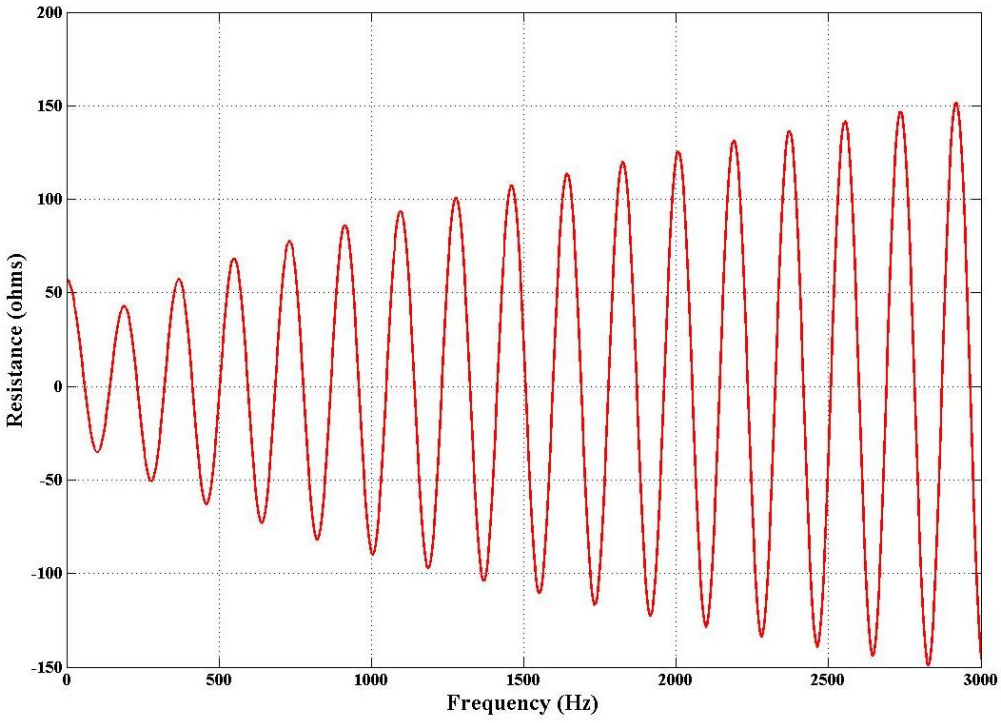

Figure 4.12: Oscillatory behavior of the resistance of the 1000 mile transmission line.

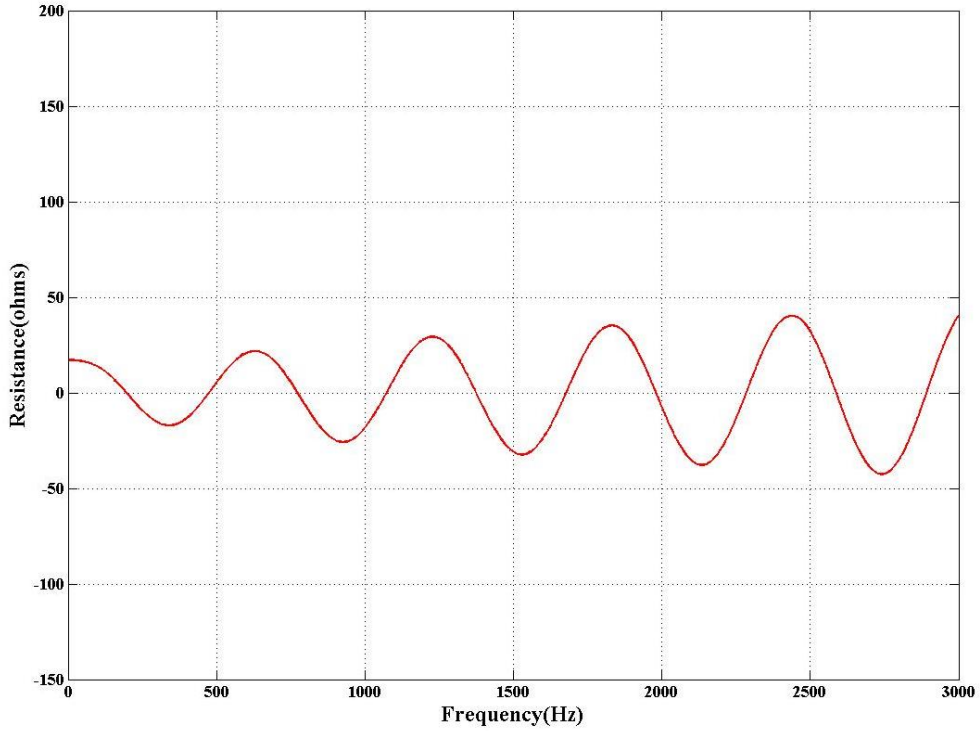

Figure 4.13: Oscillatory behavior of the resistance of the 300 mile transmission line.

Step 2. Oscillation Frequency Change: As also seen from Figures 4.12 and 4.13, the oscillation frequency increases with line length. This change in oscillation frequency with respect to length was approximated using a sixth order polynomial function given by,

$$per(l) = a_1 l^6 + a_2 l^5 + a_3 l^4 + a_4 l^3 + a_5 l^2 + a_6 l + a_7, \tag{4.33}$$

where, $per(l)$ is the period of one full oscillation of resistance value, l is the length of the line and for falcon cable type,

$a_1 = 1.0782 \times 10^{-13}$, $a_2 = -3.9400 \times 10^{-10}$,

$a_3 = 5.7877 \times 10^{-7}$, $a_4 = -4.377 \times 10^{-4}$,

$a_5 = 0.1813$, $a_6 = -40.4520$, and

$a_7 = 4.4259 \times 10^{3}$.

To determine the co-efficients of (4.33), real part of (4.17) was calculated from 1 mile to 1000 miles in steps of 1 mile. The oscillation frequency change obtained from

the analytical equation and from Equation (4.17) are plotted in Figure 4.14. It is observed that the approximated curve nearly coincides with the curve obtained from the analytical equations, with a maximum difference of 4.3%.

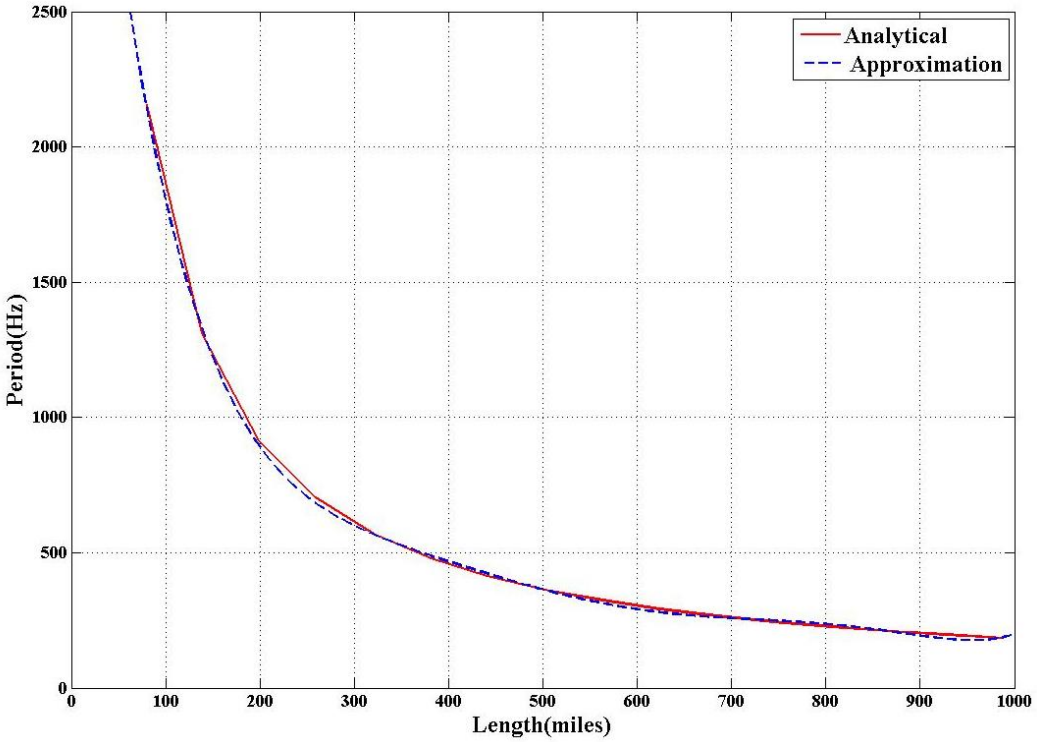

Figure 4.14: Resistance oscillation period of the transmission line versus length.

Step 3. Amplitude Change: From Figure 4.12 and 4.13, it is clear that the resistance value increases as both length and frequency increase. The dc resistance of a round solid cable is given as,

$$R_{dc} = \rho \frac{l}{A}, \tag{4.34}$$

where, ρ is the resistivity, l is the length and A is the area of the cross section of the cable. This expression is used when frequency dependency is not considered, i.e. at zero frequency. The oscillatory nature of the resistance is expressed by a cosine function. The peak amplitude of the oscillation is also required to provide a complete expression for the oscillation. For a 1000 mile long line, the peak amplitude change

of the apparent resistance against frequency for the falcon cable type is shown in Figure 4.15. As seen in Figure 4.15, the curve plotted using the analytical Equation (4.17) shows a dip in peak amplitude at low frequencies up to 167 Hz, followed by a steady increase in peak amplitude. The resistance under consideration here is not the physical resistance of the cable, but the overall resistive nature of the line as given by the real part of the final impedance Equation (4.17). Hence, detail investigation of this amplitude dip of the apparent resistant is out of the scope of this research, however, the relationship of this amplitude dip in terms of line length and signal frequency is derived. This dip in amplitude of the apparent resistance at low frequency is referred to as *apparent low frequency effect* in this thesis. Because the amplitude is exhibiting two different behaviors, two different equations are used to approximate peak amplitude: an exponential function for low frequency and polynomial equation for higher frequencies. The approximation is done in such a way that the addition of the two expressions approximates the whole behavior of the apparent resistance amplitude change.

The peak amplitude at lower frequencies is best approximated by,

$$peak(f, l) = r_{dc} l \, e^{(b_1 l + b_2) f}, \quad 0 \leq f \leq 3000, \tag{4.35}$$

where f is the frequency of the AC signal, and,

$b_1 = -9.0303 \times 10^{-6}$,

$b_2 = -1.5333 \times 10^{-3}$.

At lower frequencies, the apparent low frequency effect is more dominant, and hence this approximation is referred to as apparent low frequency approximation.

For the higher frequencies, the peak amplitude is best approximated using the following equation,

$$peak(f, l) = c \, l \sqrt{f}, \quad 0 \leq f \leq 3000, \tag{4.36}$$

where $c = 2.8315 \times 10^{-3}$. At higher frequencies, the apparent resistance amplitude change show resemblance to the real resistance amplitude changes because of the

skin effect for a ACSR conductor. This effect is more dominant at higher frequencies and this approximation is referred to as skin effect approximation. The resultant expression for peak amplitude is the combination of Equations (4.35) and (4.36) to include both effects:

$$peak(f,l) = r_{dc}l\, e^{(b_1 l + b_2)f} + (c\, l\sqrt{f}). \tag{4.37}$$

Here, when $f = 0$, $peak(f,l)$ reduces to $r_{dc}l$ only, which is the dc resistance of the line. As seen from Figure 4.15, the curve from approximated equation nearly coincides with the curve from the analytical equations. It is observed that the average error of the approximated equation is within 3%.

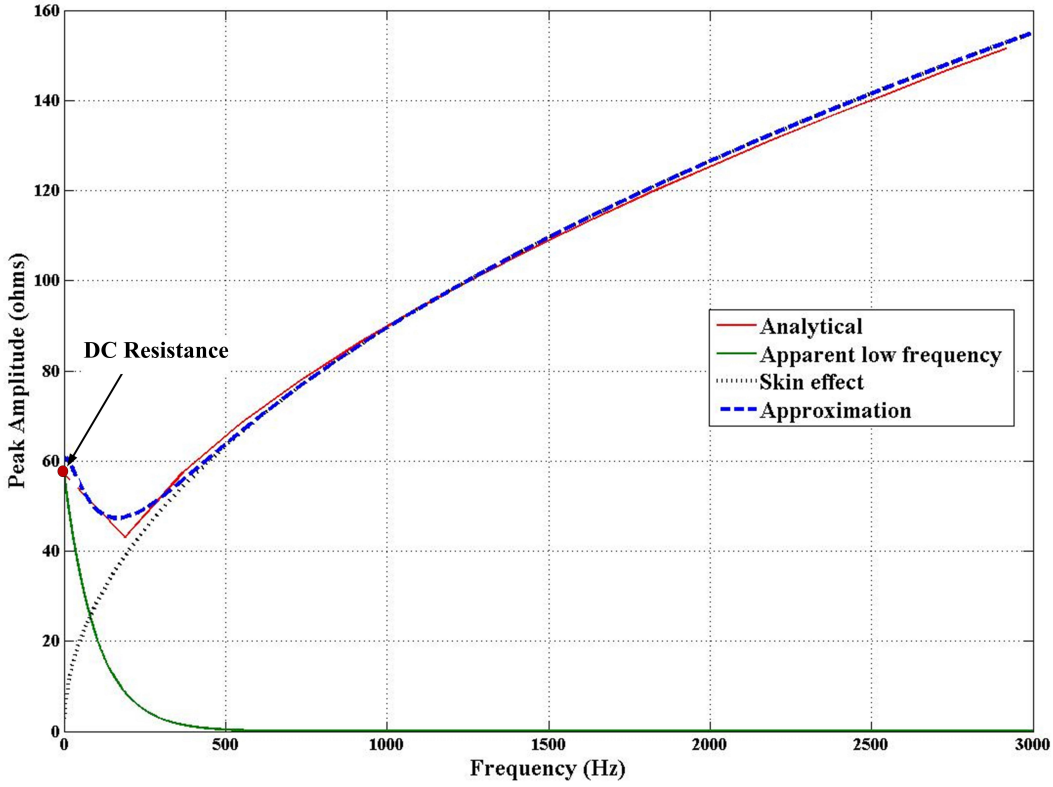

Figure 4.15: Peak resistance amplitude change for a 1000 miles long line.

Step 4. Final Expression: After approximating oscillation type, change in frequency of oscillation, amplitude and change in amplitude, the overall approximated equation can be written. Based on the approximation methods used, the apparent resistance

of a transmission line can be expressed by,

$$R(f,l) = [r_{dc} l\, e^{(b_1 l + b_2)f} + (c\, l\sqrt{f})] \cos\left(\frac{2\pi f}{per(l)}\right). \tag{4.38}$$

Although the specific numbers shown in this equation are valid for the line under consideration(falcon conductor type), the procedure would be the same for other conductor types as well. When the new approximated equation as given in (4.38) is plotted, the Figure 4.16 is obtained.

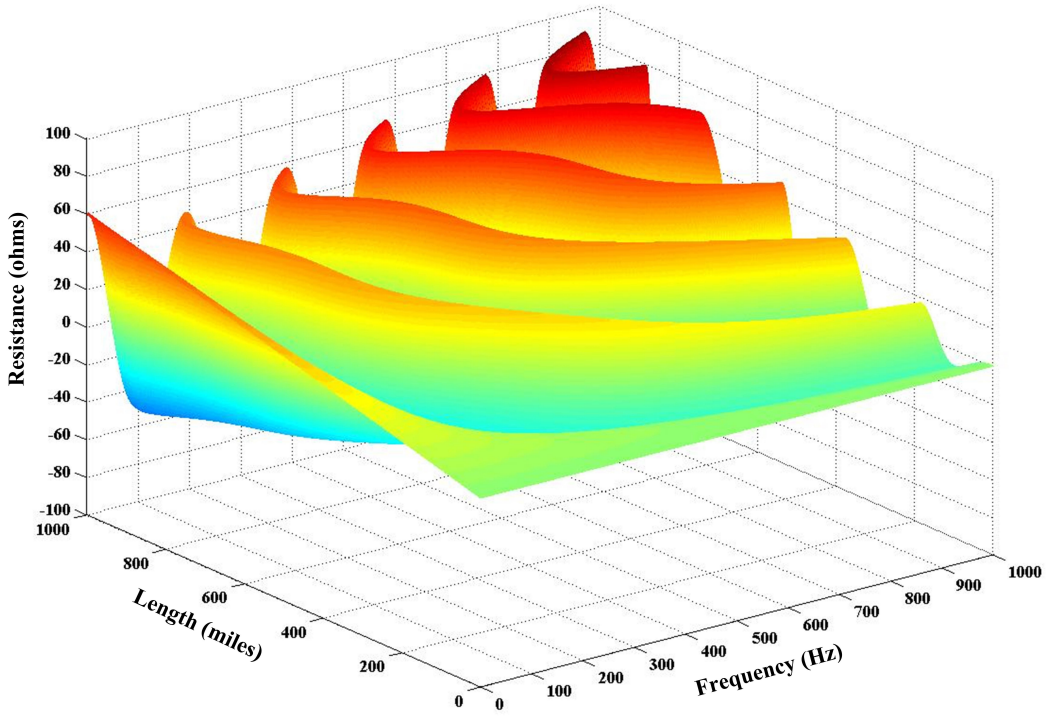

Figure 4.16: Resistance of a transmission line from approximated equation.

4.3.4 Verification and Error Analysis

The least square error approximation method is used for the approximation of the analytical model expression to obtain the proposed approximated expression. For oscillation detection, apparent resistance curve matched exactly with cosine wave and hence error for the nature of oscillation is zero. The oscillation frequency change is approximated using the sixth order polynomial function. From Figure 4.14, it is seen that the curve from approximated equation nearly coincides with the curve from

the analytical equations with maximum difference of 4.3%. For amplitude change approximation, two different equations were used. One was exponential and other a polynomial approximation. As seen from Figure 4.15, the curve from approximated equation nearly coincides with the curve from the analytical equations with average error within 3%. An overall comparison can be done by looking at the plots in Figures 4.11 and 4.16, obtained from the analytical and approximated equations. Define the percentage error as,

$$\text{Error}(\eta) = \frac{|R_{an}| - |R_{app}|}{R_{an}} \times 100\%. \tag{4.39}$$

where, R_{an} is the resistance obtained using the analytical equation and R_{app} is the resistance obtained using the approximated equation. Calculated resistance values for select lengths and frequencies are shown in Table 4.3. Percentage differences between the results obtained with the analytical equations and approximated equations are also shown.

Table 4.3: Apparent resistance calculation–select results.

Line Variables		Resistance Values		
length(miles)	freq.(Hz)	Analytical(Ohms)	Approx.(Ohms)	% difference
100	60	6.03	6.06	0.50
100	120	6.72	6.72	0.00
350	540	23.70	24.30	2.53
445	600	29.80	28.70	3.69
500	390	28.3	27.90	1.41
800	720	66.05	57.36	59.11
850	480	8.24	9.38	13.83
1000	540	64.90	14.37	77.86

A good approximation has been observed for lengths less than 800 miles and frequencies less than 600 Hz. The accuracy of the approximated equation beyond this range (length above 800 miles and frequency above 600 Hz) substantially decreases.

4.3.5 Further Simplification for Frequency-Dependent Distribution Lines

When distributions lines are under consideration, the variable length l in Equation (4.38) can be removed and approximation can be done considering only the frequency as the dependent variable. It has been observed that, for shorter lines less than 3 miles long, the frequency-dependent series resistance and reactance show almost linear dependency on frequency, also seen in Figure 3.3. Hence, the approximated equations for the electrical parameters i.e. series resistance and series reactance are achieved by using first or second order polynomial equations. The one mile-long line of falcon conductor is considered as an example, and the analytical Equations (3.12) and (3.13) are approximated using the polynomial functions. The series resistance approximation is achieved by a linear expression as shown in (4.40).

$$R = (a_1 + a_2 f)\,\Omega. \tag{4.40}$$

For falcon cable,

$a_1 = 0.0560$, and,

$a_2 = 8.898 \times 10^{-4}$.

The series inductive reactance approximation is achieved by a quadratic expression as shown in (4.41).

$$X_L = j(b_1 + b_2 f - b_3 f^2)\,\Omega. \tag{4.41}$$

For falcon cable,

$b_1 = 0.0296$,

$b_2 = 0.0140$, and,

$b_3 = -3.72 \times 10^{-7}$.

The values of a_1, a_2, b_1, b_2, and b_3 for a typical tower geometry of single phase line for multiple conductors are tabulated in Table 4.4.

Table 4.4: Co-efficients values for select conductors for a typical tower geometry.

	Resistance			Reactance			
Conductor	a_1	$a_2 \times 10^{-4}$	% Error	b_1	b_2	$b_3 \times 10^{-7}$	% Error
Bluejay	0.0865	9.609	2.20	0.0319	0.0145	3.65	1.11
Bobolink	0.0658	9.119	2.33	0.0296	0.0142	3.59	1.37
Cardinal	0.1104	9.878	1.96	0.0313	0.0147	3.65	1.32
Condor	0.1386	10.77	0.97	0.0327	0.0149	3.67	1.27
Crane	0.1226	10.04	1.93	0.0318	0.0148	3.66	1.31
Crow	0.1542	10.20	2.15	0.0331	0.0150	3.71	1.26
Curlew	0.0988	9.562	2.15	0.0308	0.0146	3.65	1.54
Dove	0.2093	9.194	4.09	0.0335	0.0154	3.92	1.65
Duck	0.1874	11.35	1.05	0.0332	0.0153	3.90	1.61
Eagle	0.2041	9.272	3.93	0.0357	0.0152	3.83	0.96
Falcon	0.0560	8.898	2.39	0.0296	0.0140	3.72	1.04
Goose	0.1765	11.03	1.17	0.0350	0.0152	3.83	0.99
Grackle	0.0829	9.390	2.14	0.0307	0.0144	3.77	1.01
Parrot	0.0603	8.993	2.33	0.0298	0.0141	3.73	1.00
Pheasant	0.0762	9.278	2.19	0.0304	0.0143	3.76	1.02
Squab	0.1748	9.889	2.78	0.0329	0.0152	3.97	1.40

The shunt capacitive admittance does not deviate appreciably when using the analytical equations as compared to the conventional expression. Hence the conventional expression is used as in (4.42).

$$Y_C = c\,\omega\ \Omega. \tag{4.42}$$

For falcon cable, $c = 1.8608 \times 10^{-6}$. The shunt conductance is neglected. These constants a_n, b_n and c_n are dependent on line geometry and conductor type. Since the tower geometry and the types of cables are standardized, the constant values can be tabulated for quick reference. Numerical results of line series resistance and reactance for some select frequencies are shown in Table 4.5. In Table 4.5, R is the series resistance and X_L is the series reactance. Considering up to the 25th harmonic, the average error of the series resistance in the constant exact PI model is 82.8% and in proposed model is only 1.63%. Similarly, the average error of series reactance in exact PI model is 19.19% and in the proposed model is 0.98%. The errors arising due to the constant exact PI model have been significantly reduced while using the proposed expressions.

Table 4.5: Series resistance and reactance comparison at select frequencies.

	Analytical		Exact PI		Proposed	
	f (Hz)	Value (Ω)	Value (Ω)	% diff	Value (Ω)	% diff
R	60	0.34	0.34	0.00	0.34	0.00
	180	0.91	0.34	45.5	0.61	2.53
	300	1.47	0.34	76.8	1.42	3.57
	420	2.02	0.34	83.1	1.96	3.13
	540	2.56	0.34	86.6	2.50	2.57
	660	3.10	0.34	88.9	3.04	2.02
	840	3.89	0.34	91.23	3.85	1.22
	1140	5.20	0.34	93.4	5.20	0.00
	1320	5.97	0.34	94.28	6.01	0.63
	1500	6.73	0.34	97.9	6.82	1.25
X_L	60	2.59	2.59	0.00	2.60	0.40
	180	7.19	7.78	8.16	6.96	3.22
	300	11.54	12.97	12.38	11.25	2.49
	420	15.74	18.16	15.33	15.47	1.70
	540	19.85	23.35	17.62	19.63	1.10
	660	23.88	28.54	19.51	23.72	0.67
	840	29.81	36.32	21.84	29.72	0.30
	1140	39.46	49.29	24.92	39.38	0.19
	1320	45.14	57.08	26.45	44.97	0.36
	1500	50.75	64.86	27.81	50.41	0.66

4.3.6 Discussion

The approximated equations can have multiple advantages. The first thing to mention which is achieved using such approximation is the speed of execution in digital simulations. Matlab is used in Windows 7 having 64 bit operating system with Intel(R) Core(TM)2 CPU 6700 @ 2.66 GHz and 2.66 GHz with 4.00 GB memory. In this system, the time taken to calculate resistance for a given cable type, length and frequency of interest were calculated. The time taken by the analytical expression was 1.8175 ms and time taken by the approximated equation was only 7.0 μs. The majority of time in computation of the analytical expression was taken by the execution of the kelvin functions. The expression of the resistance explicitly as a function of length and frequency could be used in analyzing power losses involving harmonics. It can be used to model frequency dependent transmission line models for harmonic analysis as well.

This section discussed a technique to simplify the expressions for the frequency-dependent power distribution line parameters, namely: series resistance and series inductance. Shunt conductance and shunt susceptance have very small deviation and conventional expressions are used. Polynomial approximation techniques, which implement least square methods, are applied to obtain simplified parametric variables. Although this modeling approach has multiple advantages, this method does not yet provide the generic frequency-dependent power line model. There is also a room for minimizing the error of this approximated model. Next chapter discusses about a novel approach of frequency-dependent power line modeling which provides a generic frequency-dependent power line model and highly minimized the errors seen in this modeling approach.

CHAPTER 5: NOVEL FREQUENCY-DEPENDENT POWER LINE MODELS FOR STEADY STATE ANALYSIS

5.1 Overview

This chapter discusses the development and derivation of a generic frequency-dependent electric power line model intended to use for steady state harmonic analysis. First, the modeling approach is briefly discussed. Then the model expressions are derived using the rational approximation method-Vector Fitting technique. After that, the model expressions are represented in terms of passive R-L-C components. The derivation of the circuits are shown. Derivation for both single phase and three phase lines are discussed.

5.2 Modeling Approach

A novel frequency-dependent model for electric power lines to be used in steady-state harmonic studies is derived. First, the differential equations representing the distributed nature of the line electrical parameters are considered; frequency dependency due to the effect of ground return and the skin effect is then incorporated. These derived equations represent what in this thesis is defined as analytical model, used as benchmark for model comparison. The analytical model has been described and derived in chapter 3. The vector fitting technique, used in frequency-dependent transmission line modeling for electromagnetic transient (EMT) analysis, is used here to approximate the analytical model and derive a frequency-dependent frequency-domain model. A passive circuit realization of the proposed model in a PI structure is presented and can be directly implemented in steady-state analysis tools such as harmonic power flow solvers.

5.3 Proposed Frequency-Dependent Line Model

The *proposed model* is derived from the *analytical model* (3.10) and (3.11) using the vector fitting technique [49]. Each element of the numerical ($phase \times phase$) matrices $Z'_a(f)$ and $Y'_a(f)$ is approximated by the rational pole-residue model as shown in (5.1) to obtain the *proposed model*.

$$f(s) = \sum_{n=1}^{N} \frac{c_n}{s - a_n} + d + s\,h. \tag{5.1}$$

The residues c_n and poles a_n are either real quantities or come in complex conjugate pairs, while d and h are real. Specifically, the approximation to obtain c_n, a_n, d and h is performed in two stages as explained below.

In the first stage, an initial guess of the starting poles $\bar{a}_n$ is made. An unknown function $\sigma(s)$ is introduced and multiplied by $f(s)$ to create an augmented problem as shown in (5.2).

$$\begin{bmatrix} \sigma(s)f(s) \\ \\ \sigma(s) \end{bmatrix} \approx \begin{bmatrix} \sum\limits_{n=1}^{N} \frac{c_n}{s-\bar{a}_n} + d + s\,h \\ \\ \sum\limits_{n=1}^{N} \frac{\tilde{c}_n}{s-\bar{a}_n} + 1 \end{bmatrix}. \tag{5.2}$$

After multiplying the second row of (5.2) with $f(s)$, we can write,

$$\left(\sum_{n=1}^{N} \frac{c_n}{s - \bar{a}_n} + d + s\,h \right) \approx \left(\sum_{n=1}^{N} \frac{\tilde{c}_n}{s - \bar{a}_n} + 1 \right) f(s). \tag{5.3}$$

This can be written in compact form as,

$$(\sigma\, f)_{fit}(s) \approx \sigma_{fit}(s)\, f(s), \tag{5.4}$$

with the unknowns c_n, d, h and $\tilde{c}_n$. For multiple frequency points, this is an overdetermined problem in linear form,

$$A\,x = b\,, \tag{5.5}$$

where the unknowns are in the solution vector x. Now, $f(s)$ approximation is obtained from (5.3). The functions can be expressed in partial fractions in terms of zeros and

poles as,

$$(\sigma\, f)_{fit}(s) = h\frac{\prod_{n=1}^{N+1}(s - z_n)}{\prod_{n=1}^{N}(s - \bar{a}_n)}\,, \text{ and} \tag{5.6}$$

$$\sigma_{fit}(s) = \frac{\prod_{n=1}^{N}(s - \tilde{z}_n)}{\prod_{n=1}^{N}(s - \bar{a}_n)}\,. \tag{5.7}$$

Using (5.6) and (5.7), the following expression is obtained,

$$f(s) = \frac{(\sigma\, f)_{fit}(s)}{\sigma_{fit}(s)} = h\frac{\prod_{n=1}^{N+1}(s - z_n)}{\prod_{n=1}^{N}(s - \tilde{z}_n)}\,. \tag{5.8}$$

Equation (5.8) shows that the poles of $f(s)$ are equal to the zeros of $\sigma_{fit}(s)$.

In the second stage, residues can be identified by using the original Equation (5.1). This again creates an overdetermined linear problem of form $Ax = b$. The solution vector x then has the c_n, d and h. For higher level of detail on the vector fitting technique, including discussion on stability, one can look at [49].

The *proposed model* series impedance Z'_p and shunt admittance Y'_p are therefore obtained from this approximation of the *analytical model*. Z'_p and Y'_p are expressed as the rational pole-residue model, i.e. a transfer function, in the form of ratio of zeros to poles as,

$$Z'_p = \frac{Zr_z(s)}{Pl_z(s)}\,, \tag{5.9}$$

$$\frac{Y'_p}{2} = \frac{Zr_y(s)}{Pl_y(s)}\,, \tag{5.10}$$

where the subscript z indicates impedance and y indicates admittance, $Zr_z(s)$ is the set of zeros and $Pl_y(s)$ is the set of poles. Hence, the series and shunt elements of the proposed PI-structure model are represented by transfer functions as shown in

Figure 5.1.

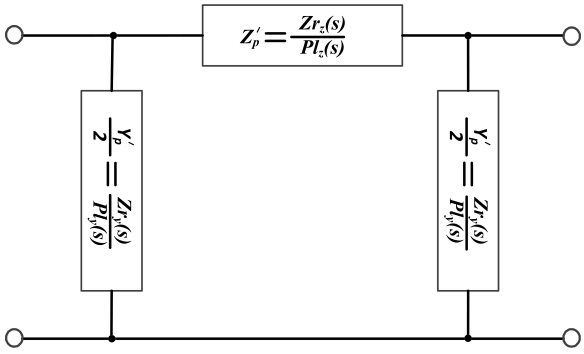

Figure 5.1: Proposed model with shunt and series elements in PI structure expressed as transfer functions.

Since the *proposed model* is derived for use in steady state harmonic analysis, the model accuracy at inter-harmonic frequencies is not as critical. Hence, a weight is introduced in (5.5) to achieve prioritized accuracy based on the frequency as,

$$\boldsymbol{W}\,\boldsymbol{A}\,\boldsymbol{x} = \boldsymbol{W}\,\boldsymbol{b}\,, \tag{5.11}$$

where $\boldsymbol{W}$ is the introduced weighting diagonal matrix of order $N \times N$, $\boldsymbol{A}$ is the matrix of order $N \times P$, $\boldsymbol{b}$ is the matrix of order $N \times 1$, N is the number of frequency points under consideration and P is the number of unknowns to solve for. This ensures desired accuracy at the harmonic frequencies without unnecessarily increasing the order of approximation, i.e. the number of poles. Generally, the use of $2N$ poles, where N is the number of frequencies of interest, results in an accurate representation of the analytical model behavior. As shown in subsequent sections, for shorter lines, 8 poles can be more than sufficient for up to the 25th harmonic frequency.

The proposed line model is derived by approximating the derived benchmark analytical model. The analytical model can be used for higher accuracy; however, for each frequency of interest, a separate analytical model has to be used. The proposed model avoids this need for multiple models by providing a single generic model for all harmonic frequencies of interest without much affecting accuracy. Also, the simulation time is faster while using the proposed model as compared to the analytical

model. The simulation speed of the proposed model can be faster than the analytical model by a factor of 2 to few hundreds, depending on the length of the line, the number of harmonic frequencies under consideration and the predefined error of accuracy. This speed during the simulation comes with the cost of off-line model derivation time since the proposed model is derived by approximating analytical model which requires the analytical model itself to be derived and executed. Once the off-line modeling of each line in a system is computed, the computational effort in system level analysis(such as HPF) is much smaller than if the analytical model were used.

5.4 Passive Circuit Realization

The transfer function obtained from the approximation can be realized using passive components. Hence, each series and shunt element can be represented by an R-L-C network. The pole residue model of the derived model can be compared to the Laplace domain impedance of appropriate circuit. Because each of the shunt or series element are being synthesized, single port circuit structure is considered.

The pole residue model in (5.1) can be rewritten as,

$$f(s) = \frac{c_1}{s - a_1} + \frac{c_2}{s - a_2} + ... + \frac{c_N}{s - a_N} + d + s\,h. \tag{5.12}$$

The residues c_n and poles a_n are either real quantities or come in complex conjugate pairs, while d and h are real. Depending on the residues' and poles' real or complex status, the passive circuit can be different. Both types of derivations are shown as follows.

5.4.1 Real Residues and Poles

The last expression of (5.12), $d + sh$ can be expressed as an impedance because of its equivalent form $R + sL$. The first term of (5.12) can be represented by a parallel R-C circuit as shown in Figure 5.2.

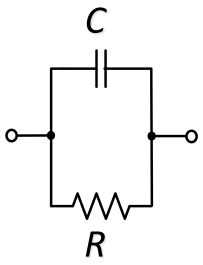

Figure 5.2: R-C parallel circuit.

For a parallel R-C circuit, the impedance can be calculated as,

$$Z_{RC} = \frac{R \times \frac{1}{Cs}}{R + \frac{1}{Cs}} = \frac{\frac{1}{C}}{s + \frac{1}{RC}}. \tag{5.13}$$

Equation (5.13) can be compared to the first term of (5.12). Comparing the c_1 and a_1, the values of R and C can be calculated as,

$$C = \frac{1}{c_1}, \text{ and} \tag{5.14}$$

$$R = -\left(\frac{c_1}{a_1}\right). \tag{5.15}$$

Similarly, each of the successive expression of (5.12) can be compared to (5.13) and the values of R and C can be calculated and then can be connected in series to match the full expression. The equivalent figure is as shown in Figure 5.3.

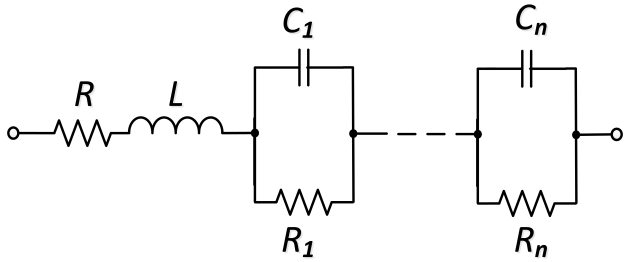

Figure 5.3: R-L-C synthesis of real residues c_n and poles a_n.

5.4.2 Complex Conjugate Residues and Poles

If the c_n and a_n in (5.1) are complex, then another network has to be derived. Since the residues and poles c_n and a_n always comes in conjugate pairs, (5.1) can be rewritten as,

$$f(s) = \frac{p_1 + q_1 j}{s - (x_1 + y_1 j)} + \frac{p_1 - q_1 j}{s - (x_1 - y_1 j)} + ... + \frac{p_N + q_N j}{s - (x_N + y_N j)} + \frac{p_N - q_N j}{s - (x_N - y_N j)} + d + s\,h, \tag{5.16}$$

where,

$c_1 = p_1 + q_1 j$, and

$a_1 = x_1 + y_1 j$ and so on.

The last expression of (5.16), $(d + sh)$ is represented as discussed earlier as an impedance. The first two expressions of (5.16) can be combined as,

$$\frac{p_1 + q_1 j}{s - (x_1 + y_1 j)} + \frac{p_1 - q_1 j}{s - (x_1 - y_1 j)} = \frac{2p_1 s - 2p_1 x_1 - 2q_1 y_1}{s^2 - 2sx_1 + x_1^2 + y_1^2} \tag{5.17}$$

The transfer function as seen in (5.17) is of second order. Hence, two energy storing components, i.e. L and C has to be used. A number of different circuit combination has been tested. The network block as shown in Figure 5.4 was a match.

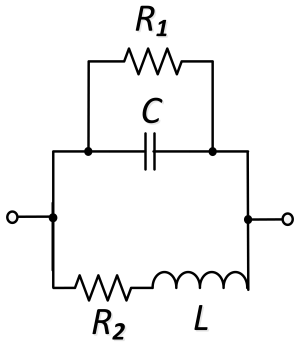

Figure 5.4: R-L-C block.

The impedance function if the network in Laplace domain is given as,

$$Z = \frac{(R_1 + Ls)\left(\dfrac{\dfrac{1}{C}}{s + \dfrac{1}{R_2 C}}\right)}{R_1 + Ls + \left(\dfrac{\dfrac{1}{C}}{s + \dfrac{1}{R_2 C}}\right)} \tag{5.18}$$

This can be simplified to make it comparable to (5.17) as,

$$Z = \frac{\dfrac{R_1}{LC} + \dfrac{s}{C}}{s^2 + \left(\dfrac{R_1}{L} + \dfrac{1}{R_2 C}\right) s + \dfrac{1}{L}\left(\dfrac{R_1}{R_2 C} + \dfrac{1}{C}\right)} \tag{5.19}$$

Comparing (5.17) and (5.19), we can write,

$$\frac{1}{C} = 2p_1, \tag{5.20}$$

$$\frac{R_1}{LC} = -2p_1 x_1 - 2q_1 y_1, \tag{5.21}$$

$$\frac{R_1}{L} + \frac{1}{R_2 C} = -2x_1, \text{ and} \tag{5.22}$$

$$\frac{1}{L}\left(\frac{R_1}{R_2 C} + \frac{1}{C}\right) = x_1^2 + y_1^2. \tag{5.23}$$

This gives four equations and four variables to solve. Solving (5.20) - (5.23), the values of R_1, R_2, L and C can be calculated in terms of p_1, q_1, x_1 and y_1. This can be repeated for all other residues and poles. Then the resulting network is the series connection of these blocks as shown in Figure 5.5.

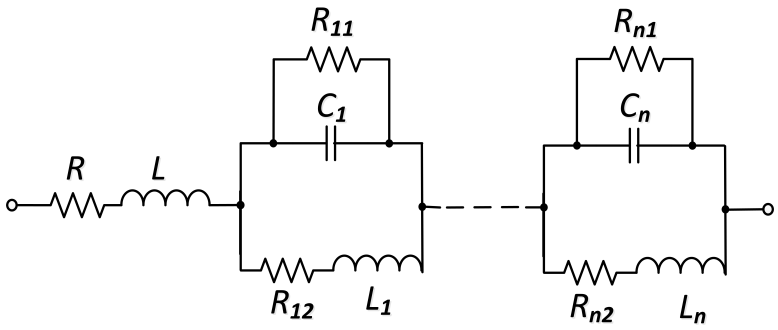

Figure 5.5: *R-L-C* synthesis of complex conjugate pair residues c_n and poles a_n.

A pair of real residues and a pair of real poles can also be represented by Figure 5.5. The first two expressions in (5.12) can be combined and expressed as,

$$\frac{c_1}{s-a_1}+\frac{c_2}{s-a_2}=\frac{s(c_1+c_2)-(c_1a_2+c_2a_1)}{s^2-(a_1+a_2)s+a_1a_2}. \tag{5.24}$$

This can be compared with (5.19) and we have,

$$\frac{R_1}{LC}=-(c_1a_2+c_2a_1), \tag{5.25}$$

$$\frac{1}{C}=c_1+c_2, \tag{5.26}$$

$$\frac{R_1}{L}+\frac{1}{R_2C}=-(a_1+a_2), \text{ and} \tag{5.27}$$

$$\frac{1}{L}\left(\frac{R_1}{R_2C}+\frac{1}{C}\right)=a_1a_2. \tag{5.28}$$

Solving (5.25)-(5.28), the values of the R_1, R_2, L and C can be obtained.

5.4.3 *R-L-C* Network: Single Phase Line

The transfer function of the form (5.1) can be represented by an *R-L-C* network. The residues c_n and poles a_n are either real quantities or come in complex conjugate pairs, while d and h are real. If the residue c_n and poles a_n are real quantities, the synthesized circuit could be represented by series of parallel *R-C* elements with one R and L to represent d and h as shown in Figure 5.3. If the residue c_n and poles a_n

are complex conjugate, the synthesized circuit could be represented by a circuit with R-L-C elements with one R and L to represent d and h as shown in Figure 5.5.

5.4.4 R-L-C Network: Multi Phase Line

Fig 5.5 shows the R-L-C realization of a single phase line. For a multi-phase line, the mutual impedance can be represented by a mutually coupled transformer. Moreover, the effect of mutual admittance is included by inserting a network block between the lines. For a balanced three phase line, the circuit representation is as shown in Figure 5.6.

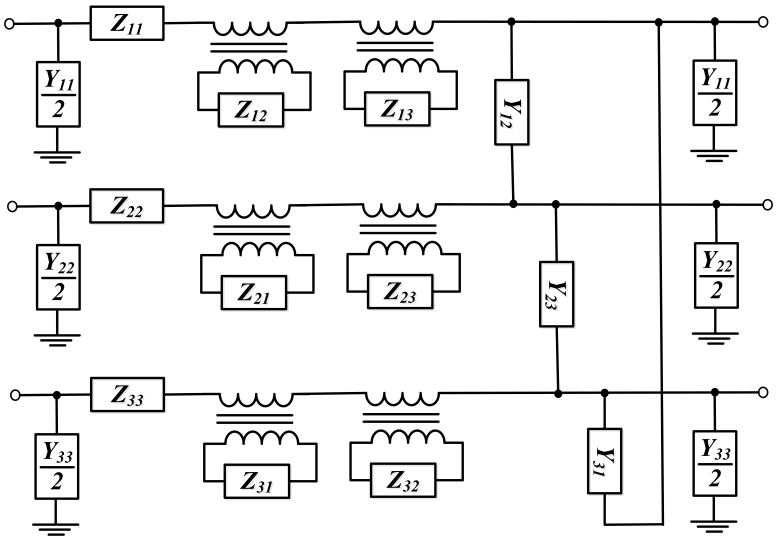

Figure 5.6: R-L-C synthesis of a three-phase line with mutual parameters.

In an unbalanced multi phase case, different amounts of current are flowing in the individual phases. Though the value of the mutual impedance remains the same, the change in current in one phase affects the change in another phase voltage. During this study, the authors have found that, in many cases of distribution lines, the mutual impedances and admittances have almost linear dependency on frequency for distribution lines up to 3 miles length. The series and shunt mutual reactances for a 3 mile overhead line with dove cable is shown in Figure 5.7. For this reason, they can simply be represented by an inductor or a capacitor. The R-L-C network as shown in Figure 5.6 can be changed to address the unbalance by obtaining a generic

approximated circuit as shown in Figure 5.8.

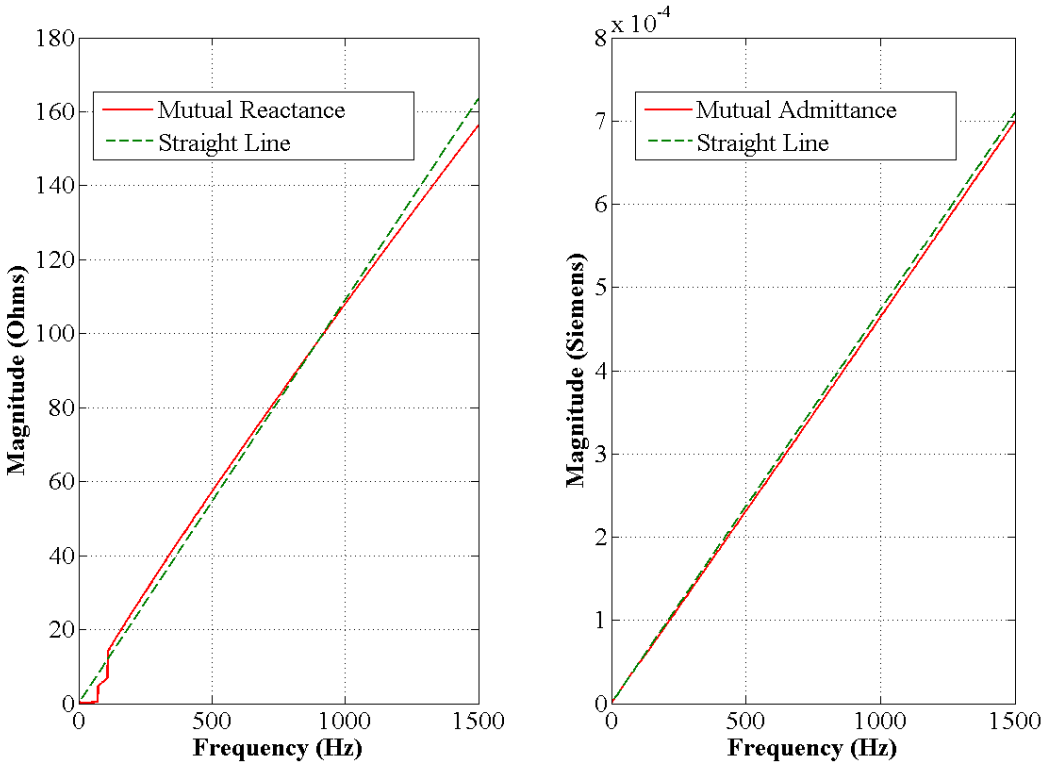

Figure 5.7: Series and shunt mutual reactances for a 3 mile overhead line with dove cable.

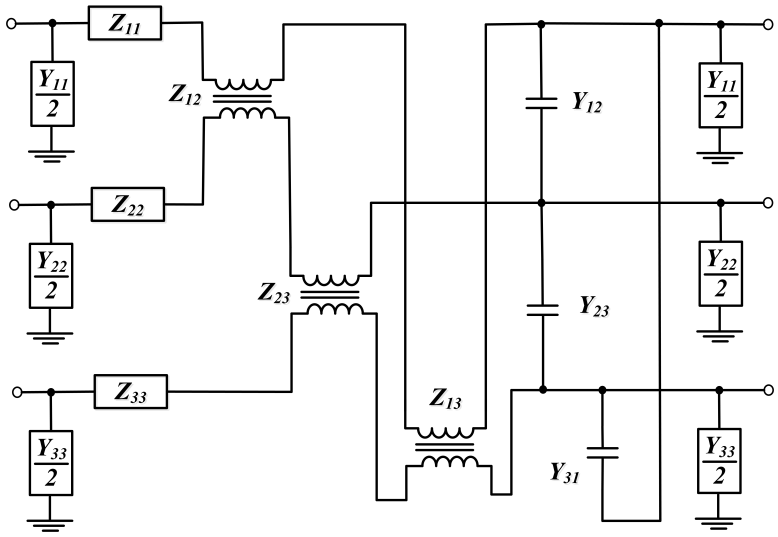

Figure 5.8: Simplified *R-L-C* synthesis of a three-phase line with mutual parameters.

5.5 Proposed Line Modeling Algorithm

This section summarizes the procedure used to derive the proposed Vector-fitted frequency-dependent line model. The proposed line model has two predefined modeling criteria to be set before model derivation:

- Number of harmonic frequencies of interest, N, and
- Level of accuracy explained in terms of absolute mean error between the analytical model and proposed the model series impedance and shunt admittances, λ.

For the test cases presented in this thesis, for example, the number of harmonic frequencies of interest was set to 25, i.e. $N = 25$ and the error limit was set to a maximum 2% i.e. $\lambda \leq 2\%$.

Next, the line information is to be collected:

- Physical properties of the line;
- Line geometry and line length.

The description of the step-by-step procedure follows.

Step 1. Analytical Line Derivation: After the predefined line modeling criteria has been set and the line information has been collected, the analytical model, which includes the frequency-dependent effects of the ground return and the skin effect is derived (as discussed in detail in chapter 3). The analytical model is composed of the set of N number of exact PI models for N number of harmonic frequencies of interest. The frequency response of up to $60N$ Hz is calculated for series impedance and shunt admittance.

Step 2. Approximation Procedure: The analytical line model is then approximated using the vector fitting technique. Specifically, the N number of exact PI models is approximated to a single exact PI model. Each of the shunt and series element of the N exact PI models is approximated using the pole residue model and expressed as transfer function as a ratio of zeros to poles. For each series and shunt element,

the approximation procedure is carried out. The approximation starts with 2 poles. If the 2-pole approximation results in a model accuracy within the average mean error of $\lambda\%$ from the analytical model, this step is complete. Else, then the poles are increased in increment of 2 until the $\lambda\%$ error limit is achieved as described in the vector fitting technique. It has been observed that to maintain an error limit of 2%, a maximum $2N$ number of poles were need to approximated N number of harmonic frequencies of interest for a line length up to 80 miles in the three phase line case and up to 120 miles for the single phase line case. Beyond these line lengths, it was observed that a larger than $2N$ number of poles were needed to approximate within the example 2% error.

Step 3. Circuit Realization: The approximated functions are then realized in circuit by using only passive components. First, shunt and series elements are realized in circuit representation as described in previously in section 5.4. After that, the mutual parameters are treated. The same circuit realization as shown in Figure 5.5 can be used for mutual parameters. However, it has been observed that the mutual parameters showed an approximately linear dependency on frequency. For this reason, the mutual impedance is approximated by an inductor and the mutual admittance by a capacitance. The values of the mutual parameters are replaced directly from the slope of the approximated line, calculated from linear regression of the data for mutual parameters. The details of the circuit realization procedure are discussed previously in section 5.4.

The modeling procedure is graphically summarized in the flowchart as shown in Figure 5.9. The proposed model used in steady state harmonic analysis is more accurate than commonly used steady-state line models such as the PI model and retains approximately the similar accuracy of the transient models for the frequencies of interest. This is verified with various test cases, which are presented in the next chapter. Hence, this model removes the necessity to run time domain simulations if one wants

to use accurate frequency-dependent line models. This makes the simulation time faster for accurate steady state harmonic analysis in system level studies.

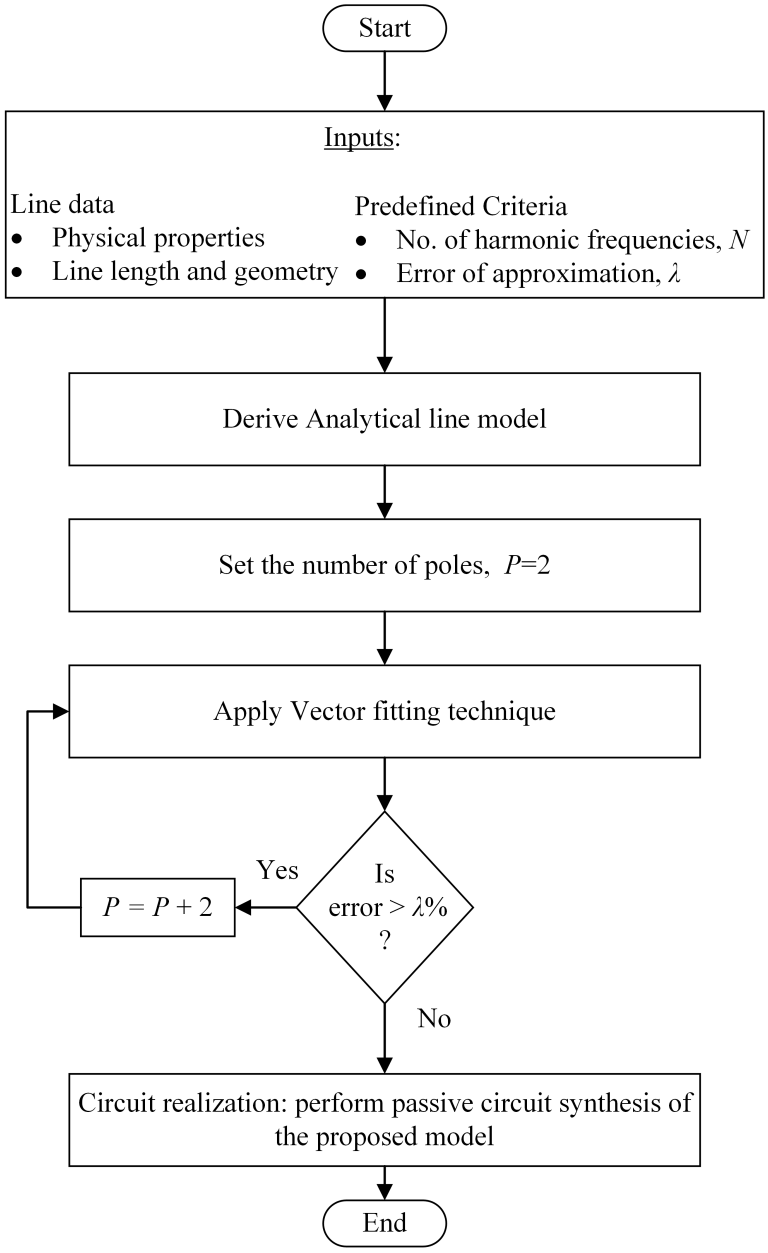

Figure 5.9: Flowchart to derive the proposed line model.

CHAPTER 6: MODEL EVALUATION AND SIMULATION RESULTS

6.1 Overview

This chapter discusses the development of the test cases used to evaluate the proposed frequency-dependent power line models and the simulation results. First, the types of lines and cables used in the test cases are discussed. Then the test cases are presented. After that, single phase and multi phase harmonic power flow is performed for the test cases using the proposed line model, the analytical line model(as benchmark) and other commonly used line models. The proposed model performance is compared to the other line models in terms of harmonic power flow results, and resulting harmonic distortions levels and harmonic losses. The R-L-C circuit representations for some example test cases are also computed.

6.2 Test Lines and Cables

In different test cases, multiple types of cables are used. Different overhead ACSR and underground concentric neutral and tape shielded cables are used. The line types are discussed briefly in the following subsections.

6.2.1 Overhead Lines

The cables used in the test case overhead lines are Aluminum-Conductor Steel Reinforced (ACSR) cables. The outer strands are high-purity aluminum alloy, chosen for its excellent conductivity, low weight and low cost. The strand at the center is designed for strength and support the weight so that the aluminum is not stretched. Hence, the center strand is steel chosen for its ductility. ACSR cables comes in several sizes, which are typically standardized. One example of 24/7 ACSR cable cross section is shown in Figure 6.1.

The ACSR cable types used in this research are listed as follows.

- ACSR 1,590,000 54/19
- ACSR 556,500 26/7
- ACSR 4/0 6/1
- ACSR 1/0

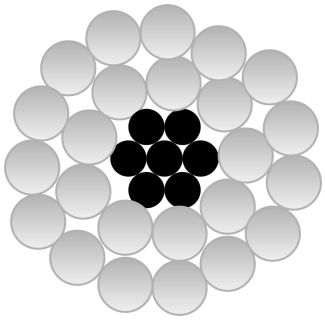

Figure 6.1: Cross section of 24/7 ACSR cable.

6.2.2 Underground Lines

Underground cables are laid out for mainly aesthetic purpose. Though they are more expensive, they also have some advantages over overhead lines. Underground lines are less vulnerable to air borne elements like wind and ice. Also, in some areas like downtown districts of cities, they are more practical than overhead lines. In this research, two types of underground cables, namely concentric neutral and tape shielded cables are used. These cables are used in IEEE 13 node test feeder.

The cross section of a concentric neutral cable is shown in Figure 6.2. The cable consists of a central phase conductor covered by a thin layer of nonmetallic semi-conducting screen to which is bonded the insulating material. The insulation is then covered by a semi-conducting insulating screen. The solid strands of concentric neutral are spiraled around the semi conducting screen with a uniform spacing between the strands. Some cables will also have an insulating jacket encircling the neutral strands [68].

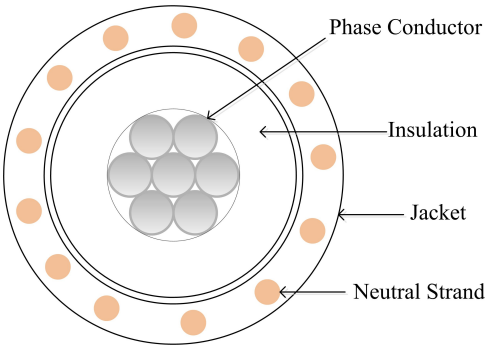

Figure 6.2: Cross section of a concentric neutral cable.

The cross section of a tape shielded cable is show in Figure 6.3. The cable consists of a central phase conductor covered by a thin layer of nonmetallic semi-conducting screen to which is bonded the insulating material. The insulation is covered by a semi-conducing insulating screen. The shield is bare copper tape helically applied around the insulation screen. An insulating jacket encircles the tape shield [68].

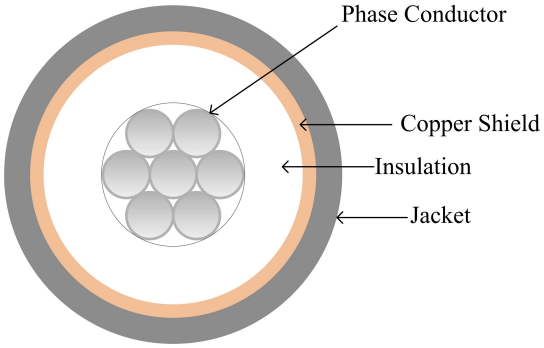

Figure 6.3: Cross section of a tape shielded cable.

The types of underground cables used in this work are listed as follows.

1. Concentric neutral cable
    - phase line: AA 250,000 cmil
    - neutral line: 13 Concentric Copper 14 kcmil
2. Tape shielded cable
    - phase line: AA 1/0 cmil
    - neutral line: Copper 1/0

6.3 Single Line Test Cases for Model Evaluation

In the first test case, the line parameter values are calculated using different models and compared against each other. Then after, a two bus case with a single phase line is considered. Line parameters, as well as the receiving end voltages obtained using different models are compared. Then, a three phase line is considered and receiving end voltages obtained using different models are compared. The *R-L-C* network of the single phase and three phase lines are also derived.

6.3.1 Case I: Series Impedance Evaluation

A three-phase balanced and transposed overhead line of falcon cable type is considered for this study. The conductors are assumed to be equilaterally spaced at 15 ft and tower height is assumed to be 50 ft. Because the balanced three phase line is considered, per phase analysis can be done and hence, calculations for only one phase are shown.

First, the values of the series resistance and series reactance at frequencies from 1 Hz to 1500 Hz using different models are calculated. For a unit length line, the results are as shown in Figure 6.4. Fig. 6.4 also shows the frequency response obtained using the *analytical model* and the *constant exact PI model*. It is noted that the *proposed model*'s error with respect to the *analytical model* (benchmark) is less than the error obtained with the *constant exact PI model*.

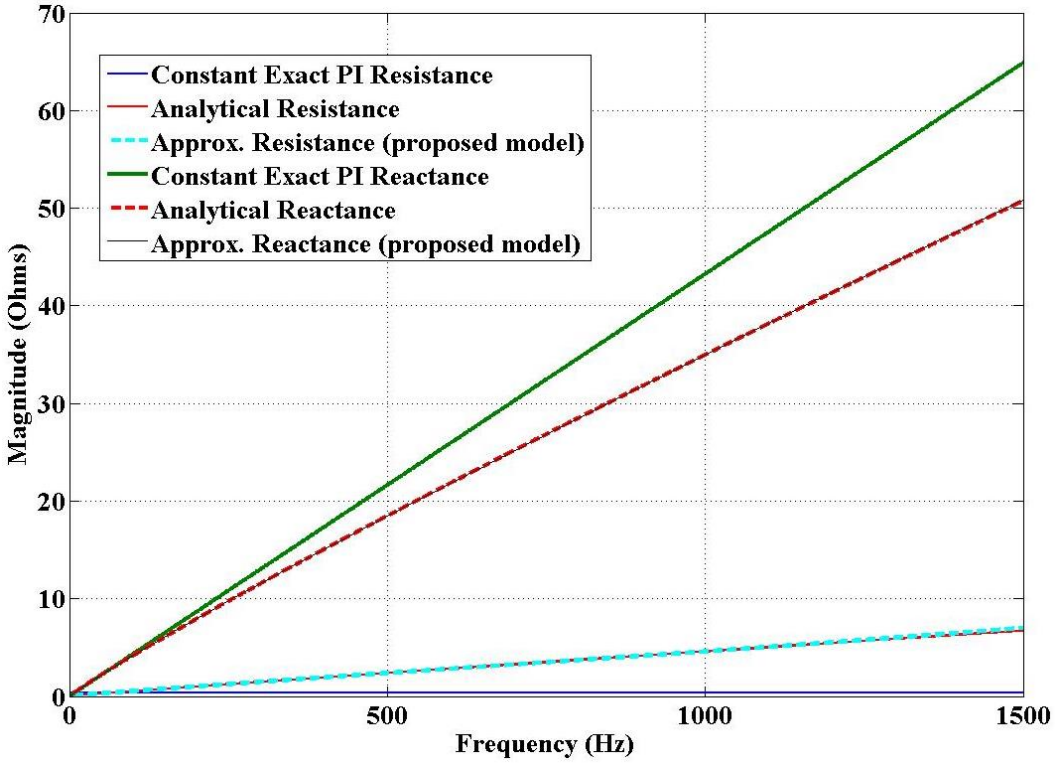

Figure 6.4: Line parameter comparison of different models for a unit length line of falcon cable.

6.3.1.1 Pole Numbers and Frequency Window

This test line was evaluated with different number of poles in the approximation process and also on different frequency window. Fig. 6.5 shows magnitude of the impedance vs. frequency resulting from the use of different numbers of poles in the Vector Fitting technique and their comparison with the *analytical* and the *constant exact PI* models. Various forms of the *proposed model* are presented; specifically, models with 2, 10, 20 and 30 poles in 5 kHz and 1.5 kHz approximation window are considered. It is observed that if more poles are used, the accuracy increases. The decrease in approximation window also increases accuracy. The 2-pole and 10-pole approximations are shown in Figure 6.6 in smaller frequency window to show that the approximation results are better in smaller frequency window. One can compare how the same 10-pole approximation is behaving in 5000 Hz approximation window in Figure 6.5 and in 1500 Hz approximation window in Figure 6.6, latter being more

accurate.

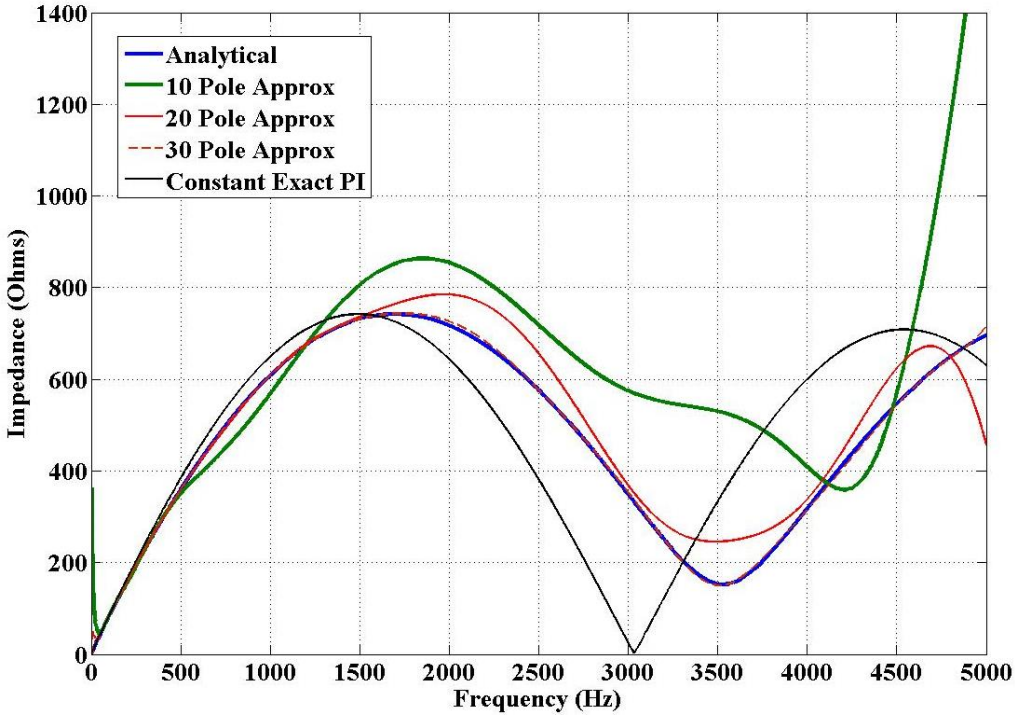

Figure 6.5: Series impedance of the 20 mile falcon cable line for various models.

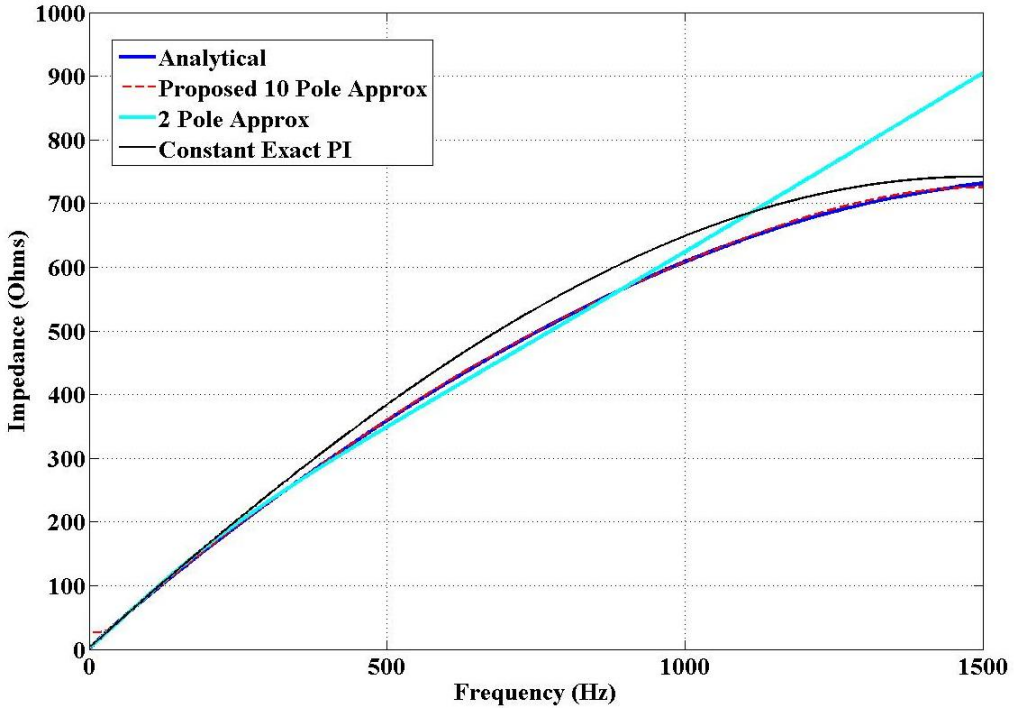

Figure 6.6: Equivalent impedance of the *proposed model* and other models.

6.3.1.2 Series Impedance Comparison

The percentage error of the 10-pole approximation function is calculated and compared with the other models. Table 6.1 shows the comparison between all the models. For the first 25 harmonic frequencies as shown in Table 6.1, it is clear that the *proposed model* is more accurate than the *constant exact PI model*. The individual percentage error of the proposed model is always below 1% and the maximum error is only 0.84% which occurs at the 25th harmonic. The *constant exact PI* has an average error of 5.31%, the 30 pole approximation done over 5 kHz window has 1.26% error and the *proposed model* has only 0.25% error. This clearly shows that the smaller window of approximation reduces the number of poles required significantly. It is seen that the *proposed model* of the 10th order in 1.5 kHz window is more accurate than the 30 pole model approximated in 5 kHz window.

Table 6.1: Frequency-dependent impedance values for different models.

freq.	Analytical	Constant Exact PI		30 poles(5KHz Win.)		10 poles(1.5KHz Win.)	
(Hz)	Z(Ohms)	Z(Ohms)	% Error	Z(Ohms)	% Error	Z(Ohms)	% Error
60	52.31	52.31	0.00	52.31	0.00	52.31	0.00
120	99.39	101.54	2.16	94.85	4.56	99.52	0.13
180	144.31	149.50	3.59	145.62	0.91	144.21	0.07
240	187.60	196.28	4.62	181.13	3.45	187.60	0.00
300	229.44	241.86	5.41	228.91	0.23	229.25	0.08
360	269.89	286.16	6.03	266.81	1.14	269.67	0.08
420	308.97	329.07	6.51	300.80	2.64	309.16	0.06
480	346.65	370.48	6.88	340.89	1.66	347.55	0.26
540	382.91	410.28	7.15	380.78	0.56	384.42	0.39
600	417.69	448.33	7.33	414.64	0.73	419.45	0.42
660	450.95	484.52	7.44	443.96	1.55	452.52	0.35
720	482.65	518.72	7.47	472.83	2.03	483.66	0.21
780	512.72	550.84	7.44	503.26	1.84	513.04	0.06
840	541.11	580.75	7.33	534.28	1.26	540.86	0.05
900	567.78	608.37	7.15	563.70	0.72	567.29	0.09
960	592.69	633.60	6.90	589.82	0.48	592.43	0.04
1020	615.78	656.35	6.59	612.20	0.58	616.25	0.08
1080	637.02	676.54	6.20	631.46	0.87	638.63	0.25
1140	656.38	694.12	5.75	648.66	1.18	659.30	0.45
1200	673.82	709.02	5.22	664.77	1.34	677.93	0.61
1260	689.31	721.19	4.62	680.28	1.31	694.11	0.70
1320	702.84	730.60	3.95	695.17	1.09	707.39	0.65
1380	714.38	737.21	3.20	708.98	0.76	717.31	0.41
1440	723.92	741.01	2.36	721.09	0.39	723.43	0.07
1500	731.46	741.98	1.44	730.89	0.08	725.33	0.84

6.3.2 Case II: Two Bus Single Phase System

In this section, two bus system with a line is considered. The first test line for single phase case is the falcon cable line discussed in previous section. The second test line is a three-phase three-wire 20-mile unbalanced line of dove cable. The conductors are asymmetrically spaced as follows: Phase A-B: 2.5ft, A-C: 7ft & B-C: 4.5ft and the tower height is 28 ft. The derived analytical model is used as benchmark; other models for comparison include the *simple PI model*, the *constant exact PI model*, the *EMT model* and a *cascaded PI model*. Since the *proposed model* has multiple *R-L-C* circuit elements, the uniformly segmented *cascaded PI model* with the same number of elements is included as one of the models for comparison.

6.3.2.1 Balanced Three-Phase/Single-Phase Test Case

A three-phase three-wire 25-mile long balanced line of falcon cable is considered. The conductors are assumed to be equilaterally spaced at 15 ft and tower height is assumed to be 50 ft. As the line is balanced, per phase analysis is performed. The single phase case with a phase and neutral wire could also be Kron reduced [69] to have a single element in the impedance or admittance matrices.

First the impedance values of the line is compared. The differences in series impedance values for various models and the benchmark *analytical model* are shown in Figure 6.7 for frequencies up to 1.5 kHz. From the figure it is clear that the *proposed model* impedances nearly coincide with the *analytical model* for all considered frequencies. The average error in model impedance with respect to the analytical model is 1.81% for the *proposed model*, 12.57% for the *constant exact PI model*, 44.72% for the *simple PI model* and 27.78% for the *cascaded PI model*.

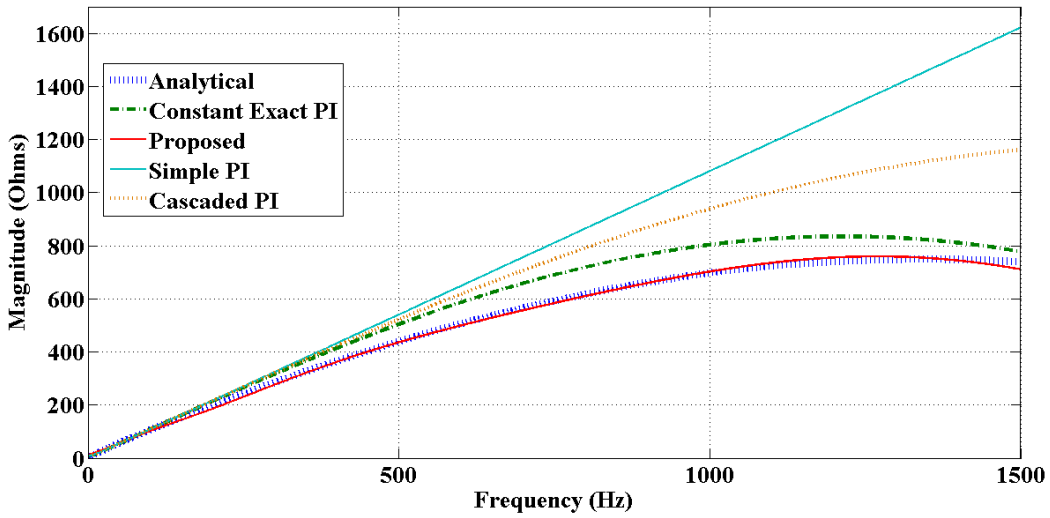

Figure 6.7: Series impedance magnitude for different line models of the 25 mile falcon cable.

Now the steady state harmonic voltages obtained using various line models are compared. Constant impedance load is used and calculated assuming that at 60 Hz, real power consumed at nominal voltage is 1 MW and reactive power consumed

is 300 kVar. Frequency-dependent impedances and admittances will have a major effect on harmonic voltage calculations. The EMT model does not have an equivalent PI structure and hence, the impedance values of this time domain model cannot be directly compared with steady-state models. However, time domain models and steady-state models can be compared in terms of receiving-end voltages or currents. In this example, the steady-state voltage obtained from the EMT model is compared to the voltages obtained using the *proposed model* and the other steady-state models. Given a known voltage source at the line sending end, a frequency scan is performed and the receiving end voltage is obtained for all considered line models. Receiving-end voltage in pu for different models is shown in Figure 6.8. Differences in receiving-end voltage between the analytical and the other models are shown in Figure 6.9. It is observed that the results obtained from the *proposed model* are similar to the results obtained using the EMT model. This shows that the *proposed model* can be used to achieve EMT model accuracy, without the need of running time domain analysis. The average error in voltage with respect to the *analytical model* calculated voltage is 1.71% for the *proposed model*, 0.01% for the Vector Fitted EMT model, 159.01% for the *constant exact PI model*, 92.88% for the *simple PI model* and 24.33% for the *cascaded PI model*.

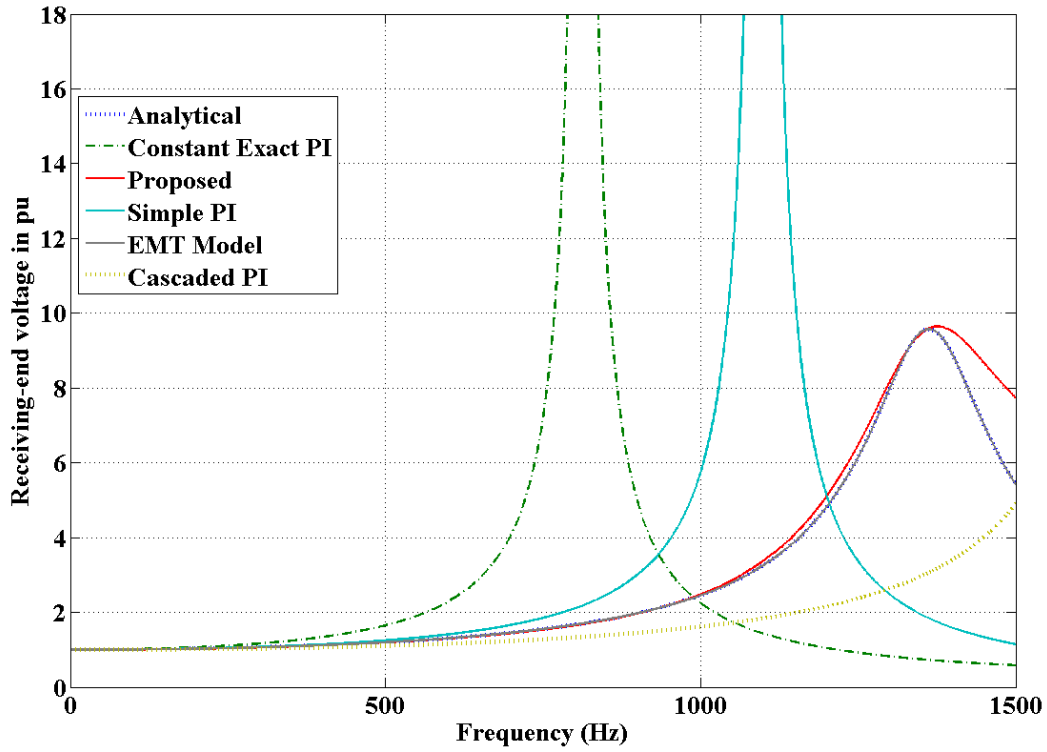

Figure 6.8: Receiving-end voltage in pu for different models for comparison for the 25-mile line of falcon conductor.

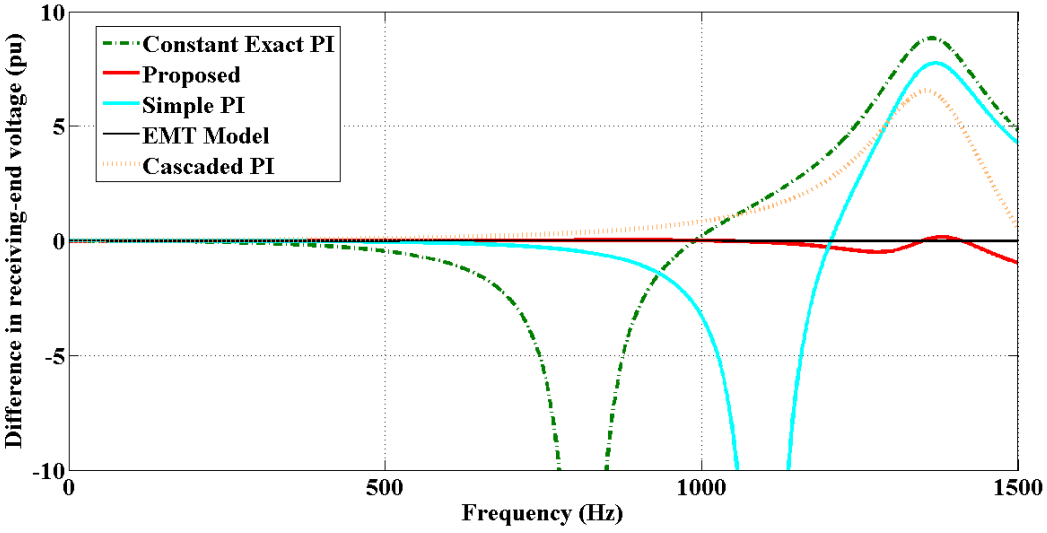

Figure 6.9: Difference in receiving-end voltage in pu between the analytical model and the other models for comparison for the 25-mile line of falcon conductor.

A long line of the same test case is also tested. Line length is considered to be 120 miles(193.12 km). First the impedance values of the line is compared. The series

impedance values for various models and the benchmark *analytical model* are shown in Figure 6.10 for frequencies up to 1.5 kHz. From the figure it is clear that the *proposed model* impedances nearly coincide with the *analytical model* for all considered frequencies. The average error in model impedance with respect to the analytical model is 1.66% for the *proposed model*, 33.16% for the *constant exact PI model*, 656.46% for the *simple PI model* and 92.39% for the *cascaded PI model*.

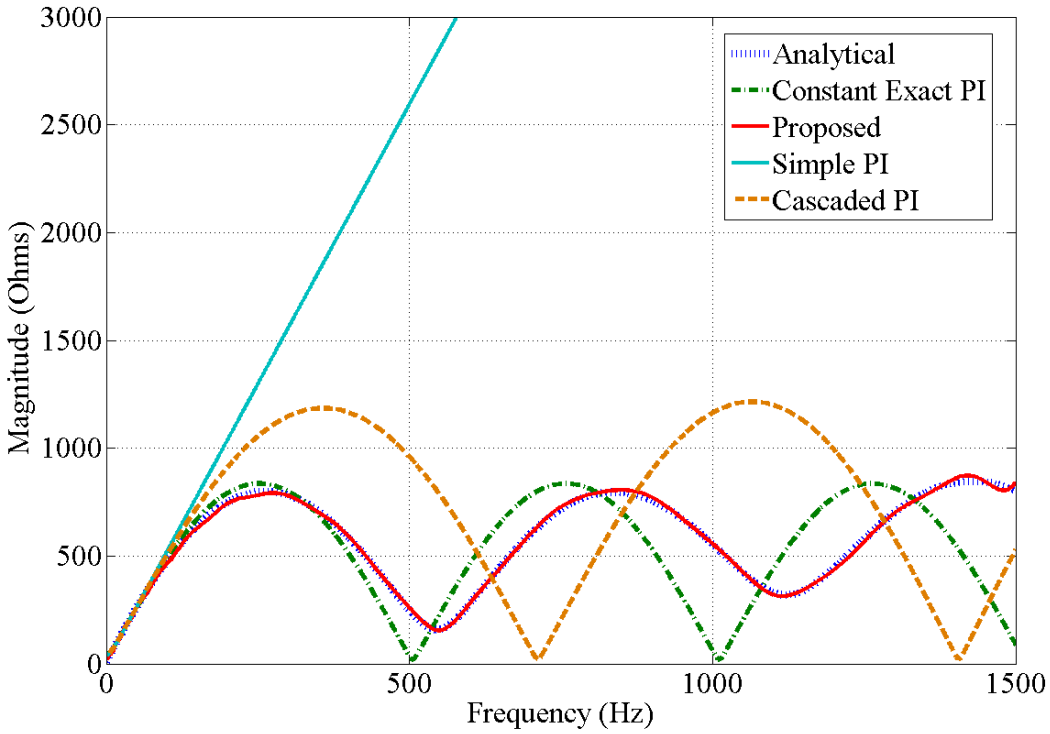

Figure 6.10: Series impedance magnitude for different line models of the 120 mile falcon cable.

Given a known voltage source at the line sending end, a frequency scan is performed and the receiving end voltage is obtained for all considered line models. Receiving-end voltage in pu for different models is shown in Figure 6.11. Differences in receiving-end voltage between the analytical and the other models are shown in Figure 6.12. It is observed that the results obtained from the *proposed model* are similar to the results obtained using the EMT model. This shows that the *proposed model* can be used to achieve EMT model accuracy, without the need of running time domain analysis.

The average error in voltage with respect to the *analytical model* calculated voltage is 1.99% for the *proposed model*, 0.006% for the Vector Fitted EMT model, 97.53% for the *constant exact PI model*, 79.04% for the *simple PI model* and 167.93% for the *cascaded PI model*.

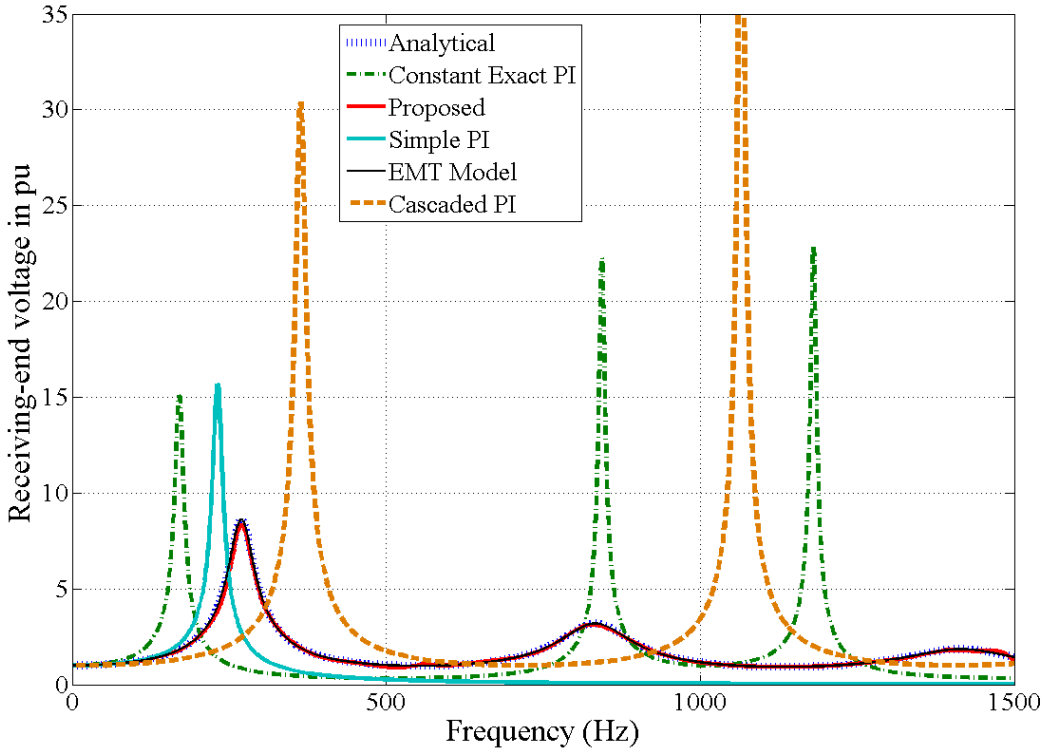

Figure 6.11: Receiving-end voltage in pu for different models for comparison for the 120-mile line of falcon conductor.

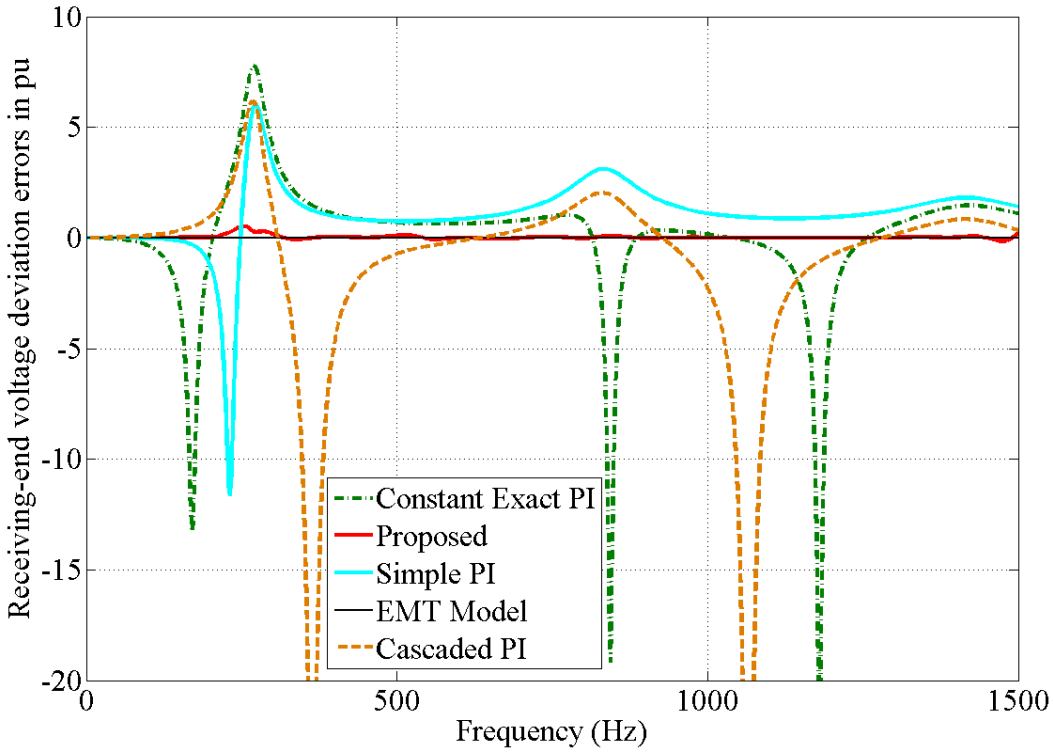

Figure 6.12: Difference in receiving-end voltage in pu between the analytical model and the other models for comparison for the 120-mile line of falcon conductor.

6.3.2.2 R-L-C Synthesis

The *proposed model* of the test line is synthesized using passive elements. The network as shown in Figure 5.5 is created for both series impedances and shunt admittances. The parameter values of the synthesized *R-L-C* circuit are shown in Table 6.2. The series impedance is approximated using the eighth order transfer function and the shunt admittance is approximated using the second order transfer function. It is seen that for this line, some of the values of the *R-L-C* elements are negative. If the software is made capable of in-taking negative values of these elements, simulations can be carried out as usual and the negative values will not create problems. It is also noted that the negative inductor can be represented by an equivalent capacitor and vice versa.

Table 6.2: Proposed line model R-L-C synthesis for the 25-mile test line.

Elements	Series Impedance			
R, L	$-32.75\,\mathrm{k\Omega}$	$0.767\,\mathrm{H}$		
R_{11}, R_{12}, L_1, C_1	$-941\,\mathrm{M\Omega}$	$-4.4\,\mathrm{M\Omega}$	$530.9\,\mathrm{H}$	$-145.2\,\mathrm{pF}$
R_{21}, R_{22}, L_2, C_2	$21.6\,\mathrm{G\Omega}$	$4.4\,\mathrm{M\Omega}$	$5.04\,\mathrm{MH}$	$0.142\,\mathrm{pF}$
R_{31}, R_{32}, L_3, C_3	$1.49\,\mathrm{k\Omega}$	$394.2\,\Omega$	$2.1\,\mathrm{H}$	$1.34\,\mathrm{\mu F}$
R_{41}, R_{42}, L_4, C_4	$31.7\,\Omega$	$47.06\,\Omega$	$1.15\,\mathrm{H}$	$472\,\mathrm{mF}$
Elements	Shunt Admittance			
R, L	$396.1\,\mathrm{m\Omega}$	$1.12\,\mathrm{nH}$		
R_{11}, R_{12}, L_1, C_1	$-0.37\,\mathrm{m\Omega}$	$5.62\,\mathrm{m\Omega}$	$110\,\mathrm{nH}$	$25.16\,\mathrm{mF}$

6.3.3 Case III: Two Bus Three Phase System

A three-phase three-wire 20-mile unbalanced line of dove cable is considered. The conductors are asymmetrically spaced as follows: Phase A-B: 2.5ft, A-C: 7ft & B-C: 4.5ft and the tower height is 28 ft. To increase the level of imbalance, single phase loads with different power ratings are connected at the receiving end of this line. A frequency scan is performed from 1 Hz to 1500 Hz, in 1 Hz steps, with a known voltage source connected at the line sending end. Phase C receiving-end voltage in pu for different models for comparison for the 20-mile line of dove conductor is shown in Figure 6.13. The receiving end voltage magnitudes obtained for different models are shown in Figure 6.14 for phase C, as an example. The *proposed model* again proves to be the most accurate as compared to the other steady-state models. The average error in voltage with respect to the *analytical model* calculated voltage is 1.81% for the *proposed model*, 107.19% for the *constant Exact PI model*, 354.01% for the *simple PI model* and 164.54% for the *cascaded PI model*.

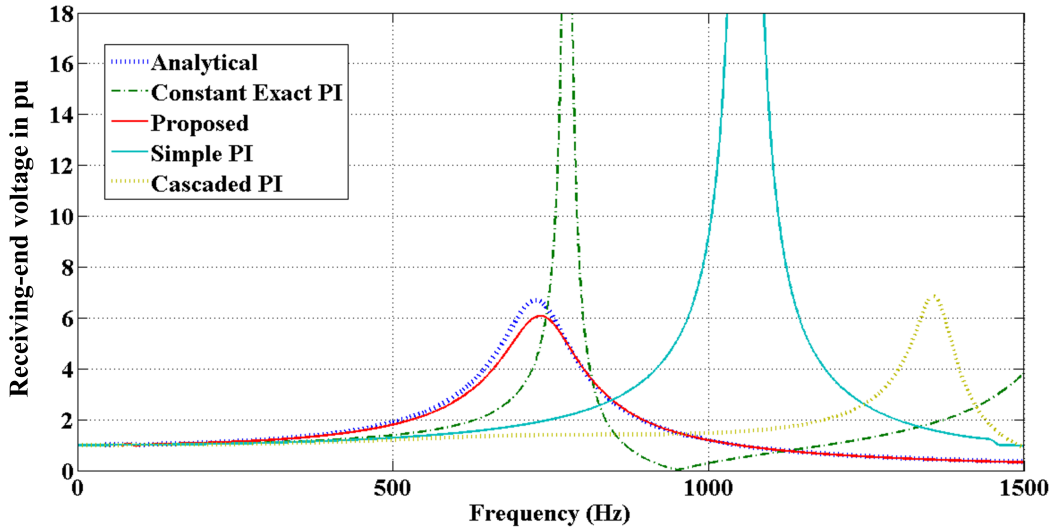

Figure 6.13: Phase C receiving-end voltage in pu for different models for comparison for the 20-mile line of dove conductor.

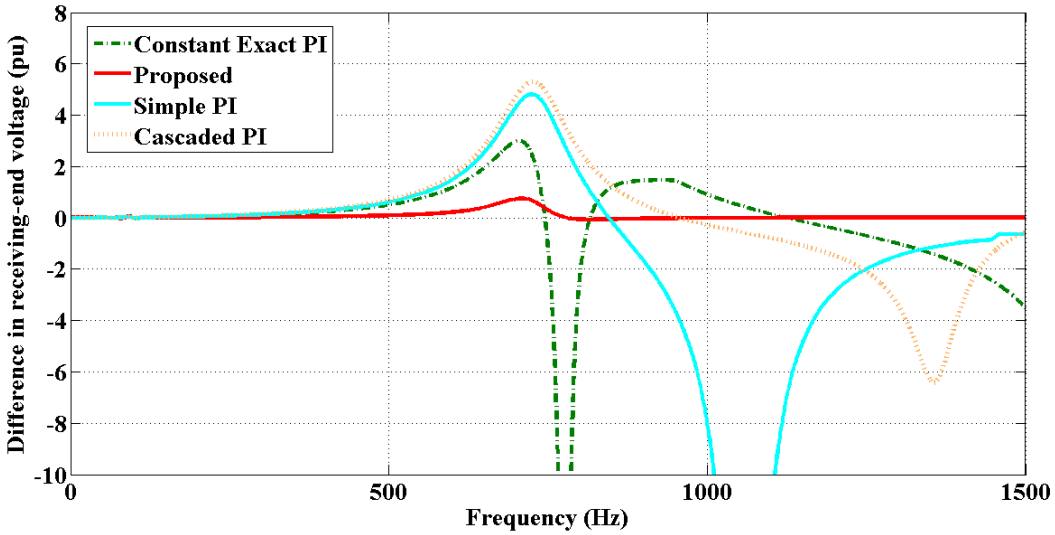

Figure 6.14: Difference in phase C receiving-end voltage in pu between the analytical model and the other models for comparison for the 20-mile line of dove conductor.

Phase C receiving-end voltage angle of different models for comparison for the 20-mile line of dove conductor is shown in Figure 6.15. The receiving end voltage angle differences for different line models are shown in Figure 6.16. It is observed that the results obtained from the *proposed model* have similar accuracy with respect to *analytical model* as compared to the *analytical model* and much better as compared

to other steady state models. The average deviation of the calculated voltage angle is 1.81° for the *proposed model*, 69.56° for the *constant exact PI model*, 39.33° for the *simple PI model* and 67.73° for the *cascaded PI model*.

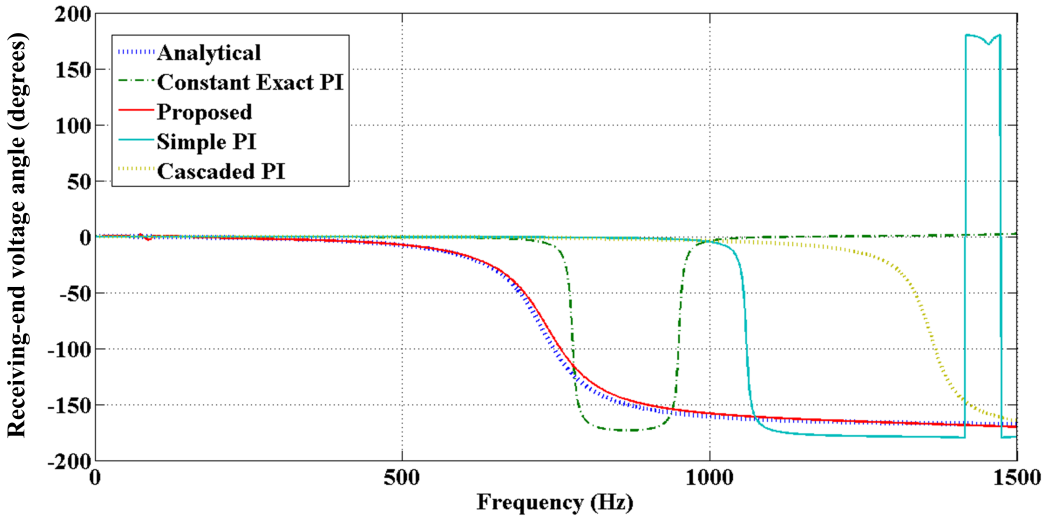

Figure 6.15: Phase C receiving-end voltage angle of different models for comparison for the 20-mile line of dove conductor.

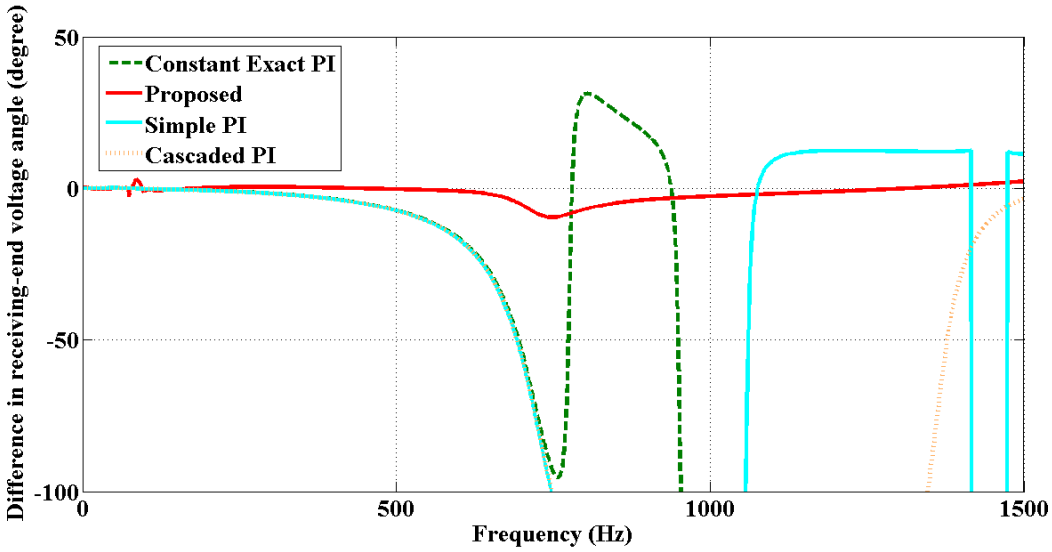

Figure 6.16: Difference in phase C receiving-end voltage angle between the analytical model and the other models for comparison for the 20-mile line of dove conductor.

6.3.3.1 R-L-C Synthesis

Similarly to the single phase case, the *proposed model* for this test line is synthesized using passive elements and the network as shown in Figure 5.5 is created for both series impedances and shunt admittances. The synthesized values for all phases are shown in Table 6.3.

Table 6.3: Proposed line model R-L-C synthesis for the 20-mile test line for all phases.

Phase A Elements				
Elements	Series Impedance			
R, L	138.8 Ω	0.102 H		
R_{11}, R_{12}, L_1, C_1	−8.99 Ω	−10.31 Ω	0.292 H	0.317 mF
R_{21}, R_{22}, L_2, C_2	818.6 Ω	148.3 Ω	−102 mH	1.9 µF
R_{31}, R_{32}, L_3, C_3	0.365 Ω	−15.55 Ω	5.11 mH	0.526 mF
R_{41}, R_{42}, L_4, C_4	1.62 Ω	101 Ω	36 H	77 µF
Elements	Shunt Admittance			
R, L	−91.1 µΩ	820 nH		
R_{11}, R_{12}, L_1, C_1	−0.14 mΩ	254 µΩ	0.161 µH	8.96 F

Phase B Elements				
Elements	Series Impedance			
R, L	130.1 Ω	0.101 H		
R_{11}, R_{12}, L_1, C_1	15.61 Ω	111.7 Ω	−207 H	−2.2 µF
R_{21}, R_{22}, L_2, C_2	−0.02 Ω	8.61 Ω	−1.1 mH	−4.14 mF
R_{31}, R_{32}, L_3, C_3	0.22 Ω	−0.83 Ω	−0.52 mH	−2.89 mF
R_{41}, R_{42}, L_4, C_4	−13.87 Ω	39.71 Ω	−43.3 mH	−25 µF
Elements	Shunt Admittance			
R, L	−99.6 µΩ	953 nH		
R_{11}, R_{12}, L_1, C_1	−0.13 mΩ	194 µΩ	0.138 µH	8.68 F

Phase C Elements				
Elements	Series Impedance			
R, L	96.3 Ω	0.105 H		
R_{11}, R_{12}, L_1, C_1	5.72 Ω	−6.18 Ω	295 µH	4.77 µF
R_{21}, R_{22}, L_2, C_2	−2.65 Ω	3.40 Ω	−8.95 mH	−0.68 mF
R_{31}, R_{32}, L_3, C_3	35.53 Ω	−109.1 Ω	−76 mH	−84 µF
R_{41}, R_{42}, L_4, C_4	−0.03 Ω	0.03 Ω	16.1 µH	13.4 mF
Elements	Shunt Admittance			
R, L	111 µΩ	598 nH		
R_{11}, R_{12}, L_1, C_1	−1.52 mΩ	120 µΩ	0.9 µH	2.56 F

As derived from the analytical model in the three phase case, the mutual parameters are included in the model by using the network as shown in Figure 5.8. For short and medium length lines, the mutual parameters are accurately approximated by a linear function: frequency being the dependent variable. Hence, the mutual impedance can be represented by a transformer and the mutual admittance by a capacitor. The parameter values of the synthesized *R-L-C* circuit of the mutual parameters are shown in Table 6.4.

Table 6.4: Proposed line model R-L-C synthesis of the mutual impedance and admittance for the 20-mile test line.

Elements	Mutual Impedance		
$Z_{12}(R_{12} + j\omega L_{12})$	$5 + j\omega 0.109\,\Omega$		
$Z_{13}(R_{13} + j\omega L_{13})$	$20 + j\omega 0.113\,\Omega$		
$Z_{23}(R_{23} + j\omega L_{23})$	$19 + j\omega 0.114\,\Omega$		
Elements	Mutual Admittance		
C_{12}, C_{13}, C_{23}	525 nF	140 nF	303 nF

The simplified circuit representation of this three phase line is shown in Figure 6.17.

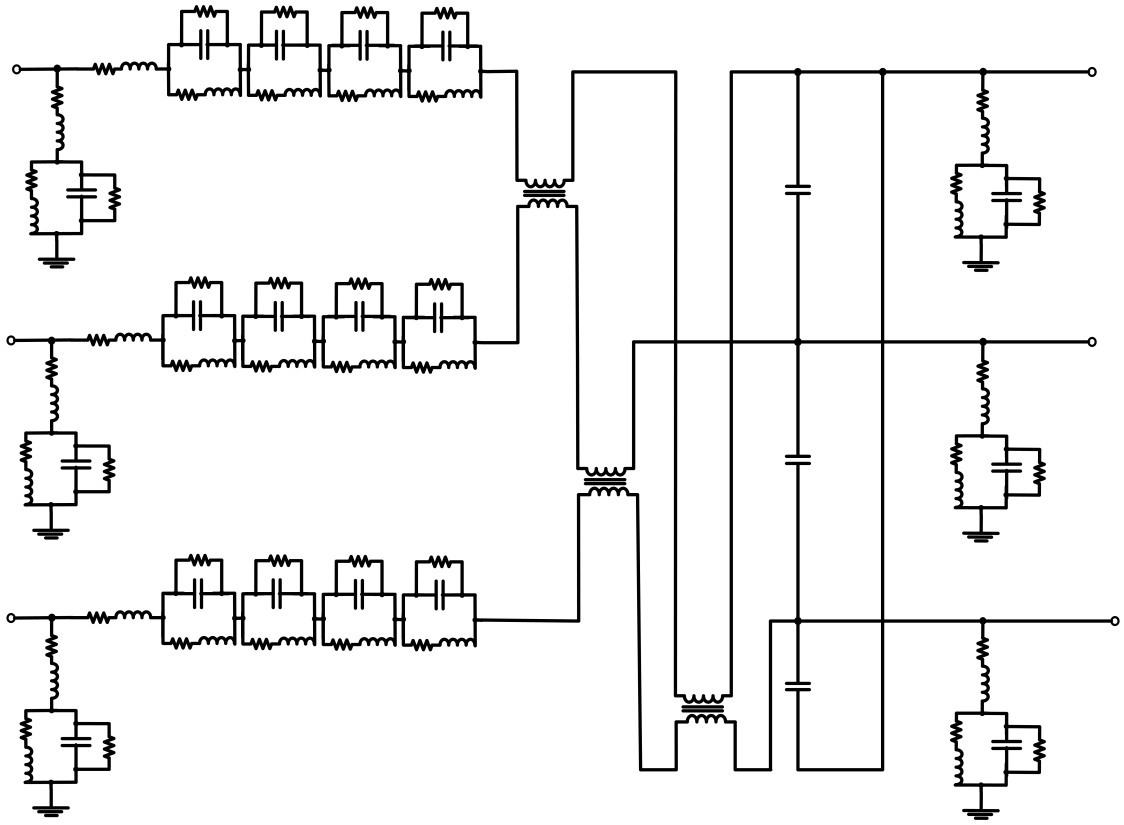

Figure 6.17: Simplified circuit representation of three phase 20 mile Dove conductor type.

6.4 Harmonic Power Flow in IEEE 13 Node Test Feeder

In order to perform a preliminary evaluation of the new frequency-dependent line model performance in system level studies, the IEEE 13 node test feeder [70] was used. The single line diagram of the test feeder is shown in Figure 6.18. This feeder is characterized by multi-phase unbalanced overhead and underground lines. The line impedances and admittance provided by IEEE are for the fundamental frequency of 60 Hz. In order to evaluate the proposed modeling approach, the authors have calculated the line parameter values for a frequency range from 1 to 1500 Hz using various line models.

6.4.1 Harmonic Current Injection

To test HPF on the test feeder, arbitrary nonlinear loads are assumed at different buses. The nonlinearity is created by injecting harmonic currents in the system. The

nodes with harmonic current injection are:

- Node 646: 11th harmonic current is injected at phase B and the magnitude is 10% of the fundamental current.
- Node 652: 5th harmonic current is injected at phase A and the magnitude is 10% of the fundamental current.
- Node 675: 7th harmonic current is injected at phase A, 13th harmonic current is injected at phase B and 19th harmonic current is injected at phase C. The magnitude of each is 10% of the fundamental current.

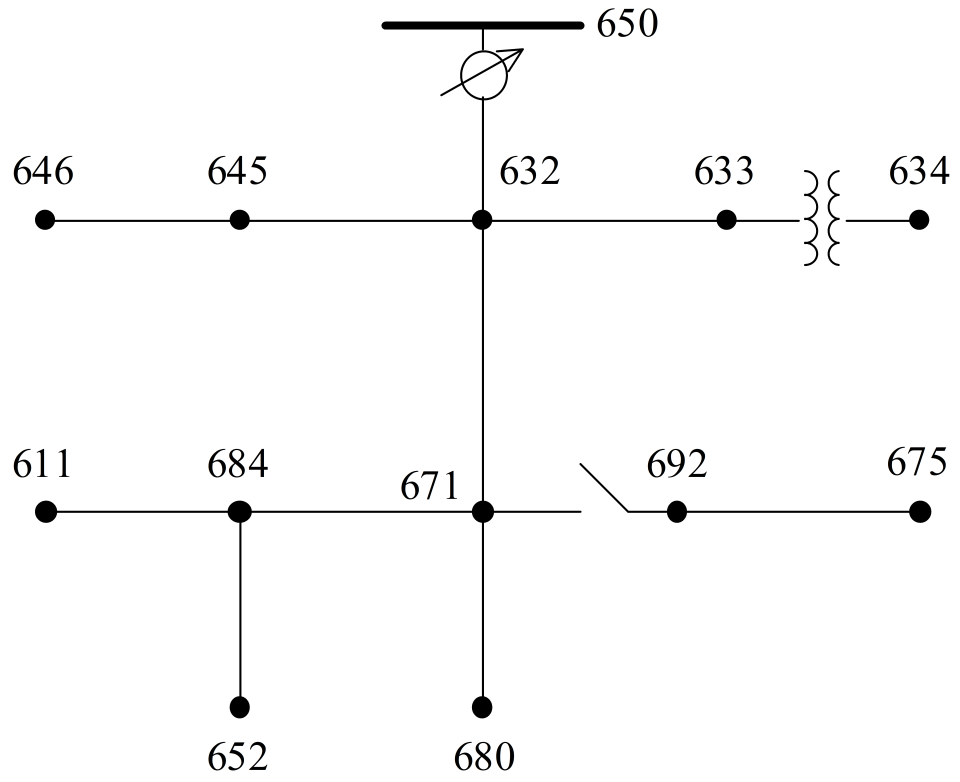

Figure 6.18: Single line diagram of IEEE 13 node test feeder.

6.4.2 Comparison in Harmonic Distortion

The load ratings are increased from the base case IEEE 13 node test feeder [70] evenly such that the line fundamental substation current is a few kilo amperes. The

THD at various points is calculated from (6.1).

$$\text{THD} = \frac{\sqrt{\sum_{n=2}^{N} F_n^2}}{F_1}. \tag{6.1}$$

where F is either rms voltage or rms current, n the harmonic number, N is the highest harmonic number under consideration and F_1 is the fundamental frequency rms value. Harmonic power flow is performed and multiple line models are compared. For clarity, the models under comparison are numbered as shown in Table 6.5.

Table 6.5: Line model numbering.

Model No.	Model Type
1	Analytical Model–Benchmark
2	Constant Exact PI Model
3	Simple PI Model
4	Cascaded PI Model
5	Proposed Model

Voltage and current THD values at select nodes in the proximity of the nodes injecting harmonics are presented in Tables 6.6 and 6.7 respectively. It is observed that the *proposed model* THD results are very close to the *analytical model* in comparison to the other steady state models, e.g. at node 671-Phase A, the voltage THD for *analytical model* is 2.866% and that of *proposed model* is 2.805%, however for the *exact PI model*, *simple PI model* and *cascaded model* are 1.681%, 4.894% and 3.097% respectively.

Table 6.6: Voltage THD values in percentage at select nodes.

Node-Phase	Model 1	Model 2	Model 3	Model 4	Model 5
645-B	1.312	3.467	2.321	0.323	1.284
611-C	5.348	3.890	3.914	12.50	4.502
671-A	2.886	1.681	4.894	3.097	2.805
671-B	2.339	1.081	2.481	5.264	2.240
671-C	2.685	2.659	2.903	3.638	2.306

Table 6.7: Current THD values in percentage at select nodes.

Node-Phase	Model 1	Model 2	Model 3	Model 4	Model 5
645-B	0.252	0.998	0.353	0.049	0.242
611-C	2.294	1.239	1.519	4.393	1.933
671-A	0.804	0.372	1.611	0.838	0.842
671-B	0.582	0.221	0.788	1.517	0.658
671-C	0.603	0.364	0.764	0.875	0.562

6.4.3 Comparison in Harmonic Losses

For the test case, harmonic losses were calculated using the different models as shown in Table 6.5. The results are shown in Table 6.8. Harmonic losses at select frequencies are normalized with the losses incurred in the *analytical model*–the benchmark; the deviation can be seen from the base value of 1. As seen from the table, the harmonic losses calculated using the *proposed model* are within 1% difference from those obtained using the *analytical model*, while the other models have up to 110% error (with the *simple PI model* performing the worst).

Table 6.8: Normalized harmonic losses at select frequencies f.

f (Hz)	Model 1	Model 2	Model 3	Model 4	Model 5
300	1.00	1.03	1.03	1.03	0.99
420	1.00	1.16	1.50	0.77	1.00
660	1.00	0.65	2.10	0.41	0.99
780	1.00	1.00	1.62	0.71	1.00
1140	1.00	1.59	1.93	0.93	1.00

The overall system losses are also calculated. The system loss bar diagram is shown in Figure 6.19. Losses are expressed as the percentage of the system load power. It is clearly seen that the loss calculation using the *proposed model* is very accurate with the *analytical model* and other steady state models show significant deviation.

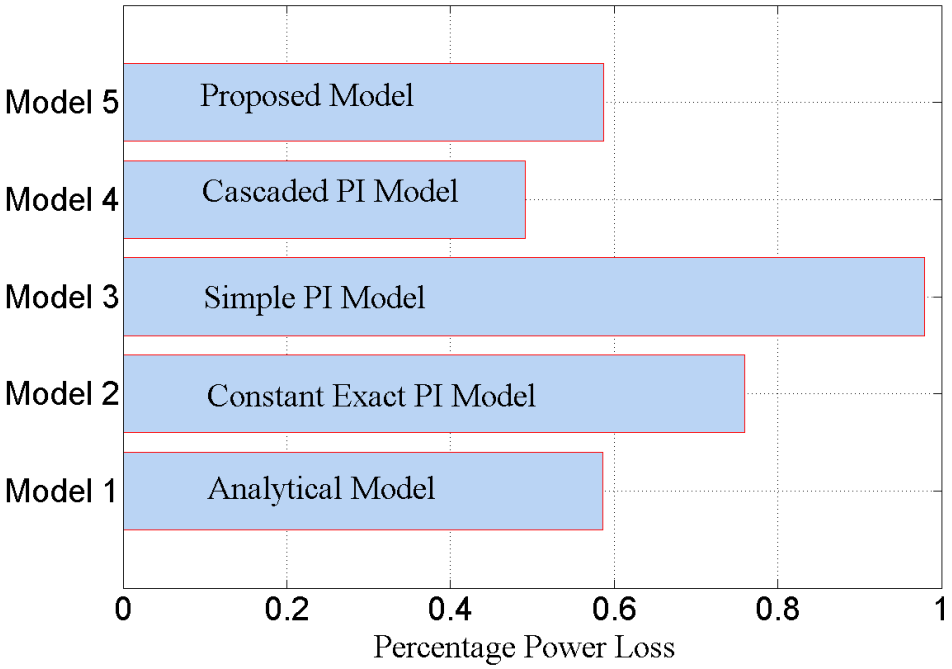

Figure 6.19: Total harmonic losses using different models.

CHAPTER 7: CONCLUSIONS AND FUTURE WORKS

7.1 Overview

The work presented in this thesis addressed the development and investigation of novel frequency-dependent electric power line models for steady state harmonic analysis. It took into account the line frequency-dependent characteristics due to the effect of the ground return and the skin effect. Multiple approaches were investigated and brought to the development of the proposed generic frequency-dependent line model. First a multi-segment line modeling approach was investigated and implemented in an harmonic power flow algorithm. Then an analytical expression capturing the real part of the line series impedance (apparent resistance) was presented, which can also be implemented for the imaginary part of the line series impedance (apparent reactance). Specifically for distribution lines, the expressions were simplified to first and second order polynomial equations. Lastly, the vector fitted generic frequency-dependent line modeling approach was presented. All the models were evaluated using different test cases and their performance compared to other commonly-used line models. Some of the metrics used for model evaluation and validation are series impedance, voltage magnitudes and angles at different buses or nodes on test cases after running harmonic power flow using different line models, voltage distortion levels etc.

In this chapter, first the summary of the research contributions is presented. Then, the differences between the EMT model and the proposed model are highlighted. Finally, possible areas of future work are discussed.

7.2 Summary of Research Contributions

The research contributions can be summarized as follows:

(a) The multi-segment frequency-dependent line model structure was used in a

non-iterative harmonic power flow tool. Results of the test studies using the proposed HPF tool were compared to results obtained using a single lumped parameter segment line model (i.e. the traditional PI model) as well as using the frequency-dependent line model(EMT model) used in the PSCAD software. In general, the results obtained using the proposed HPF tool with frequency-dependent line model structures were closer to the results obtained using the frequency-dependent line models in PSCAD than the ones obtained using a single-segment line model.

(b) An analytical expression capturing the frequency-dependent characteristics of real part of the line series impedance (apparent resistance) was presented. With this equation, the apparent resistance of the transmission line can be analyzed independently without deriving and calculating the equation for overall impedance of the line. This expression can be used directly in frequency dependent line models, including phasor domain calculations. A similar approach can be used for the imaginary part of the frequency-dependent line impedance(apparent reactance). The simplified approximated equation is compared with the analytical benchmark model and differences in computational time between the two are presented. Results have shown that during the run of the digital simulation, the approximated equation is executed 250 times faster than the analytical equation.

(c) As an extension of the work mentioned in the point above, a technique to simplify the expressions for the frequency-dependent power distribution line parameters was presented. The complex equations using the hyperbolic, logarithmic, trigonometric functions along with the Bessel functions and kelvin functions are simplified to first and second order polynomial functions. Computational time and error between the analytical expressions and the simplified expressions are compared. Results have shown that during the digital simulation, the

proposed equation is executed much faster than the analytical equations. Also the simplified expressions clearly retain the frequency-dependency of the line parameters.

(d) The proposed model presents a generic vector fitting-based frequency dependent line model to be used in frequency domain behavior analysis. The proposed model results in much higher accuracy than the simple PI, cascaded PI or constant exact PI models.

(e) The proposed frequency-dependent line modeling approach removes the necessity to run time domain simulations while still retaining very accurate frequency-dependent characteristics. This makes the model computationally efficient, and the simulation execution time faster.

(f) The PI structure of this proposed model allows for simple implementation in existing system-level analysis algorithms such as harmonic power flow.

(g) The proposed model can be synthesized in an R-L-C network and is therefore implementable in conventional simulation software. The use of passive elements also aids in maintaining model stability.

(h) The derived analytical model can be used for higher accuracy. However, for each frequency of interest, a separate analytical model has to be used. The proposed model avoids this problem by providing a single generic model for all harmonic frequencies of interest without much affecting the accuracy of analytical model. Also, the simulation time is faster when using the proposed model as compared to the analytical model.

(i) The proposed model is found to be more accurate than currently used steady state models such as the PI model or the exact PI model calibrated at 60 Hz. Hence, the proposed model has the advantage of accuracy over the currently used steady state models. Also, since the proposed frequency-dependent line modeling approach removes the necessity to run time domain simulations while

still retaining very accurate frequency-dependent characteristics as that of the EMT models, the proposed model has the advantage of speed over the EMT models for steady state harmonic analysis.

7.3 Proposed Model and EMT Model Comparison

The time domain EMT model and the frequency domain proposed model have some noticeable differences, although both models use the Vector fitting technique. The major differences between the EMT model [15] and the proposed model are listed below:

(a) Simulation Domain: The EMT model is designed to be used in for time domain simulations for transient analysis and cannot be used in frequency domain-based tools; the proposed model is developed for use in frequency domain simulations to study the propagation of harmonic frequency components. When comparing steady-state fundamental and harmonic voltages and currents obtained using both models, the proposed model is shown to retain the accuracy of the EMT model.

(b) Approximation Procedure: Both EMT and proposed model use the Vector fitting technique. In the EMT model, modal decomposition is done and propagation H and characteristic admittance Y_c are approximated. In the proposed model, the series impedance Z and shunt admittance Y of the benchmark model in a PI structure are approximated.

(c) Approximation Window: In EMT studies, a frequency response of up to 1 MHz may be required to capture transients in the microsecond time-scale. For the *proposed model*, a much smaller approximation window of up to the 25th harmonics, i.e. 1500 Hz, is considered. The smaller frequency window for steady state analysis is justified since transmission lines by nature are low pass filters and very high harmonics do not propagate in the system.

(d) Circuit Representation: The EMT model circuit representation has an active

element: a current source, but the proposed model circuit representation has all passive *R-L-C* elements. The use of all passive elements helps in creating more stable system models.

7.4 Future Work

Several suggestions can be made to extend this research:

(a) In multi-segment frequency-dependent transmission line models, the uniform segmentation of the line was considered, i.e. each segment series impedance and shunt admittance were equal. A non-uniform line model segmentation could be pursued to improve the accuracy.

(b) An analytical expression capturing the real part of the line series impedance (apparent resistance) was presented. The apparent resistance expression can be extended to use in other scenarios, e.g. in equivalent frequency-dependent network to analyze harmonic losses. A similar approach can be used for the imaginary part of the frequency-dependent line impedance(apparent reactance).

(c) The proposed vector fitted model has *R-L-C* elements. In some occasions, the passive elements turn out to be physically unrealizable. An investigation to ensure physically realizable passive elements can be pursued.

(d) For all the models investigated in this research, the focus was to study state harmonic propagation in the system. All these models could be investigated on how they respond to electrical transients.

REFERENCES

[1] "IEEE draft guide for applying harmonic limits on power systems," *IEEE P519.1/D12, July 2012*, pp. 1–124, Feb 2015.

[2] AXINO-TECH Consulting & Services Ltd. (Nov 16, 2011) [Online]. Available: http://www.axino-tech.co.nz/documents/Testing

[3] W. Xu and J. Mayordomo, "Three-phase power flow and harmonic analysis," in *Electric Energy Systems: Analysis and Operation*, Boca Raton, CRC Press, 2008.

[4] "IEEE recommended practice and requirements for harmonic control in electric power systems," *IEEE Std 519-2014 (Revision of IEEE Std 519-1992)*, pp. 1–29, June 2014.

[5] J. Arrilaga and N. R. Watson, *Power System Harmonics*. New York: John Wiley and Sons, 2nd ed., 2004.

[6] S. Govindarajan, M. Cox, and F. Berry, "Survey of harmonic levels on the southwestern electric power company system," *IEEE Trans. Power Del.*, vol. 6, pp. 1869–1875, Oct 1991.

[7] H. W. Dommel, *Electromagnetic Transients Program (EMTP) Theory Book*. Portland, Oregon: Bonneville Power Administration, 1995.

[8] PSCAD, *Version 4.4.1.0*. Manitoba, Canada: Manitoba HVDC Research Center.

[9] A. Budner, "Introduction of frequency-dependent line parameters into an electromagnetic transients program," *IEEE Trans. Power App. Syst.*, vol. PAS-89, pp. 88–97, Jan 1970.

[10] A. Semlyen and A. Dabuleanu, "Fast and accurate switching transient calculations on transmission lines with ground return using recursive convolutions," *IEEE Trans. Power App. Syst.*, vol. 94, pp. 561–571, Mar 1975.

[11] J. Marti, "Accuarte modelling of frequency-dependent transmission lines in electromagnetic transient simulations," *IEEE Trans. Power App. Syst.*, vol. PAS-101, pp. 147–157, Jan 1982.

[12] T. Noda, N. Nagaoka, and A. Ametani, "Phase domain modeling of frequency-dependent transmission lines by means of an arma model," *IEEE Trans. Power Del.*, vol. 11, pp. 401–411, Jan 1996.

[13] H. Nguyen, H. Dommel, and J. Marti, "Direct phase-domain modelling of frequency-dependent overhead transmission lines," *IEEE Trans. Power Del.*, vol. 12, pp. 1335–1342, Jul 1997.

[14] B. Gustavsen and A. Semlyen, "Calculation of transmission line transients using polar decomposition," *IEEE Trans. Power Del.*, vol. 13, pp. 855–862, Jul 1998.

[15] A. Morched, B. Gustavsen, and M. Tartibi, "A universal model for accurate calculation of electromagnetic transients on overhead lines and underground cables," *IEEE Trans. Power Del.*, vol. 14, pp. 1032–1038, Jul 1999.

[16] B. Gustavsen, "Frequency-dependent transmission line modeling utilizing transposed conditions," *IEEE Trans. Power Del.*, vol. 17, pp. 834–839, Jul 2002.

[17] T. Noda, "Application of frequency-partitioning fitting to the phase-domain frequency-dependent modeling of overhead transmission lines," *IEEE Trans. Power Del.*, vol. 30, pp. 174–183, Feb 2015.

[18] V. Cecchi, A. St.Leger, K. Miu, and C. Nwankpa, "Modeling approach for transmission lines in the presence of non-fundamental frequencies," *IEEE Trans. Power Del.*, vol. 24, pp. 2328–2335, Oct 2009.

[19] B. Poudel and V. Cecchi, "Harmonic power flow using multi-segment frequency-dependent transmission line models," in *North Amer. Power Symp. (NAPS)*, pp. 1–6, 2013.

[20] B. Poudel and V. Cecchi, "An approach for modeling frequency-dependent apparent resistance of power transmission lines," in *North Amer. Power Symp. (NAPS)*, pp. 1–6, 2014.

[21] M. Tavares, J. Pissolato, and C. Portela, "Mode domain multiphase transmission line model-use in transient studies," *IEEE Trans. Power Del.*, vol. 14, pp. 1533–1544, Oct 1999.

[22] K. Malekian, U. Schmidt, A. Hoshmeh, and A. Shirvani, "Frequency dependent model of underground cables for harmonic calculations in frequency domain," in *Information Technology and Electrical Engineering (ICITEE), 2014 6th International Conference on*, pp. 1–7, Oct 2014.

[23] A. Dounavis, R. Achar, and M. Nakhla, "Efficient passive circuit models for distributed networks with frequency-dependent parameters," *IEEE Trans. Adv. Packag.*, vol. 23, pp. 382–392, Aug 2000.

[24] B. Poudel and V. Cecchi, "Frequency-dependent transmission line modeling for steady state power system harmonic analysis," in *North Amer. Power Symp. (NAPS)*, pp. 1–6, 2015.

[25] W. M. Haynes, *CRC Handbook of Chemistry and Physics*. Boca Raton: CRC Press, 2014.

[26] J. D. Glover, M. S. Sharma and T. J. Overbye, *Power System Analysis and Design*. New Delhi: Cengage Learning, fourth ed., 2008.

[27] J. J. Grainger and W. D. Stevenson Jr., *Power System Analysis.* New Jersy: McGraw Hill Companies, Inc, 2003.

[28] A. Kennelly and H. A. Affel, "Skin-Effect Resistance Measurements of Conductors, at Radio-Frequencies up to 100,000 Cycles per Second," *Proc. Inst. of Radio Engineers*, vol. 4, pp. 523–574, Dec 1916.

[29] W. C. Johnson, *Transmission lines and networks.* New York: McGraw-Hill Book Co., 1st ed., 1950.

[30] E. Kreyszig, *Advanced Engineering Mathematics.* New York: Wiley, 1972.

[31] P. V. O'Neil, *Advanced Engineering Mathematics.* Belmont, California: Wadsworth Publishing Company, 1991.

[32] *Aluminum Electrical Conductror Handbook.* Washington D.C.: Aluminum Association, 2nd ed., 1982.

[33] J. R. Carson, "Wave propagation in overhead wires with ground return," *Bell Sys. Tech. J.*, vol. 5, pp. 539–554, Oct 1926.

[34] F. E. Terman, *Radio Engineers' Handbook.* New York: McGraw-Hill Book Co., 1943.

[35] H. B. Dwight, "Skin effect and proximity effect in tubular conductors," *Trans. Ameri. Inst. of Elect. Engineers*, vol. XLI, pp. 189–198, Jan 1922.

[36] U. A. Bakshi and M. Bakshi, *Generation, Transmission and Distribution.* Pune: Technical Publications Pune, 2009.

[37] G. Smith, "The proximity effect in systems of parallel conductors and electrically small multiturn loof antennas," tech. rep., Division of Engineering and Applied Physics, Harvard University, Cambridge, Massachusetts, 1971.

[38] D. A. Douglass and L. Kirkpatrick, "Ac resistance of acsr-magnetic and temperature effects," *IEEE Transactions on Power Apparatus and Systems*, vol. PAS-104, pp. 1578–1584, June 1985.

[39] P. N. Murgatroyd, "Calculation of proximity losses in multistranded conductor bunches," *IEE Proc. A - Physical Science, Measurement and Instrumentation, Manage. and Educ.*, vol. 136, pp. 115–120, May 1989.

[40] X. Bian, L. Chen, D. Yu, L. Wang, and Z. Guan, "Impact of surface roughness on corona discharge for 30-year operating conductors in 500-kv ac power transmission line," *IEEE Trans. Power Del.*, vol. 27, pp. 1693–1695, July 2012.

[41] H. Saadat, *Power System Analysis.* New York: Tata McGraw-Hill, 2005.

[42] G. W. Kimbark, *Electrical Transmission of Power and Signals.* New York: John Wiley and Sons, 1958.

[43] W. H. Hayt, *Engineering Electromagnetics*. New York: McGraw-Hill Book Co., 7th ed., 1981.

[44] G. Bekefi and A. H. Barrett, *Electromagnetic Vibrations, Waves and Radiation*. Cambridge, MA: MIT Press, 1987.

[45] D'Alembert, "Recherches sur la courbe que forme une corde tenduÃ« mise en vibration," *Histoire de l'acadÃ©mie royale des sciences et belles lettres de Berlin*, vol. 3, pp. 214–219, 1747.

[46] L. Bergeron, "Du coup de belier enhydraulique au coup defoudre en electricite." Paris: Dunod, 1949. Transl., "Water Hammer in Hydraulics and Wave Surges in Electricity", (Translating Committee sponsored by ASME). New York: Wiley, 1961., 1949.

[47] A. Budak, *Passive and Active Network Analysis and Synthesis*. Boston: Houghton Mifflin, 1974.

[48] J. E. Storer, *Passive Network Synthesis*. New York: McGraw-Hill Book Co., 1957.

[49] B. Gustavsen and A. Semlyen, "Rational approximation of frequency domain responses by vector fitting," *IEEE Trans. Power Del.*, vol. 14, pp. 1052–1061, Jul 1999.

[50] MATLAB, *version 7.10.0 (R2010a)*. Natick, Massachusetts: The MathWorks Inc., 2010.

[51] D. Goldsman, R. Nance, and J. Wilson, "A brief history of simulation," in *Proc. of the 2009 Winter Simulation Conf.(WSC)*, pp. 310–313, Dec 2009.

[52] H. Dommel, "Digital computer solution of electromagnetic transients in single- and multiphase networks," *IEEE Trans. Power App. Syst.*, vol. PAS-88, pp. 388–399, April 1969.

[53] G. A. Baker, Jr., "The theory and application of the padé approximant method," in *Advances in Theoretical Physics, Volume 1* (K. A. Brueckner, ed.), p. 1, 1965.

[54] E. W. Kimbark, *Electrical Transmission of Power and Signals*. New York: John Wiley and Sons, 2nd ed., 2004.

[55] R. Zimmerman, C. Murillo-Sanchez, and R. Thomas, "Matpower: Steady-state operations, planning, and analysis tools for power systems research and education," *IEEE Trans. Power Syst.*, vol. 26, pp. 12–19, Feb 2011.

[56] CYMDIST, *Version 5.04*. Quebec, Canada: CYME International T& D Inc.

[57] Mathematica, *Version 8.0 for Students*. Champaign, Illinois: Wolfram Research.

[58] D. Xia and G. Heydt, "Harmonic power flow studies part I - formulation and solution," *IEEE Trans. Power App. Syst.*, vol. PAS-101, no. 6, pp. 1257–1265, 1982.

[59] S. Herraiz, L. Sainz, and J. Clua, "Review of harmonic load flow formulations," *IEEE Trans. Power Del.*, vol. 18, no. 3, pp. 1079–1087, 2003.

[60] W. Xu, J. Marti, and H. Dommel, "A multiphase harmonic load flow solution technique," *IEEE Trans. Power Syst.*, vol. 6, no. 1, pp. 174–182, 1991.

[61] M. Valcarel and J. Mayordomo, "Harmonic power flow for unbalanced systems," *IEEE Trans. Power Del.*, vol. 8, no. 4, pp. 2052–2059, 1993.

[62] W. Xu, J. Drakos, Y. Mansour, and A. Chang, "A three-phase converter model for harmonic analysis of hvdc systems," *IEEE Trans. Power Del.*, vol. 9, no. 3, pp. 1724–1731, 1994.

[63] D. Pileggi, N. Chandra, and A. Emanuel, "Prediction of harmonic voltages in distribution systems," *IEEE Trans. Power App. Syst.*, vol. PAS-100, no. 3, pp. 1307–1315, 1981.

[64] A. A. Mahmoud and R. D. Shultz, "A method for analyzing harmonic distribution in a.c. power systems," *IEEE Trans. Power App. Syst.*, vol. PAS-101, no. 6, pp. 1815–1824, 1982.

[65] Y. Sun, G. Zhang, W. Xu, and J. Mayordomo, "A non-iterative harmonic power flow method for accurate harmonic calculations," in *13th Int. Conf. Harmonics and Quality of Power*, pp. 1–6, 2008.

[66] *Electrical transmission and distribution reference book.* East Pittsburg, Pennsylvania: Westinghouse Electric Corporation, fourth ed., 1950.

[67] J. W. M.L. James, G.M. Smith, *Applied Numerical Methods for Digital Computation.* New York: John Wiley and Sons, 3rd ed., 1985.

[68] W. H. Kersting, *Distribution System Modeling and Analysis.* New York: CRC Press, Taylor & Francis Group, 1958.

[69] G. Kron, *Tensor Analysis of Networks.* New York: John Wiley and Sons, 1939.

[70] IEEE PES Distribution Systems Analysis Subcommittee, "Radial test feeders." http://ewh.ieee.org/soc/pes/dsacom/testfeeders/testfeeders.pdf.